Novel spectroscopic imaging techniques for quality control of multiple unit pellet system (MUPS) tablets

Dissertation

with the aim of achieving a doctoral degree

at the Faculty of Mathematics, Informatics and Natural Sciences

Department of Chemistry

Universität Hamburg

submitted by

Anna Novikova

Hamburg 2017

Reviewer of the thesis: **Professor Dr. Claudia S. Leopold**

                               Professor Dr. Patrick Théato

                               Professor Dr. Sascha Rohn

Date of thesis defence: **19th May 2017**

Date of approval for publication: **22nd May 2017**

Acknowledgements

This thesis was prepared at the University of Hamburg, Department of Chemistry, Division of Pharmaceutical Technology under supervision of Professor Dr. Claudia S. Leopold.

Foremost, I would like to thank Prof. Dr. Leopold for offering me this highly interesting research topic and for believing in me as a researcher as well as for giving me the opportunity to be a member of her research group. I want to express my deep gratitude for the interesting discussions, which guided me through my work as well as for the research freedom, which allowed me to work on my own ideas and projects and to develop myself personally and professionally.

Furthermore, I would like to thank Prof. Dr. Dr. h.c. Thomas Rades from the University of Copenhagen for the co-supervision of this work. I am grateful for the warm welcome I received during my research stay in his working group at the University of Copenhagen as well as for proof reading this thesis. Thomas motivated, inspired and supported me all the time.

Moreover, I am grateful to Prof. Dr. Patrick Théato and Prof. Dr. Sascha Rohn for the evaluation this. Furthemore, I would like to thank Prof. Dr. Hans-Ulrich Moritz and Dr. Maria Riedner for being members of the examination committee.

I thank Dr. Albrecht Sakmann for his support of this work and especially for his help with students' supervision as well as for enabling my attendance to every conference or postgraduate training. In addition, I would like to thank Petra Borbe and Kai Braunschweig for the experimental assistance, especially concerning HPLC analysis.

I deeply thank Associate Prof. Dr. Jens Michael Carstensen from the Technical University of Denmark for suppling the VideometerLab and the VideometerLabUV as well as for his support and interesting discussions concerning the imaging analysis.

Contents

Zusammenfassung

In multipartikulären Systemen wie MUPS (Multiple unit pellet system)-Tabletten werden die Vorteile der konventionellen Tabletten mit denen von Kapseln, die mit Pellets befüllt sind, kombiniert. Im Rahmen der PAT (process analytical technology)-Initiative sowie im Vergleich zu konventionellen Tabletten stellen MUPS-Tabletten zusätzliche Herausforderungen an die Qualitätskontrolle, wie z.B. die ungleichmäßige Verteilung der überzogenen Pellets in den Tabletten, sowie auf den Tablettenoberflächen. Daher bieten insbesondere schnelle und nicht destruktive spektroskopische Mapping- oder Imagingtechniken ein hohes Potenzial für die Qualitätskontrolle von MUPS-Tabletten.

In der vorliegenden Arbeit wurde die Anwendbarkeit von bildgebenden Verfahren, wie multispectral ultraviolett (UV) imaging und terahertz pulsed imaging (TPI), für die Qualitätskontrolle von MUPS-Tabletten untersucht. Da MUPS-Tabletten teilbar sind, ist die Pelletverteilung in einer Tablette bzw. auf ihrer Oberfläche von entscheidender Bedeutung und muss gewährleistet sein. Daher wurde die Eignung des UV Imagings in Kombination mit multivariater Bildanalyse zur Auswertung der Oberfläche von MUPS Tabletten in Bezug auf die Differenzierung der Pellets von den Hilfsstoffen, zur Vorhersage des Wirkstoffgehalts, sowie zur Pelletverteilung geprüft. Darüber hinaus wurde der Einfluss des Überzugspolymers und der Tablettenschichtdicke auf die beschriebenen Eigenschaften untersucht. Das Zerfallsverhalten und die anschließende Wirkstofffreisetzung der gesamten MUPS-Tablette bzw. der sich darin befindenden Pellets können jeweils durch die geschickte Wahl des Polymerüberzugs gesteuert werden. Aus diesem Grund sind die Dicke und die Homogenität des aufgebrachten Überzugs von besonderer Bedeutung. In diesem Zusammenhang wurde das UV Imaging in Kombination mit multivariater Datenanalyse für die Bestimmung der Dicke und der Homogenität des Überzuges während des

Überziehens im Labormaßstab herangezogen. Das Überzugspolymer kann den Wirkstoff in den Pellets vor Feuchtigkeit, Licht oder chemischen Interaktionen mit anderen Formulierungskomponenten schützen. Daher wurde das UV Imaging in Kombination mit multivariater Bildanalyse auch für die Überwachung des Wirkstoffabbaus der sich in den MUPS-Tabletten befindlichen Pellets während der Lagerung untersucht.

TPI gewinnt immer mehr an Bedeutung für die Analyse von festen Proben mit komplexen inneren Strukturen wie Tabletten, da diese Methode eine 3D-Abbildung der Probe erlaubt. Da die Verteilung der Pellets in einer MUPS-Tablette ein kritischer Faktor ist, wurde die Eignung von TPI zur Analyse der inneren Struktur von MUPS-Tabletten untersucht. Dabei sollte geprüft werden, ob die Pellets in einer MUPS-Tablette unter der Tablettenoberfläche visualisierbar sind.

Abstract

Multiple unit pellet system (MUPS) tablets combine advantages of coated single unit tablets and pellet containing capsules. In context with process analytical technology (PAT) and compared to single unit tablets, MUPS tablets pose additional challenges for quality control, such as an uneven distribution of the coated pellets in the tablet itself as well as at the tablet surface. Therefore, especially fast and non-destructive spectroscopic mapping or imaging techniques offer a high potential for quality control of MUPS tablets.

In this thesis, the applicability of multispectral ultraviolet (UV) imaging and terahertz pulsed imaging (TPI) for quality control analysis of MUPS tablets was investigated. As MUPS tablets are dividable, the pellet distribution within a tablet as well as at its surface is crucial and has to be homogeneous. Therefore, the applicability of UV imaging in combination with multivariate image analysis for surface evaluation of MUPS tablets was investigated with respect to the differentiation of the API pellets from the excipients matrix, estimation of the drug content as well as analysis of pellet distribution. Furthermore, the influence of the coating material as well as the tablet thickness on the described properties was analysed. The disintegration behaviour and subsequent drug release of the entire MUPS tablet or of the pellets within the MUPS tablet, respectively, may be controlled by a coating film. In this regard, the applicability of UV imaging in combination with multivariate data analysis was investigated to determine the coating thickness and its distribution at the tablet surface during lab scale coating. The applied pellet coating may protect the API from humidity, light, or chemical interactions with other formulation components. Hence, the applicability of the non-destructive UV imaging in combination with multivariate image analysis was investigated to monitor the API degradation within MUPS tablets during storage.

TPI has gained an increasing interest for analysis of solid samples such as tablets with complex internal structures, as this method allows a 3D mapping of the sample. As mentioned before, the pellet distribution within a MUPS tablet is crucial, and thus the suitability of TPI for analysis of the inner structure of the MUPS tablets was also investigated. Thereby, it was possible to visualise the pellets in a MUPS tablet also below the tablet surface.

List of Abbreviations

AOTF   Acousto-optical tuneable filters

API   Active pharmaceutical ingredient

ASA   Acetylsalicylic acid

ATR   Attenuated total reflection

CQAs   Critical quality attributes

EMA   European Medicines Agency

FDA   U.S. Food and Drug Administration

FIR   Far-infrared

GMP   Good manufacturing practice

HPLC   High performance liquid chromatography

HPMC   Hydroxypropyl methyl cellulose

IR   Infrared

LCTF   Liquid crystal tuneable filters

LV   Latent variable

MG-ST   Magnesium stearate

MCC   Microcrystalline cellulose

MIR   Mid-infrared

MSC   Multiplicative scatter correction

MUPS	Multiple units pellet system
NIR	Near-infrared
PAT	Process analytical technology
PCA	Principal component analysis
PC	Principal component
PLS	Partial least squares regression
QbD	Quality by design
RH	Relative humidity
RMSE	Root mean square error
RMSEC	Root mean squared error of calibration
RMSECV	Root mean squared error of cross validation
RMSEP	Root mean squared error of prediction
SA	Salicylic acid
SNV	Standard normal variate
Theo	Theophylline
THz	Terahertz
TPI	Terahertz pulsed imaging
UV	Ultraviolet

1. Introduction

1.1.   Multiple units pellet system tablets

1.1.1.   General aspects

Tablets represent more than 80% of all pharmaceutical dosage forms for human use [1,2], mainly because of the relatively high patient compliance resulting from oral administration and the dosing accuracy [1,3]. A further advantage of this dosage form is the rather easy manufacturing process [1], resulting in a high manufacturing speed leading to low production costs. In addition, tablets exhibit a high physicochemical stability compared to liquids or semi-solid formulations [1]. Moreover, tablets with different biopharmaceutical properties may be produced [4]. For example, tablet disintegration with subsequent drug dissolution can be controlled by coating tablet cores with a polymer film [5]. Particularly, enteric and sustained release coatings play an important role. However, the drawback of these coated single unit tablets is that they pass the stomach without disintegration resulting in high intra- and interindividual variations of the GI tract passage [6]. In addition, the division of coated single unit tablets leads to a loss of the coating functionality [6]. A more predictable transit time through the stomach may be achieved by units smaller than 1 mm as they are still able to pass the pylorus without its opening [6,7]. In contrast to coated single unit tablets, pellet containing capsules meet this requirement. Moreover, pellets with different release profiles can be filled into capsules leading to the desired release kinetics [8,9]. Nevertheless, disadvantages of capsules compared to coated single unit tablets are the low manufacturing speed and high manufacturing costs [8]. Furthermore, pellet containing capsules cannot be divided.

Multiple unit pellet system (MUPS) tablets are an increasingly investigated solid oral dosage form in pharmaceutical research and development [8], as they combine advantages of coated single unit tablets with pellet containing capsules. In contrast to single unit tablets, the active pharmaceutical ingredient (API) in MUPS tablets is

present in the core of small coated pellets [10]. MUPS tablets disintegrate in the stomach into these pellets, which pass the pylorus faster and at a more predictable rate than a coated single unit tablet. Drug release from the pellets in the intestine depends on the functionality of the applied pellet coating [6]. The disintegration process of a MUPS tablet and the passage through the pylorus is visualised in Fig. 1.
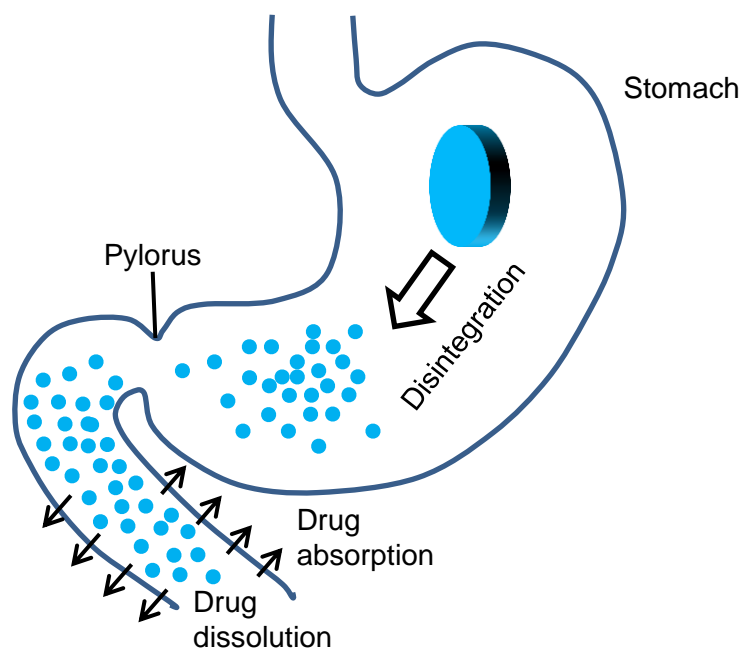
Fig. 1: Illustration of the disintegration of a MUPS tablet and the passage through the pylorus.

Combination of pellets with different release characteristics allows a higher release profile flexibility than coated single unit tablets [11]. In addition, the risk of "dose dumping" as the result of coating cracks is decreased, as single pellets only contain small amounts of API [8]. A further advantage of MUPS tablets is their dividability, thus, these tablets do not lose their coating functionality and therefore offer a comparably high dosage flexibility [11].

The dividability is also an advantage compared to pellet containing capsules. Furthermore, in comparison to capsules the production costs of MUPS tablets are lower and the risk of tampering with the dosage form is reduced [11].

1.1.2.   Special aspects of MUPS tablet manufacturing

A MUPS tablet usually consists of coated API pellets embedded in an excipient matrix. Therefore, the manufacturing process of MUPS tablets may include several steps, such as pelletisation of the API and excipients, granulation of the matrix materials, coating of the pellets, blending and compression of the components to a tablet as well as an optional final coating of the tablet. An example of possible manufacturing steps is presented in Fig. 2.
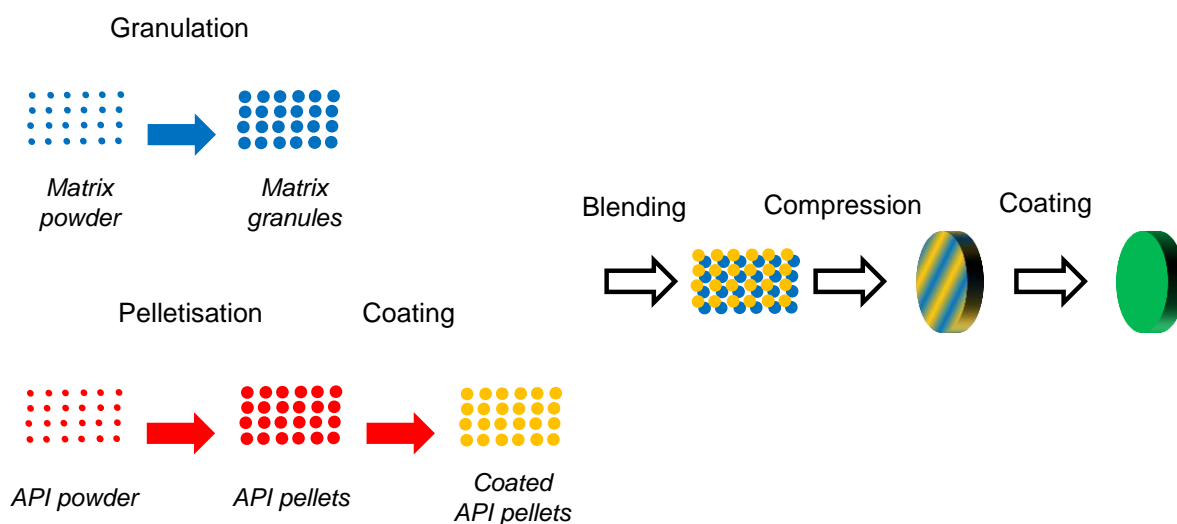
Fig. 2: Illustration of the manufacturing process of a MUPS tablet.

During the development of MUPS tablet formulations several aspects should be considered. The coated pellets have to withstand the compression force, otherwise the coating of the pellets might crack leading to a faster drug release. In the literature mainly two types of coatings are investigated: ethyl cellulose and acrylic polymers under the trade mark Eudragit® [8,11–21]. The elasticity of the applied coating serves as the main property to withstand the compression force. Ethyl cellulose coatings

have been shown to be more brittle leading to a loss of the coating functionality in many studies [11,15]. Depending on the coating type, an increasing coating level applied onto the pellets may decrease the tensile strength of the resulting tablet and increase the elastic recovery of the pellets [8,11]. Coatings prepared from organic solution have been observed to be more flexible than coatings prepared from aqueous dispersions [15,21]. For the pellets to remain intact during the compression process Lehmann et al. suggested that the coating film should show an elongation at break of at least 75% [22]. The elongation at break may be increased by addition of a plasticiser to a coating formulation [23,24]. With increasing concentration of a plasticiser in a coating formulation the elasticity of the coating increases leading to an improved resistance of the coating against the compression force [25]. Of course, the type of plasticiser also has an influence on the resulting elasticity of the coating [26].

In addition to the coating, the pellet core also has an influence on the resistance of the coated pellet to the compression force [8]. In the literature different opinions about the hardness requirements for the pallet cores may be found. In general, it is suggested that pellet core and coating film should have similar properties [27,28]. The studies about compression of uncoated pellets have shown that the pellet cores should exhibit some elasticity to withstand the compression force by deformation instead of fracture [29,30]. In addition, a high porosity of the uncoated pellets leads to an increased elasticity of the pellets and to a higher tensile strength of the resulting tablet [31,32]. Furthermore, the manufacturing process of the pellets also has an influence on the physical properties of the pellets and thus on the ability to withstand the compression force [33]. Surprisingly, coated pellets with high hardness showed less coating rupture after compression than softer and more porous pellets because they undergo less deformation or fracture during compression [14,34]. Opitz also suggested that the cores should exhibit low porosity and be of spherical shape as

well as showing low deformation during the compression [35]. Moreover, Regnarsson et al. found that an increasing particle size resulted in increasing damage of the coating [36]. This was also confirmed by Haslam et al. [37].

The tableting excipients may also contribute to the ability of coated pellets to withstand the compression force. The compression energy that is brought into the system during compression should ideally be completely absorbed by tableting excipients called cushioning agents, and transferred into bonds without damage to the coated pellets [38]. In the literature, different types of deformation behaviour of cushioning agents are suggested to be advantageous. In older studies the advantage of plastic deformation of cushioning agents has been described, as they lead to hard tablets [11]. In contrast, Picker et al. showed that cushioning agents with elastic deformation behaviour result in less pronounced damage of the coated pellets as the compression energy is used for the elastic recovery of the cushioning agents [39]. Furthermore, the excipients should prevent a direct contact between the pellets, which would lead to a fusion of the pellets resulting in slower drug release [19]. Theoretically, 29% of excipient powder is sufficient to prevent the contact between the coated pellets and thus their fusion [11]. The excipients should allow a high tablet hardness even at low compression forces and not influence drug release [11]. With increasing amount of cushioning agent the tensile strength of the resulting tablet increases and damage to coated pellets decreases [11,14]. Additionally, a rapid disintegration of the tablet in the stomach should be guaranteed [11]. The cushioning agents may be incorporated into the tablet in various forms such as pellets, granules or powder and consist of different materials [40]. For example, microcrystalline cellulose (MCC) and polyethylene glycol have been shown to be advantageous [41]. However, the ingredient composition of MUPS tablets may be heterogeneous with regard to particle size, and thus surface area as well as the density of the ingredients

[11,42–44]. Therefore, segregation of the ingredients at different stages of the tablet manufacturing process may occur [11,42–44]. The matrix excipients should enable a homogeneous distribution of the pellets within the tablet leading to content and weight uniformity [11].

The mentioned studies show that a lot of aspects have to be considered during the MUPS tablet manufacturing process to obtain tablets of the desired quality.

1.2.   PAT in the QbD context with special focus on MUPS tablets

As already described, the tablet manufacturing process and particularly manufacturing of MUPS tablets includes several processing steps. Therefore, the quality of each intermediate product is crucial because it also serves as a starting material for the next production step. Joseph Juran, the pioneer of the quality by design (QbD) concept, suggested that quality should be designed into the product, and the possible problems with the product that might follow are related to the way how this product was designed [45]. Therefore, the sentence '*Quality should be built into the product, and testing alone cannot be relied on to ensure product quality.*' turned into a philosophy in the pharmaceutical field [46]. In this regard, quality control of each manufacturing step is required to build the quality into the process resulting in an end product with the desired attributes [47–50]. Thus, understanding of the manufacturing process plays a major role. The authorities, such as the European Medicines Agency (EMA) and the U.S. Food and Drug Administration (FDA), strictly regulate the environment of the manufacturing process by Good Manufacturing Practice (GMP) frameworks [51–53]. These guidelines include requirements for various topics concerning the manufacturing process. Among other requirements, the process has to be clearly defined, controlled and documented [51–53]. As a result of these strict requirements, the quality of the products continuously increased. However, there has been an innovation delay concerning the production improvement and associated quality control [48,54]. Currently, solid oral dosage forms are still frequently produced in batches, which are examined by often time-consuming tests of only randomly chosen samples in spatially separated laboratories [55,56]. To solve the problem with the delay of innovations in the pharmaceutical industry, two initiatives were launched by the FDA in 2004 to optimise the regulatory frameworks and to support innovation in pharmaceutical manufacturing [47,48,54].

One of the main goals of these frameworks is the understanding of the process, which leads to an efficient manufacture and to a high quality of the product [47,48]. In this context, the end points of the single manufacturing steps should be determined based on the quality of the intermediate product and not on the process time. Therefore, during process development, quality target product profiles (QTPP) should be established. QTTPs represent the planned characteristics of the product [50]. Ideally, these should be achieved to ensure the desired quality with regard to safety and efficacy of the product [50]. The QTTP profiles may include content uniformity, tablet appearance (e.g. homogeneity of the coating) and drug stability [57]. Based on the QTPPs, the critical quality attributes (CQAs) of a dosage form can be defined [50,58]. *'A CQA is a physical, chemical, biological, or microbiological property or characteristic that should be within an appropriate limit, range, or distribution to ensure the desired product quality.'* [50] These CQAs should be monitored during each manufacturing step. Therefore, the FDA Guidances for Industry support process analytical technology (PAT) approaches [48,59]. In contrast to the mentioned tests of representative samples in spatially separated laboratories, PAT tools allow a complete control of the critical parameters during production, and in many cases even a better process understanding [55].

In general, there are four different measurement methods in process analysis that are applied to ensure the product quality in the pharmaceutical industry (Fig. 3) [60].

a   **Off-line**

Manufacturing environment | Laboratory

Process

Analyser

Sample

b   **At-line**

Manufacturing environment

Process

Analyser

Sample

c   **On-line**

Manufacturing environment

Process

Analyser

d   **In-line**

Manufacturing environment
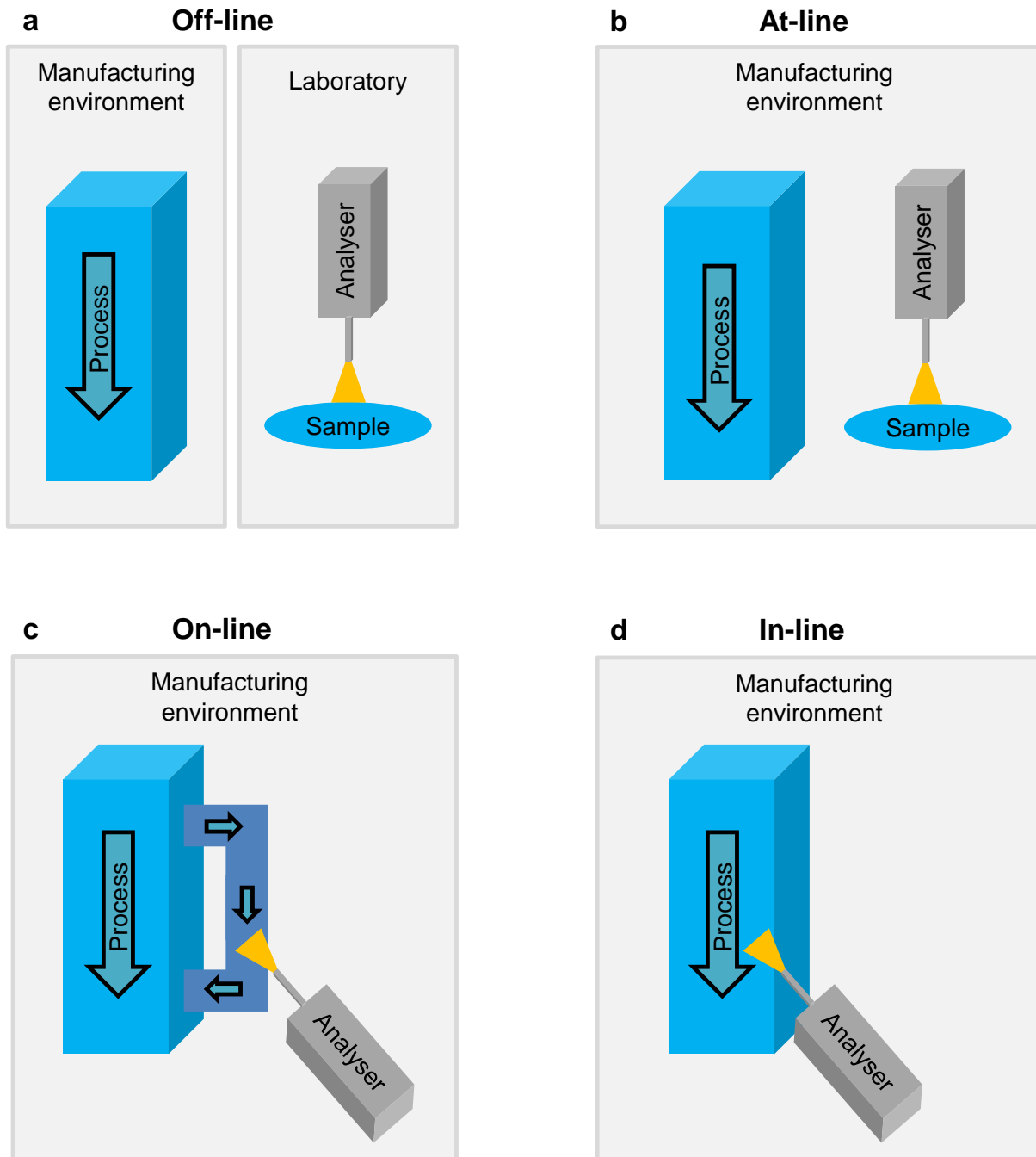
Process

Analyser

Fig. 3: Measurements methods in process analysis; modified from [60].

As described above, most quality tests are performed in spatially separated laboratories on preselected samples and not in the same environment as the manufacturing process (Fig. 3a) [60]. This measurement procedure is known as the off-line measurement method [60]. A drawback of this method is a lag time between

an unsatisfactory analytical result being found and the reaction thereon resulting from the spatial separation [60]. In contrast to off-line measurements, real-time process monitoring which can be achieved by at-line, in-line and on-line measurements serves as a fast and accurate measurement method to obtain the desired information on the sample [48,61]. During at-line measurements the sample is analysed during the process in the manufacturing environment close to the production line [48,60]. However, the sample is still removed from the process, but the reaction time is considerably reduced compared to off-line measurements (Fig. 3b) [48,60]. Nevertheless, the reaction time is still rather slow [60]. In case of on-line measurements, the sample remains in the manufacturing environment, but is temporarily separated from the main production line and analysed for example during passage through a sampling loop (Fig. 3c) [60]. After passage through the sampling loop, the sample is brought back into the process [48,60]. As shown in Fig. 3d, during in-line measurements the process analyser is placed directly into the manufacturing machine and is therefore in direct contact with the product, allowing analysis of the current status of the product [60].

For real process monitoring, PAT requires fast, non-invasive, and non-destructive analytical techniques. Thus, spectroscopic techniques exhibit a great potential as PAT tools. Spectroscopic methods such as near-infrared (NIR) and Raman spectroscopy are already established in different manufacturing areas as PAT tools [55,62–65]. Nevertheless, the delay of innovation described above led to a need to catch-up for the pharmaceutical industry. Therefore, research on spectroscopic techniques with PAT potential is of increasing interest in academia and industry.

In context with PAT, many quality attributes of MUPS tablets may become crucial and should be monitored. As described above, QTTP profiles such as content uniformity,

tablet appearance and drug stability might be used to define the CQAs [57]. These QTTP profiles are especially interesting in combination with MUPS tablet quality attributes. As already described, the composition of the MUPS tablets may be heterogeneous and segregation of the ingredients at different stages of the tablet manufacturing process may occur [42–44]. As dividability is an advantage of MUPS tablets, content uniformity and the pellet distribution within the MUPS tablets should be monitored. The disintegration behaviour and subsequent drug release of the entire MUPS tablet or of the pellets within the MUPS tablet, respectively, may be controlled by a coating film. Therefore, the thickness and the uniformity of the applied coating are CQAs and have to be controlled. The applied functional coating on the pellets may protect the API from humidity, light, or chemical interactions with other formulation components [66,67]. Therefore, methods to monitor the API stability within the coated drug pellets of a MUPS tablet may attract interest in the near future.

1.3.   Spectroscopic techniques for PAT

1.3.1.   General aspects

Spectroscopic techniques, as described above, exhibit a great potential as PAT tools resulting from the possibility of a fast, non-invasive and non-destructive measurement [65,68,69]. In general, the main principle of spectroscopic measurements is the propagation of light with chosen energies through the sample such as a tablet. Thereby, the propagated light is influenced by the optical properties of the sample, for example the absorption and scattering coefficients [70,71]. These optical properties of the sample depend on various sample attributes such as chemical structure, concentration and physical properties [70]. Thus, spectroscopic techniques allow both qualitative as well as quantitative, non-destructive analysis of the samples, making simultaneous in-line analysis of various attributes possible [72].

Two measurement approaches for spectroscopic techniques, transmission and reflection, play a major role. The main difference between these two measurement approaches is the passage of the light beam in the sample as shown in Fig. 4. If the measurement is performed in transmission mode, the light beam passes through the sample. Thus, information on the composition of a bulk sample may be obtained [73]. A drawback of this approach might be the limitation of light propagation by the sample thickness, as the light beam has to propagate through the whole sample before reaching a detector [73]. For this reason, opacity of the sample might also be a problem [73]. Hence, time-consuming and destructive sample preparation is necessary. However, opaque samples with various thicknesses may be analysed in reflectance mode, where the incident light beam is reflected by the tablet surface and the reflected light beam is captured by the detector [73]. If only information on the sample surface is needed, no thickness limitation exists [73]. Thus, measurements with this approach are fast and non-destructive, as usually no sample preparation is

needed. The disadvantage of reflection analysis is the possibility to collect information on the component distribution only at the tablet surface [73]. In addition, the spectra can be noisy, as the light is diffusely reflected by the sample surface before it reaches the detector [73]. This thesis focuses on the reflection techniques, as they are fast and non-destructive and therefore exhibit a high potential for quality control analysis.

Transmission technique   **Reflectance technique**

Light source   Light source   Detector

Light beam   Incident light beam   Reflected light beam

Sample   Sample

Detector
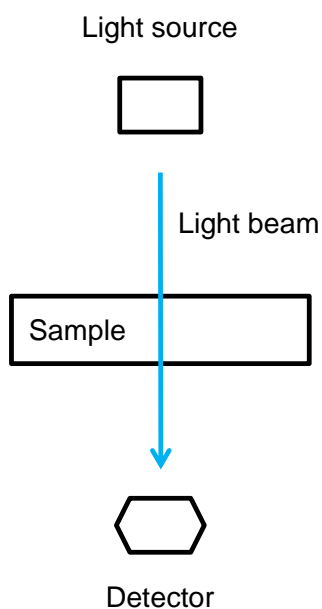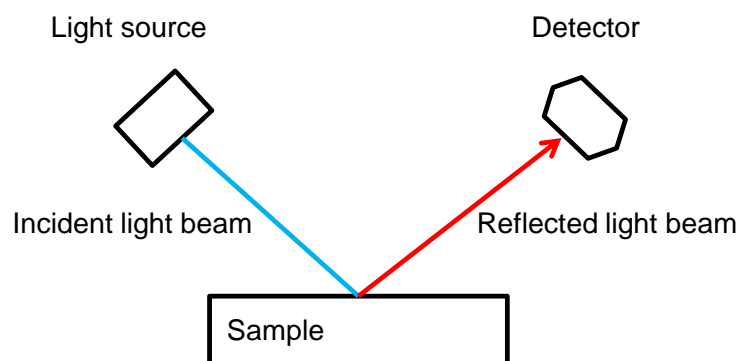
Fig. 4: Comparison of spectroscopic transmission and reflectance techniques for analysis of a sample.

In general, two types of the spectroscopic measurements are possible: single point and imaging (or mapping) measurements. Single point measurements are fast, but allow recording of the information only at one point or of the sample mean [64]. For several research applications, such as the distribution of the API at the sample

surface, acquirement of spatial spectral information is essential. The spatial spectral information may be collected in two ways, by mapping or imaging [74–76]. In a mapping experimental set up, the sample is measured sequentially [75], by moving a spot of the sample into the light beam (Fig. 5).
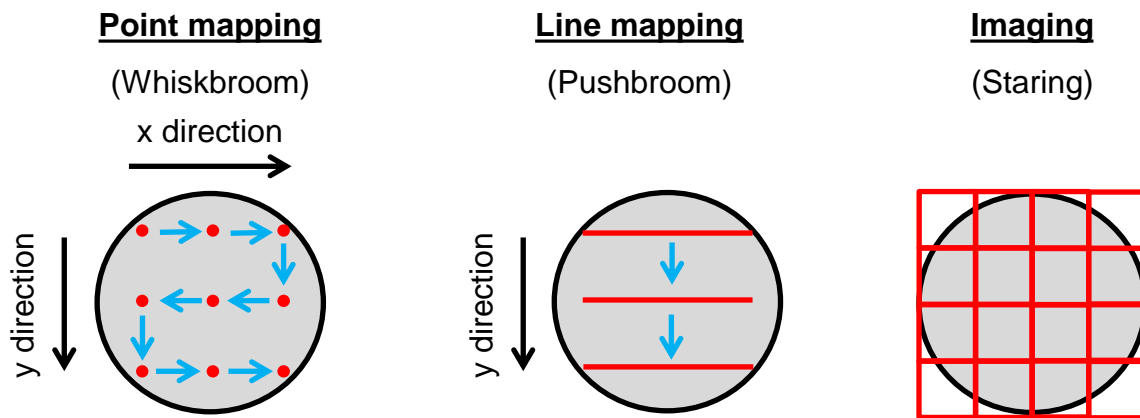
Fig. 5: Visualisation of different imaging techniques applied on a circular sample.

By point mapping (Whiskbroom) the sample is scanned point-by-point by moving in the xy direction [77]. Thereby, for each analysed spot ("point" or pixel) a full spectrum is acquired. The advantage of this technique is high flexibility in spatial resolution, sample size and spectral range. However, scanning of the sample point-by-point is time-consuming. Thus, the spatial resolution is usually kept low to decrease the measurement time [77]. This technique is commonly used for NIR, Raman and MIR analysis [75].

Line mapping (Pushbroom) is faster than point mapping, as a full spectrum is acquired for each pixel in a line at the same time [77]. To collect the spatial information of the whole sample the sample is moved in only one direction (x or y

direction) [75,77]. This technique exhibits a high potential for in-line and on-line quality control of manufacturing processes [77].

Imaging (Staring) methods record a spectrum of each pixel of the sample with an array detector without movement of the sample or the detector [75,77]. These methods may be performed by application of a rotating wheel with various bandpass filters for wavelength selection [77]. Thereby, a sample is illuminated with the light of a chosen energy and the absorbance or reflectance intensity of each pixel is recorded [75]. Thereafter, the rotation wheel switches to the next bandpass filter and the next absorbance or reflectance values may be recorded leading to the acquirement of a full spectrum of each pixel at the sample surface [75]. The disadvantage of this method is low flexibility [77] with respect to wavelength selection. A more flexible way to obtain the desired radiation wavelength is the application of liquid crystal tuneable filters (LCTF) or acousto-optical tuneable filters (AOTF). These filters are the mostly used devices because the filter change is done automatically and thus more wavelengths are available [77,78]. The main advantage of imaging is the possible high spatial resolution at low spectral resolution [77]. However, the sample has to be stationary and thus only at-line quality control is feasible [77].

Mapping and imaging experimental setups provide spectral and spacial information on the sample that allows localization and identification of the ingredients [72]. Quite often in the literature mapping and imaging methods are subsumed up under the term 'imaging'. However, if the sample is moved in x and y direction, this experimental setup should not be called imaging [75]. However, the images that are acquired by mapping techniques are treated in the same way during the following analysis of spectral data sets as those acquired by imaging [75]. The data obtained

by mapping or imaging result in a three-dimensional data cube [64]. As shown in Fig. 6 a spectrum is collected for each pixel of a tablet surface (marked in red).
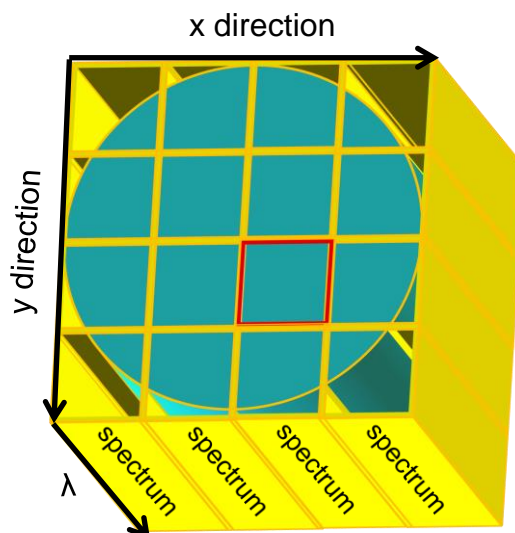
Fig. 6: Schematic visualisation of a three-dimensional data cube obtained for tablet surface analysis.

Depending on the dimensions of the obtained images, i.e. on the number of the applied wavelengths, a different terminology is used. If the number of the wavelengths is higher than ten, the imaging technique is called hyperspectral imaging, if it is lower than ten, it is called multispectral imaging [75]. With regard to the limited space for data storage, multispectral imaging exhibits a high potential in quality control. Mapping or imaging may be performed by illumination of the sample with the radiation of various energies of the electromagnetic spectrum. In the following chapters the most commonly applied analytical techniques and their PAT potentials are discussed.

1.3.2. *Mid-infrared spectroscopy*

Mid-infrared (MIR) spectroscopy covers the range of the electromagnetic spectrum between 2.6 and 26 µm (4000–400 cm^{-1}) [72]. Absorption of the radiation in this range results in fundamental vibration of the molecules [56,73]. One advantage of MIR is that various molecules show strong absorbance in this range allowing an analysis of these molecules [73]. In addition, based on the spectral information, it is possible to analyse the structure of molecules (peak location) and to quantify the amount of them in a sample (peak intensity) [73]. Compared to high performance liquid chromatography (HPLC), MIR spectroscopy is quite fast (few min per measurement) and simple to perform [73]. MIR spectroscopy has a high absorption cross section resulting in high sensitivity allowing the determination of even low API contents [72]. However, because of the relatively high absorption cross section, many drugs have to be measured in diluted form or other techniques such as attenuated total reflection (ATR) have to be applied. Thus, in-line analytics of high dose APIs is challenging [72]. Another important disadvantage of MIR spectroscopy for in-line quality control is the limited application of fiber optics complicating remote sampling [56]. In addition, with increasing number of the components in the sample the spectrum of the sample becomes more complex resulting in problematic interpretation of the spectra of sample mixtures [73]. To decrease the complexity of these spectra, a spectral subtraction may be applied [73]. Spectra of several components are subtracted from the total spectrum such that the remaining spectra only contains the components of interest [73]. Another important drawback of MIR spectroscopy that should be mentioned is its sensitivity towards water [73]. Thus, the water absorption band may overlap with absorption bands of the sample and therefore has to be subtracted from the sample spectrum leading to complicated data

processing [73]. Therefore, this technique appears less suitable for quality control during manufacturing process with high water content (granulation) [79].

1.3.3. Near-infrared spectroscopy

Near-infrared (NIR) spectroscopy uses the range of the electromagnetic spectrum between 780 and 2526 nm (12820 – 3959 cm^{-1}) and is a well investigated method for analysis of pharmaceutical formulations [65]. The absorption of radiation in the NIR range mostly leads to overtones or combinations of fundamental vibrations in the molecules [56,65,71]. Hence, NIR spectra are less well resolved compared to MIR showing broad overlapping bands of these vibrations and overtones [71]. Therefore, the NIR spectra are more difficult to interpret and to link spectral information to the physicochemical properties of the sample [56,65,80]. For that reason, the potential of NIR as a powerful spectroscopic tool was entirely recognised only with the implementation of chemometrics [56]. Additionally, the suitability of light-fibre probes for remote sampling accelerated the application of NIR for PAT analysis [56]. One advantage of NIR compared to MIR is the weaker absorptivity of materials in the NIR range resulting in the possibility to measure the samples directly, i.e. undiluted [81]. Furthermore, even samples with high scattering such as turbid solids may be analysed in transmission and reflectance mode without special preparation [65]. Additionally, weaker absorptivity leads to a higher penetration depth of the radiation allowing analysis of thicker samples compared to MIR [65,81]. The investigated samples might be analysed through glass and several plastic materials [72]. Another advantage of NIR is the possibility to obtain physical as well as chemical information on the sample from one measurement [65]. As mentioned above, the NIR absorption provides information on chemical properties and scattering effects [65]. If the physical information is unneeded, scattering effects may disturb the measurement and need special data processing [65]. Nonetheless, despite numerous advantages, NIR is unsuitable in certain cases, because it shows a high water sensitivity and a low absorption cross section, making quantification of low API concentrations difficult

[79]. Nevertheless, NIR spectroscopy is widely used in the pharmaceutical field

because of the described advantages [63–65,72,80].

1.3.4. Raman spectroscopy

Raman spectroscopy is another frequently applied method for analysis of pharmaceutical formulations. The Raman effect is the inelastic scattering of light often in the same range of energies as infrared spectroscopy [63]. During Raman measurement the sample is irradiated with monochromatic laser light [56]. Thereby, the excitation frequency of the laser light can vary between the UV and the NIR region, resulting in a high frequency flexibility for this technique [81]. The molecule is excited by the radiation to a virtual energy level, then the molecule may return back to the ground state by elastic scattering emitting the light of the same energy as the excitation light (Rayleigh scattering) [56,81,82]. However, this scattering provides no information on the molecular vibrations [56]. If the molecule does not return to the ground state, it returns to the first energy level by inelastic scattering emitting light of lower energies compared to the excitation light (Stokes Raman scattering) [56,72,82]. This measurable energy difference can be related to the vibrational energy of the absorption and thus to chemical bond vibrations [56,72,82]. The Raman scattering emitting frequencies may vary from 17 to 4000 cm^{-1}, covering the FIR and MIR range [81]. For this reason, Raman spectra usually look similar to MIR spectra characterised by narrow peaks identifying the investiagted molecule [72]. In fact, the two techniques are complimentary: if a functional group in a molecule has a weak signal in the MIR spectrum it usually presents a strong signal in the Raman spectrum and vice versa [72,82]. As mentioned above, Raman spectra provide sharp bands making their interpretation easier than that of NIR spectra even without chemometrics [83].

Raman measurements are non-invasive and need no or little pretreatment permitting on-line monitoring of the manufacturing process [72,83]. Additionally, because of the high energy of the excitation light, analysis through plastic and glass is feasible

allowing tests directly in the primary packaging [72,83]. Furthermore, remote sampling with fiber optics is also possible with Raman spectroscopy [83]. Another advantage of Raman spectroscopy is the API detection in the presence of water [63,83]. However, as a result of the relatively weak signal, Raman scattering may be overlaid by other spectroscopic phenomena such as fluorescence, complicating API quantification [55,72,83]. An additional disadvantage of Raman spectroscopy is the low signal-to-noise ratio [75]. Therefore, a longer integration time than during NIR mapping is needed resulting in longer measurement times [75]. Finally, because of the high energies of the excitation light a thermal decomposition of the sample may occur [83]. However, Raman spectroscopy is a valuable tool for pharmaceutical quality analysis [64].

1.3.5.   Terahertz spectroscopy (Far-infrared)

Within the past ten years, Terahertz (THz) spectroscopy has attracted the attention of pharmaceutical researchers [84,85]. THz radiation refers to the part of the electromagnetic spectrum between microwaves and the IR region (2-133 cm^{-1}, 0.1 - 4 THz) [85]. Because of the low attenuation of pharmaceutical excipients at THz frequencies it is possible to penetrate deep into pharmaceutical dosage forms, thus enabling a range of unique imaging applications [85–87]. Light absorption at these frequencies leads to dipole moment oscillations at lower frequencies than in the MIR region [81].

Terahertz pulsed imaging (TPI) is a mapping technique that uses short pulses (< 1 ps) of THz radiation [88,89]. The THz pulse beam propagates into the tablet and is reflected if a change of the refractive index occurs. This phenomenon may be observed at the interface between two different types of materials or as a result of a distinct density change within one material [90]. Additionally, during propagation of the THz pulse beam through the material, changes in the absorption coefficient occur [90]. Therefore, pronounced changes in the refractive index and/or absorption coefficient can be analysed as a single event or as a combination of both [90]. Based on these changes a contrast image can be created [90]. Therefore, by application of this technology a wide range of small organic molecules [91] and their different crystal structures [92,93], distribution of the components in a sample [94] as well as degradation products in polymers [95] can be identified.

The main advantage of THz spectroscopy is the high penetration depth of THz radiation [88,89], thus allowing analysis of the 3D structure of pharmaceutical samples. Therefore, THz spectroscopy has gained increasing interest for analysis of solid dosage forms with a complex internal structure [89]. THz is sensitive to polar

liquids and has been shown to be advantageous compared to IR techniques regarding water quantification because of its detection sensitivity, acquisition speed and reduced scattering effects [88]. Nevertheless, the low spatial resolution of TPI between 150 and 250 µm [96] might be a limitation for some applications. Additionally, the depth resolution limit depends on the frequencies of the THz beam and on the refractive indices of the materials and lies approximately between 30 and 50 µm [96]. Nonetheless, the application of THz spectroscopy for in-line monitoring of processes has already been described in the literature, for example for monitoring of the coating process [97].

1.3.6. UV spectroscopy

Ultraviolet (UV) radiation represents a rather small region of the electromagnetic spectrum in the range between 100 - 400 nm [98]. Currently, mainly the wavelengths above 200 nm are used in pharmaceutical control applications. Generally, UV spectra are less informative than MIR spectra making API identification more challenging and may require application of multivariate techniques [79]. Nevertheless, UV spectroscopy holds a great potential, as robust detectors and light sources for the wavelengths below 200 nm should be available soon, allowing analysis of fundamental spectral signatures on bonds (for example C-C) [79]. These signatures are similar to the signatures measured by MIR spectroscopy [79]. However, UV spectroscopy below 200 nm is expected to be affordable at a lower price and will probably be more robust [79]. Furthermore, because of the robustness of this technique, the spectra are reproducible revealing a high potential for in-line control and monitoring [79]. Moreover, UV radiation exhibits a higher absorption cross section allowing the collection of chemical information even at low API concentrations [79,99,100]. Furthermore, many substances show a high UV scattering coefficient providing physical information such as the density distribution on a tablet surface [79,99–101]. An advantage of UV imaging is the potential to achieve a higher spatial resolution resulting from the short wavelength of UV compared to NIR or MIR radiation [77,100]. For example, in the whiskbroom constellation UV imaging might achieve a spatial resolution of 300 nm, on the one hand because of the short wavelength and bright illumination sources and on the other hand because of the high detector sensitivity [77]. Another advantage of UV spectroscopy, especially for imaging purposes, is the high data acquisition speed that can be achieved because of the high absorptivity of most solids in this spectral range as well as the bright illumination sources and sensitive array detectors. So far, UV spectroscopy for

analysis of solids has not been widely described in the pharmaceutical literature. However, UV spectroscopy exhibits potential for in-line process control because of its high robustness, low cost, high sensitivity of the detectors and a high absorption cross section [60,79].

1.4.   Analysis of spectral data sets

1.4.1. *General aspects*

The analysis of spectral data sets varies depending on the measurement constellation. For single point measurements, usually only two data analysis steps are needed. Each spectral data set has to be pre-processed and afterwards analysed by uni- or multivariate analysis. Data sets obtained from spectroscopic mapping or imaging result in three-dimensional data cubes. In a first step, the regions of interest, for example pixels belonging to the tablet, are separated from the background [57]. In a second step, the three-dimensional data cube is unfolded by transferring into a new two-dimensional matrix [57]. In a third step, with this two-dimensional matrix spectral pre-processing is performed [57,102,103]. Uni- or multivariate data analysis represents the forth step [57]. Finally, the analysed two-dimensional matrix is refolded into a three-dimensional data cube allowing spatial visualisation of the results [57]. Thus, spectroscopic mapping or imaging provides spectral and furthermore spatial information on the sample.

1.4.2. Spectral pre-processing

As mentioned above, preliminary spectral pre-processing might be performed before further analysis of the spectral data set. In general, the main goal of pre-processing is to improve data analysis by elimination of the spectral variance that is not based on changes in the desired information, for example concentration changes [104,105]. Therefore, the selection of appropriate pre-processing methods depends on the type of needed information [71,105]. In this context, a carefully chosen pre-processing method can highly improve the performance of the resulting multivariate model. Common pre-processing methods for spectral data are summarized in Table 1.

In this thesis, standard normal variate (SNV) correction and mean centering were applied. SNV is a frequently applied pre-processing method removing the multiplicative interferences of scatter and particle size [104]. Mean centering is one of the most commonly applied pre-processing methods and removes the spectral offset [108]. Thereby, the mean of the spectral values is subtracted from all variables removing the intercepts at each wavelength [107]. The overall interpretation of the spectral data remains unchanged [108], as only the overall spectral features common to all spectra are removed [107]. SNV correction eliminates the spectral variances resulting from multiplicative interferences of light scattering and particle size [104]. The SNV correction removes baseline shifts and variations in the slope of the spectra while the shape of the spectra remains unchanged [105]. Thereby, the mean and standard deviation of each variable in the spectrum are calculated. Subsequently, the mean is subtracted from each spectral value and divided by the standard deviation [102,109].

Table 1: Several data pre-processing methods for multivariate data analysis.

	Pre-processing method	Purpose
Filtering		
	Offset correction	To correct a parallel baseline shift [104]
	De-trending	To remove offset and curvilinearity, which occurs in the case of powdered, densely packed samples [104]
	First derivative	To resolve peak overlap (or enhance resolution) and to remove a constant background [104,106]
	Second derivative	To resolve peak overlap (or enhance resolution) and to remove a linear background [104,106]
Normalisation	Standard normal variate (SNV) correction	To remove the multiplicative interferences of scatter and particle size [104]
	Multiplicative scatter correction (MSC)	To compensate for different scatter and particle sizes [104]
	Normalisation	To remove differences in total spectral intensity [107]
Centering	Mean centering	To remove intercepts at each wavenumber and thus spectral features common to all samples [107]

Filtering pre-processing methods that are frequently applied for different purposes to spectroscopic data sets, especially to NIR data, are shown in Table 1. Beside the SNV correction, other frequently applied normalisation pre-processing methods are also mentioned in Table 1.

In general, pre-processing methods should be applied cautiously avoiding a combination of several methods, because this may lead to a significant change of the raw data [102,104,109].

1.4.3. Multivariate data analysis

The spectral data analysis can be divided into univariate and more complex multivariate analysis. Univariate analysis extracts only one variable, for example peak area, peak height, or ratio of two peak heights from a sample spectrum [110,111]. In contrast to univariate analysis, multivariate analysis is based on many variables, which provide information on the sample [72]. The main advantage of multivariate analysis is that many components within one sample can be analysed simultaneously in absence of characteristic peaks of each component [72,112,113]. A drawback is the complexity of this method, especially for researches, who are new to the subject. Multivariate data analysis is a significant improvement for the applicability of the spectroscopic techniques, particularly imaging, as PAT tools [65,68]. Especially for NIR spectroscopy, multivariate data analysis offers additional application possibilities [56]. Combination of UV spectroscopy with multivariate data analysis may improve the suitability of UV spectroscopy for quality control.

Among other multivariate analysis techniques, principal component analysis (PCA) and partial least squares (PLS) regression have been shown to be suitable for analysis of the complex data sets [114].

1.4.3.1. Principal component analysis

PCA is the most commonly used method for multivariate analysis of scientific data and was introduced by Karl Pearson [115]. In the context of PCA, it is useful to regard a data set as a matrix, the rows are the 'objects', for example samples or pixels at the tablet surface, while the columns are 'variables', for example reflection values at different wavelengths. The PCA algorithm allows to detect similarities and trends in the data without the need for calibration or previous information on the

sample [116]. Thereby, the aim of the PCA application may be to find relationships between the investigated objects, for example in identifying classes of objects [117]. Thus, it is possible to find outliers that do not belong to the classes. Nevertheless, the main goal of the PCA is data reduction and almost every data matrix can be simplified by PCA [117,118]. The mathematical background of the PCA is widely described in the literature [117]. The main principal of data reduction by PCA is schematically visualised in Fig. 7.
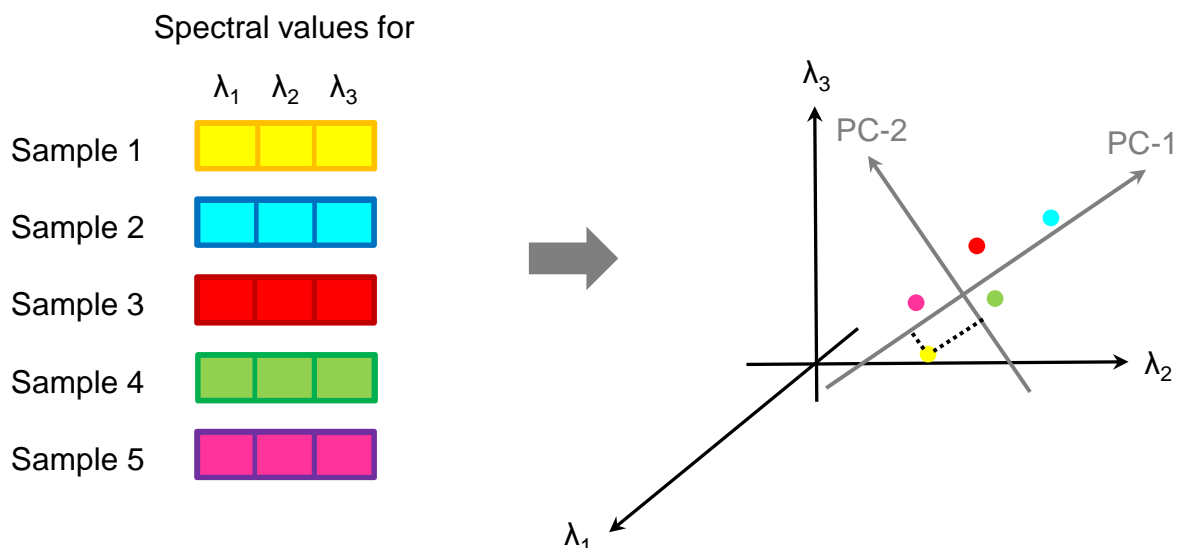
Fig. 7: Schematic visualisation of data reduction by PCA, modified from [72].

In this Fig., the spectral values of five samples (dots) are recorded at three different wavelengths (λ_1, λ_2, λ_3). Each wavelength corresponds to an axis. As three wavelengths were selected, the resulting space is three-dimensional. Each sample (dot) has a defined position in this three-dimensional space based on its spectral values for each wavelength. In this space a new axis, called the first principal component (PC-1) is constructed in a least-square sense to explain as much data

variance as possible [72]. The second axis, called PC-2 is constructed orthogonally to PC-1 and explains the remaining variance, which is not covered by PC-1 [72]. The projections of the data dots onto the new axes are called 'scores' [72]. The weight of each initial variable with regard to the variance within the dataset is represented by the loadings and reveals the degree of covariance between the variables [112,119]. In general, PCA has become a widely used statistical technique for analysis of scientific data sets [72,120].

1.4.3.2. Partial least squares regression

The PLS approach was introduced by the Swedish statistician Herman Wold and his son Svante Wold [121–123]. PLS is a commonly used algorithm for regression of scientific data [55,119,124]. The main goal of PLS is again data reduction. However, in contrast to PCA where the maximum variance is the main criterion for the decomposition step, the main objective of the PLS regression is to predict the Y data set (dependent variable) based on the X data set (independent variable) and to find correlation between X and Y [119,125–128]. Thereby, the matrix containing the X data set, for example the spectra of different samples, is projected into a new space by construction of new axes, in this case called latent variables (LVs) instead of PCs [119]. Thereafter, the matrix containing the Y data set, for example the concentrations of the components in the sample, is projected onto the LVs [72]. The mathematical background of PLS is described extensively in the literature [72,119,121,122,129,130]. Depending on the dimensions of the Y matrix, one may distinguish between PLS1 and PLS2 [130]. PLS1 is calculated based on the Y matrix as vector, for example a data vector with only concentration values for one component, while PLS2 is calculated based on several Y values for each sample, for

example the concentrations of several components [130,131]. PLS applied to hyperspectral imaging shows several advantages compared to classic spectroscopy [72]. The Y values, for example API concentrations or coating thicknesses, can be predicted for each pixel at the sample surface allowing the collection of the spatial information on the distribution of the Y values at the sample surface [72]. In addition, the three-dimensional data cube may contain many data sets allowing a separation of the data between calibration and validation sets. As already mentioned, the application of PLS for prediction of the independent variables from the dependent variables is described in detail in the literature [125].

1.5. Application of spectral techniques for non-destructive analysis of tablets

1.5.1. General aspects

As already mentioned, solid oral dosage forms are commonly produced in batches, which are examined by often time-consuming off-line tests of only randomly chosen samples [55,56]. An advantage of spectroscopic techniques is the option of a total control and additional spatial information on the sample. Moreover, spectroscopic techniques and especially imaging techniques are applicable to non-destructive, non-invasive and fast quality control investigations during the whole manufacturing process and even during storage. Therefore, ongoing research on new spectroscopic techniques with PAT potential is of particular importance. Several fast and non-destructive spectroscopic techniques with in-line potential such as NIR spectroscopy [65,132] and Raman spectroscopy [55,68,83,133] have been widely described in the pharmaceutical literature. Furthermore, NIR and Raman spectroscopy are already established in different manufacturing fields as PAT tools [62–65,134]. MUPS tablets have a heterogeneous inner structure, as they consist of coated API pellets surrounded by powder excipients. Hence, techniques with the option to obtain spatial information on the sample are more suitable to analyse the surface of MUPS tablets or their inner structure, than single point measurements. As described above, the crucial attributes of MUPS tablets during the manufacturing process are the pellet distribution within the tablet, as the MUPS tablets are dividable, the coating thickness of the pellets and/or the whole tablet, as well as the degradation of the API in the coated API pellets within the tablets during storage time. Therefore, fast and non-destructive methods for quality control or monitoring of these attributes are needed.

1.5.2.   Analysis of API quantification and distribution within a tablet[1]

Many studies are dealing with the applicability of NIR spectroscopy to monitor various quality parameters of single unit tablets during the manufacturing process [135–138]. Moreover, particularly NIR spectroscopy has been demonstrated to be a powerful imaging tool for monitoring of API content uniformity and API distribution of single unit tablets [139–143]. In only one publication the applicability of NIR mapping for the distribution analysis of various components in MUPS tablets is described [144]. Application of Raman mapping to analyse the distribution of the ingredients in single unit tablets, mainly in combination with multivariate analysis, has been extensively described in the literature [145–150]. Surprisingly, the application of Raman mapping to analyse the pellet distribution within MUPS tablets has not yet been described in the literature, but is potentially possible. The suitability of THz chemical imaging to analyse the distribution of the ingredients in single unit tablets was investigated by Ajito et al. [94]. The application of TPI for chemical imaging as well as for API quantification has also been published in the literature [92,151]. Compared to NIR and Raman imaging, TPI provides the possibility of mapping in a 3D tablet matrix [90]. Therefore, chemical imaging in depth of lactose and tartaric acid on a model tablet was performed by TPI [152]. However, this model tablet consisted of polyethylene, which is almost translucent for THz radiation, which means that scattering effects on the THz radiation in depth were minimised [90,152]. This method offers a great potential for chemical imaging in depth. Nevertheless further studies are needed to develop a robust method to implement this imaging procedure. Furthermore, many coated tablets show either a strong absorption or scattering of NIR radiation [90], thus complicating the API mapping in coated tablets, whereas TPI propagates through the coating allowing the analysis of the tablet structure below the

---

[1]Parts of this chapter have been published as shown on page 167 in appendix B.

coating. As described above, a main advantage of TPI is the propagation of THz radiation through most pharmaceutical materials, enabling a high penetration depth and thus allowing analysis of the 3D structure of pharmaceutical samples. Therefore, THz technologies have gained increasing interest for pharmaceutical applications to analyse solid dosage forms with complex inner structures [89]. Therefore, this technology exhibits a high potential for the analysis of MUPS tablets.

Multispectral UV imaging with six distinct wavelengths has recently been described, but only few publications deal with the analysis of various tablet properties by UV imaging [100,101,153,154]. Wu et al. successfully tried to distinguish between API and tablet matrix as well as between the crystalline and the amorphous form of an API within tablets by multispectral UV imaging [100]. Klukkert et al. used multispectral UV imaging for identity control and API quantification in single unit tablets [101]. As mentioned before, one of the properties of MUPS tablets is a heterogeneous surface, consisting of coated API pellets surrounded by matrix excipients. The application of single point measurements is therefore meaningless as no spatial information is obtained. Hence, from the described experimental set ups only mapping or imaging can be used as PAT tool for analysis of the MUPS tablet surface with regard to API distribution and API content. Compared to NIR imaging, advantages of UV imaging include the higher absorption cross section [100] providing chemical information of even low API concentrations, and higher scattering at the surface providing morphological information [79]. Generally, multispectral UV imaging allows fast data acquisition because of the reduced number of the applied wavelengths.

1.5.3. Analysis of the coating quality[2]

Tablet disintegration and subsequent drug dissolution kinetics may be controlled by coating of tablet cores with a polymer film. Therefore, the thickness and the uniformity of the applied coating become critical CQAs and have to be controlled.

To monitor the film thickness during the coating process several methods have traditionally been used. One of the simplest approaches is to quantify the loss of mass in the vessel containing the coating dispersion [155]. Another commonly used method is to remove a predetermined amount of tablets from the coating process at pre-set intervals to determine the polymer weight gain compared to the same amount of uncoated tablets. Both methods allow an indirect determination of the coating thickness and are based on a number of assumptions such as an uniform coating distribution on each tablet as well as a complete mass transfer of the polymer to the tablet surfaces. However, it is well known that differences in the decrease of mass of the tablets resulting from friability, loss of polymer due to spray drying as well as residual solvent may affect the tablet mass and hence the polymer weight gain [156]. Other off-line methods to analyse the coating quality include disintegration and dissolution experiments. These off-line methods have the advantage of the direct determination of the CQAs, i.e. the dissolution or disintegration profiles. However, they are destructive and time-consuming and thus unsuitable for real-time analysis.

In contrast to the indirect methods outlined above optical and scanning electron microscopy are well established for the direct measurement of the coating thickness. Although such methods are also destructive in that they require the preparation of a cross-section through a tablet prior to analysis and are therefore used off-line, it is possible to measure the coating thickness at several spots of the tablet surface and

---

[2]Parts of this chapter have been published as shown on page 167 in appendix B.

hence to derive an estimate of coating uniformity [155,157]. However, it is challenging to prepare cross-sections of coated tablets without deformation of the coating, as the polymers typically used for coated tablet formulations readily undergo plastic deformation if shear stress is applied [156].

To better understand the coating process the application of fast and non-destructive sensing techniques with in-line potential is attractive. NIR spectroscopy and Raman spectroscopy are examples for such techniques. They are indirect in that they estimate the coating thickness based on a chemometric model that quantifies changes in the chemical composition (vibrational spectral signatures that are specific to the coating formulation and/or the tablet core formulation). Examples of NIR [158–161] and Raman spectroscopy [162,163] as PAT in-line methods to determine the mean coating thickness of tablets or pellets during the coating process are well documented. Furthermore, analysis of the coating thickness distribution on the tablet surface with NIR chemical imaging is also described in the literature [143]. Cairós et al. presented an approach to analyse the surface of coated tablets with NIR spectroscopy in combination with multivariate data analysis, especially with PCA, without previous knowledge of the sample properties [164].

As already described, imaging methods allow the measurement of the spatial variability in the coating thickness [155]. Apart from the established NIR and Raman imaging methods, TPI can also be used for coating characterisation. TPI as a mapping technique uses short pulses of THz radiation to determine the coating thickness of coated tablets [88,89]. It is a direct thickness measurement, as the thickness is determined without further calibration based on the time delay between the reflection of the THz pulse that originates from the surface of the coated tablet and the subsequent reflection from the interface between the coating and the tablet

core. With this technique it is possible to measure the distribution of the coating thickness across the surface of a tablet [88]. Therefore, the main applications of TPI in the pharmaceutical field are the determination of the coating thickness [96] and the analysis of its uniformity [90] as well as the in-line monitoring of a coating process [97].

A further imaging technique to analyse the quality of tablet coatings is UV imaging. In a recent study, it was shown that multispectral UV imaging with six distinct wavelengths is a valuable technique to analyse coating defects on coloured coated tablets [154]. As already mentioned, an advantage of this imaging method is its high data acquisition speed that can be achieved because of the high absorptivity of most tablet formulations in the UV spectral range together with the availability of bright illumination sources and sensitive array detectors [77]. However, the potential of UV imaging to determine the coating thickness and its distribution on the tablet surface remains unclear.

1.5.4.   Monitoring of API degradation[3]

In contrast to a single unit tablet, the API in MUPS tablets is present in the form of small coated pellets [10]. The applied coating on the pellets may protect the API from humidity, light, or chemical interactions with other formulation components [66,67]. Therefore, methods to monitor the API stability within coated drug pellets are currently attracting interest.

Depending on the approval country, stability tests should be carried out at different storage condition zones in the world [165]. Accordingly, the World Health Organization suggests four main climatic zones [166,167]. The guideline of the International Council for Harmonisation "Stability testing of new drug substances and products Q1A(R2)" recommends storage conditions for stability studies in the climatic zones I and II [168]. Thus, several stability studies might be required for one pharmaceutical product depending on the climatic zone of the approval country. Analysis of the degradation products during these stability studies is usually performed by well-established analytical methods such as HPLC or mass spectrometry. However, these analytical methods are time-consuming, destructive and costly [169,170]. In addition, the drug concentration cannot be determined for each sample (tablet), and information on an individual sample can only be obtained at one sampling time point. Furthermore, these techniques deliver only an average concentration of the degradation product in the investigated sample. Therefore, no information on the distribution of the degradation product at the sample surface is obtained. Thus, the application of spectroscopic techniques to monitor the stability of all samples during a stability study is possible at any time point. Surprisingly, only few publications deal with the application of spectroscopic techniques to determine API degradation in stability studies. In the context of the model API used in this thesis for

---

[3]Parts of this chapter have been published as shown on page 167 in appendix B.

the stability study, acetylsalicylic acid (ASA), Drennen et al. (1990) used NIR
spectroscopy to determine the amount of salicylic acid (SA) as degradation product
of ASA and the amount of absorbed water during a stability study of ASA tablets
[171]. The amount of SA as degradation product of ASA could also be predicted by
NIR spectroscopy in combination with PCA through the blister packaging [172]. Wang
et al. applied Raman spectroscopy to monitor the shelf-life of ASA tablets [173].

1.6.   Objective of this work

MUPS tablets are solid oral dosage forms of particular pharmaceutical interest, as they combine advantages of coated single unit tablets with pellet containing capsules. In the context of PAT, MUPS tablets represent an additional challenge for quality control compared to single unit tablets because of the uneven distribution of the API within the MUPS tablets resulting from the presence of API clusters (pellets) as compared to conventional tablets. In addition, in MUPS tablets the pellets are coated with a polymer coating, which might further complicate especially the surface analysis. Therefore, spectroscopic mapping or imaging techniques are of increasing interest for quality control of MUPS tablets. UV imaging for analysis of pharmaceutical solid samples such as tablets is only scarcely described in the literature. Nevertheless, this technique offers several advantages compared to other more common spectroscopic mapping or imaging techniques and is thus of increasing interest for quality control. In this context, the aim of this thesis was to investigate the suitability of multispectral UV imaging with six distinct wavelengths for the quality control of specific attributes of MUPS tablets. Compared to single unit tablets, MUPS tablets are dividable and thus a homogeneous distribution of the pellets within the tablet has to be ensured. Therefore, the suitability of UV imaging to differentiate between the coated API pellets and the tablet excipients as well as to determine the pellet amount and pellet distribution at the tablet surface was investigated. Furthermore, the influence of the tablet thickness on the tablet surface analysis by UV imaging with regard to the pellet amount and pellet distribution was investigated.

The coating thickness has a significant influence on the drug release from a MUPS tablet. Therefore, the applicability of multispectral UV imaging for determination of the coating layer thickness of coated tablets as well as for analysis of the spatial

distribution of the coating layer thickness at the tablet surface was investigated. In this proof-of-concept study single unit tablets were used as a model dosage form to minimize the influence of different surfaces areas and sizes. Different model formulations were selected as examples for the commonly used coated single unit tablet formulations. A further aim of this thesis was to investigate the applicability of UV imaging to monitor the degradation of an API in MUPS tablets during storage, as the API stability is crucial.

In comparison to UV imaging, which is a surface analysis method, TPI offers the possibility of a tablet 3D mapping. This fast and non-destructive method has gained increasing interest in the analysis of samples with a complex internal structure. In this regard, the applicability of TPI for analysis of the inner structure of MUPS tablets below the tablet surface was also investigated.

2. Materials and Methods

2.1.   Materials

2.1.1.   Active Pharmaceutical Ingredients

Acetylsalicylic acid (ASA) and salicylic acid (SA) were purchased from Caelo (Hilden, Germany). Theophylline pellets obtained by extrusion and spheronization containing 94% theophylline (Theo), 5% povidone and 1% colloidal silicon dioxide, were supplied by Temmler (Killorglin, Ireland). Pure Theo (for HPLC calibration) was obtained by Caelo (Hilden, Germany).

2.1.2. Tableting excipients

Microcrystalline cellulose pellets (Cellets® 700) and Hydroxypropyl methyl cellulose (HPMC; Pharmacoat® 603) were obtained from Harke Pharma (Mülheim an der Ruhr, Germany). Eudragit® NE 30 D and Eudragit® RL PO were donated by Evonik (Essen, Germany). The ethyl cellulose dispersion (Aquacoat® ECD) was a donation from FMC BioPolymer (Philadelphia, USA). Microcrystalline cellulose (MCC, Ceolus® KG-802) was supplied by Asahi Kasei Chemicals (Tokyo, Japan), and crospovidone (Kollidon® CL-F) as well as povidone K 30 (Kollidon® 30) were supplied by BASF (Ludwigshafen, Germany). Triethyl citrate was obtained from Fluka (Buchs, Switzerland), talc from Fagron (Barsbuettel, Germany) and magnesium stearate (MG-ST) from Baerlocher (Unterschleissheim, Germany). Polysorbate 80 was purchased from Caelo (Hilden, Germany).

2.1.3. Chemical reagents

Acetone and isopropanol were obtained by Biesterfeld Spezialchemie (Hamburg, Germany), and acetonitrile by VWR (Darmstadt, Germany). Hydrochloric acid, phosphoric acid and trifluoroacetic acid were purchased from Carl Roth (Karlsruhe, Germany). Deionized water was prepared with a Millipore purification system (Merck Millipore, Schwalbach, Germany).

2.2. Methods of 'Multispectral UV imaging for surface analysis of MUPS tablets with special focus on the pellet distribution'[4]

2.2.1. Preparation of aqueous coating dispersions

To prepare the Eudragit® NE 30 D coating dispersion, HPMC as gelling agent was dispersed in purified water at 40 °C using an Ultra Turrax® (IKA, Staufen, Germany). After a transparent solution was formed, polysorbate 80 as a plasticiser and talc as anti-tacking agent were added and dispersed for at least ten min and subsequently slowly poured into Eudragit® NE 30 D under continuous stirring for at least five min. The resulting dispersion contained 22.7% Eudragit® NE 30 D, 6.8% talc, 0.7% polysorbate 80, and 0.7% HPMC (w/w).

For preparation of the ethyl cellulose coating dispersion, triethyl citrate as plasticiser was slowly added to Aquacoat® ECD while stirring. An HPMC solution, prepared by dispersion of HPMC as pore former in purified water at 40 °C using an Ultra Turrax®, was slowly poured into this dispersion. The resulting coating dispersion contained 77.1% Aquacoat® ECD, 5.0% triethyl citrate, and 2.1% HPMC (w/w).

---

[4]This chapter has been published as shown on page 167 in appendix B.

2.2.2. Coating of theophylline pellets

Theo pellets (mesh 900 – 1000 µm) were coated in a bottom spray fluidized bed apparatus (Solidlab 1, Bosch Packaging Technology, Schopfheim, Germany). The nozzle diameter was 0.8 mm. For the Eudragit® NE dispersion, coating parameters are shown in Table 2. The coated pellets were subsequently dried in an oven at 40 °C for 48 h. For the ethyl cellulose dispersion, coating parameters are also shown in Table 2. The coated pellets were post-dried in an oven at 60 °C for 24 h. Polymer coating levels of 5%, 12% and 19%, respectively, were applied onto the Theo pellets. The coating levels were defined as weight gain referring to the coating polymer mass.

Table 2: Process parameters used for fluid bed coating of theophylline pellets.

Process parameter	Eudragit® NE dispersion	Ethyl cellulose dispersion
Inlet air flow rate	$35 \ m^3 \ h^{-1}$	$31 \ m^3 \ h^{-1}$
Inlet air temperature	16 °C	55 °C
Atomizing air pressure	1.5 bar	1.5 bar
Microclimate	0.4 bar	0.4 bar
Spraying rate	$1.5 – 3.0 \ g \ min^{-1}$	$2.0 – 4.0 \ g \ min^{-1}$
Nozzle diameter	0.8 mm	0.8 mm

2.2.3. Preparation of MUPS tablets

For the differentiation of the API pellets from the excipients by UV imaging, six different formulations to be compacted to MUPS tablets were prepared. These formulations consisted of 70% coated pellets, 23% MCC as cushioning excipient, 6% crospovidone as disintegrant, and 1% MG-ST as lubricant (w/w). Three of these formulations were prepared with pellets coated with the Eudragit® NE dispersion, at different coating levels of 5%, 12%, and 19%, respectively. The other three formulations were prepared with pellets coated with the ethyl cellulose dispersion at coating levels of 5%, 12%, and 19%, respectively. 300 mg of each formulation were manually filled into the die and compacted at 282 MPa using the single punch mode of an instrumented rotary press (Fette 102i, Fette Compacting, Schwarzenbek, Germany), equipped with 10 mm flat-faced punches.

For analysis of the pellet distribution in the MUPS tablets another six different formulations were prepared and 250 mg of each formulation were compacted at 255 MPa in the single punch mode leading to tablets with an average thickness of 2.4 mm. The compression force was purposely decreased, because the tablets had to be dividable, which requires adequate tensile strength. The tensile strength was determined with a tablet hardness tester (Erweka TBH425, Heusenstamm, Germany). The tensile strength of the produced tablets was above 3 MPa to ensure tablets of significant hardness comparable to industrially produced tablets. Three of these formulations contained Theo pellets coated with the Eudragit® NE dispersion (coating level 5%) at pellet contents of 30%, 50%, and 70% (w/w). The other three formulations contained Theo pellets coated with the ethyl cellulose dispersion (coating level 5%) at the same pellet contents as above. The content of MCC in the six formulations correspondingly varied between 63%, 43% and 23% (w/w) depending on the coated pellet content. The content of the other excipients was kept

constant in all formulations. The formulations were intentionally not optimised with regard to the prevention of segregation. Hence, the obtained tablets showed a highly variable pellet content. The API content and thus the actual number of pellets in the tablets was determined by HPLC (Section 2.2.6).

To examine the influence of the tablet thickness on the predictive power of the surface analysis in terms of pellet content and distribution, the formulation containing 50% (w/w) of pellets coated with the ethyl cellulose dispersion was used to prepare tablets with three additional tablet thicknesses. For preparation of these tablets, 112 mg, 185 mg, and 350 mg of the selected formulation, respectively, were manually filled into the die and compressed at 255 MPa to obtain tablets with thicknesses of 1.1 mm, 1.8 mm, and 3.3 mm.

For the spectral calibration set, plain flat faced tablets of uncoated Theo pellets (n = 10), MCC (n = 10), and crospovidone (n = 10), respectively, with a diameter of 10 mm each were prepared. For the first part of the study tablets were obtained by manually filling 300 mg of each compound into the die of the tablet machine and compression at 282 MPa. For the second and third part of the study 250 mg of each substance were filled manually into the die and compressed at 255 MPa.

All tableting experiments were performed under controlled conditions (21 °C / 45% RH).

2.2.4. Tablet surface imaging

2.2.4.1. UV imaging

All tablets were imaged (bottom and top side) with an UV spectral imager (VideometerLabUV, Videometer, Hørsholm, Denmark) equipped with a CCD camera capturing diffused reflectance light at six wavelengths (254, 280, 300, 313, 334 and 365 nm) using Mercury-Xenon as UV light source. The instrument covers a field of view of 7.4 cm x 9.9 cm (960 pixels x 1280 pixels); this allows to image up to 20 tablets simultaneously. The pixel size is 77 μm. The recording time of a multispectral image depends on the strobe time, which in this case was 20 s. To operate the instrument, the VideometerLab software (ver. 2.1, Videometer, Hørsholm, Denmark) was used. The working principal of the UV imager (Fig. 8) has previously been described in the literature [100,154]. Briefly, high intensity UV light is transmitted through band pass filters until it reaches an integrating sphere with an inner highly reflective diffuse coating, where it gets diffused by many internal reflections resulting in a homogeneous illumination of the sample surface.

2.2.4.2. Scanning electron microscopy (SEM)

SEM was used to study the morphology of the surface of the MUPS tablets. SEM pictures were taken with a Leo 1525 scanning electron microscope (Zeiss, Jena, Germany) with a working voltage of 5.00 kV.
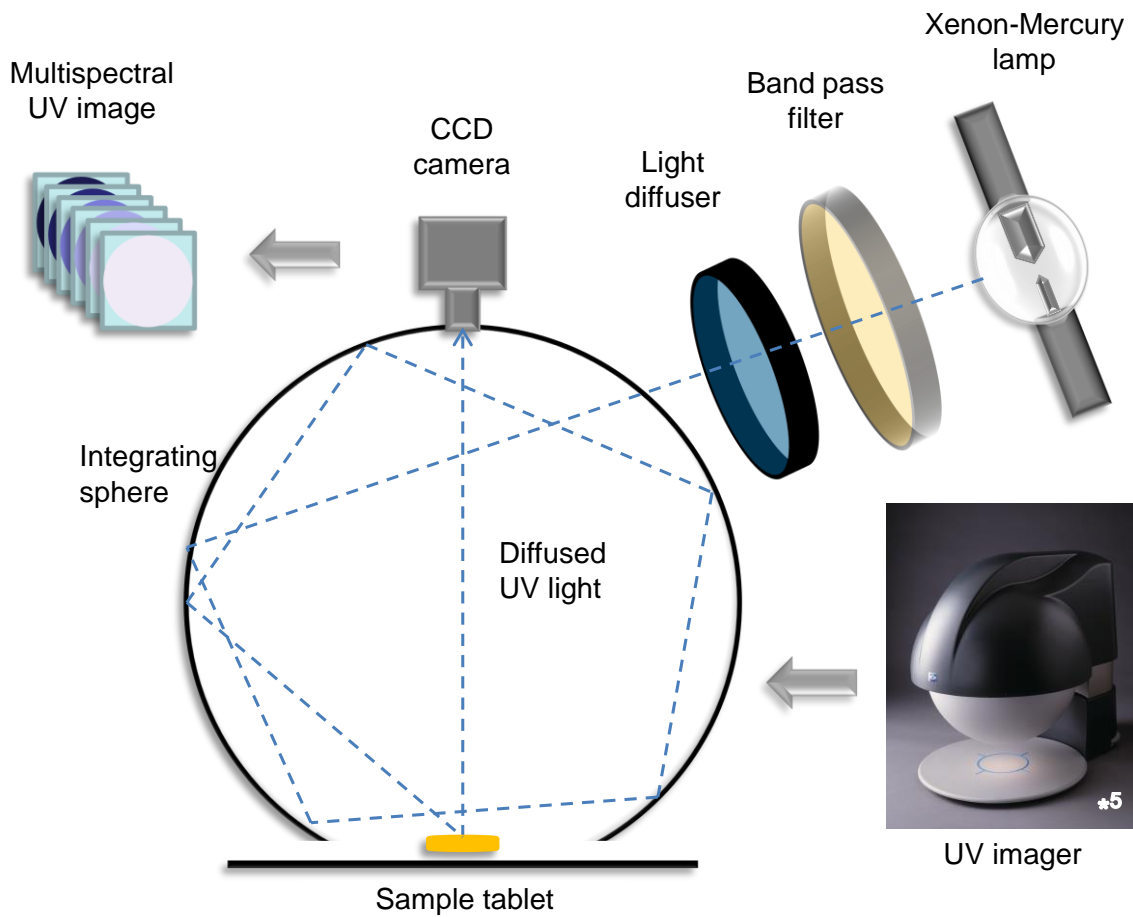
Fig. 8: Working principle of the UV imager; modified from [154].

2.2.5. Multivariate image analysis for pellet detection and quantification

Analysis of the images was performed with an in-house written Matlab® (ver. R2013a, Mathworks, Natick, USA) script. The software was combined with the PLS_Toolbox (ver. 7.3, Eigenvector Research, Wenatchee, USA) for multivariate data analysis and the Image Processing Toolbox (ver. 8.0, Mathworks, Natick, USA). Spectral differences in UV imaging as a result of different tablet densities caused by slightly different thicknesses and tensile strengths were minimised by SNV correction [102,116].

For the purpose of tablet surface analysis a four step pellet quantification procedure was performed. In the first step (Fig. 9), PCA was applied to the images to separate the pixels belonging to a tablet from the background by setting a hard threshold in the PC-1 scores [116]. Subsequently, the centre and radius of the whole tablet were determined using a circle-detecting Matlab® algorithm based on the Circle Hough Transformation [174].

In the second step, based on the spectral calibration set a PLS regression approach was used to visualise the differences between the coated API pellets and the excipients within a MUPS tablet [119]. For the calculation of the PLS model the standard SIMPLS algorithm of the PLS_Toolbox software was applied [129]. The calibration of the PLS model was performed with ten plain Theo, MCC, and crospovidone tablets, respectively. Based on the results of a preliminary cross validation (random subsets, 10 splits, 6 iterations) and an evaluation of the root mean square error of calibration (RMSEC) as well as of the root mean square error of cross validation (RMSECV) values as a function of LVs [102,175], a calibration model with two LVs was calculated resulting in an RMSEC of 1.35% and an RMSECV of 1.52%. This model was used to predict the Theo content of each pixel of the UV image of a

tablet based on its UV spectrum. Subsequently, a binary image was created after defining a second threshold, based on the PLS predicted values (Fig. 9). Thereafter, the centres of the pellets were detected by the circle-detecting Matlab[®] algorithm and used to determine the number of pellets.

| UV imaging | PCA for background segmentation | Binary image based on PLS prediction for Theo content | Detection of the pellets | Division of the surface into sectors |

| Adjacent sectors form a half | Moving theoretical division line | Inhomogeneous pellet distribution | Tablet division; HPLC analysis |
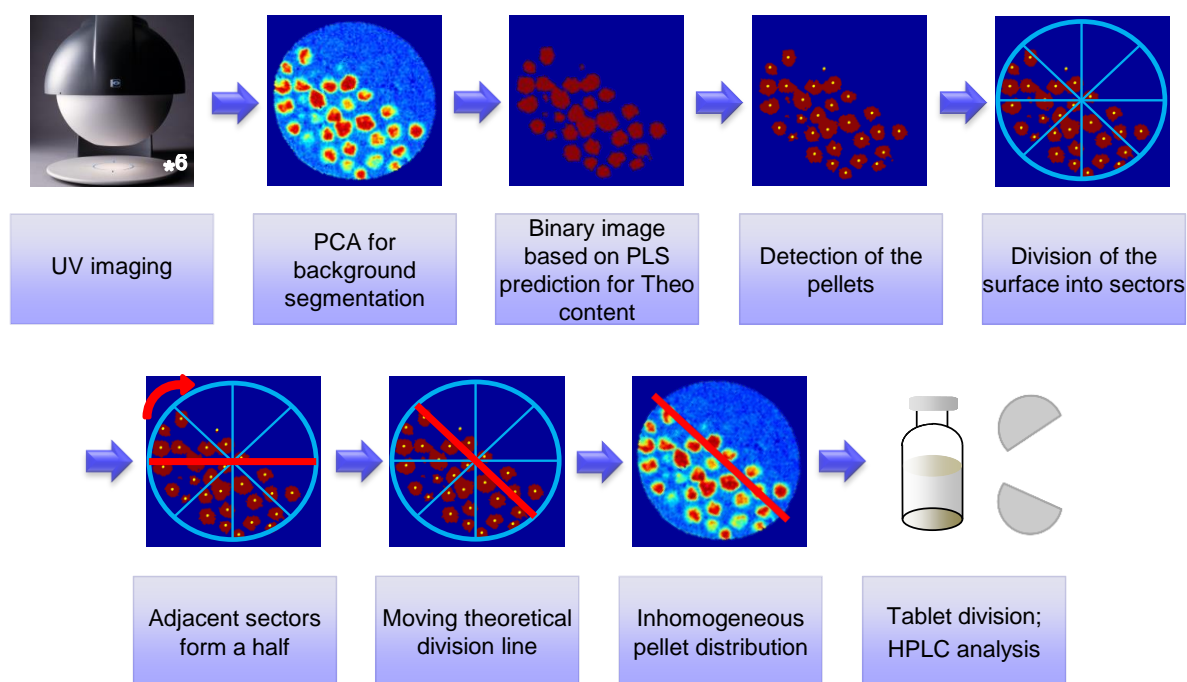
Fig. 9: Pathway for analysis of pellet detection and quantification.

In the third step, the images of the surfaces (top and bottom) of the tablet were divided into 60 sectors each (Fig. 9) resulting in 30 adjacent sectors per half. The two tablet halves were separated from each other by a theoretical division line. A sector-wise movement of the theoretical division line resulted in different theoretical possibilities of tablet division. For all these theoretical possibilities, the ratio of the numbers of pellets for the two halves was calculated. A ratio of unity indicates a

---

[6]Printed with permission of Videometer A/S

homogeneous distribution of the pellets throughout the tablet surfaces and a ratio close to zero indicates a high degree of inhomogeneity regarding the distribution of the pellets. Therefore, the lowest resulting ratio representing the highest pellet inhomogeneity was selected for practical division of the tablet performed with gavel and chisel.

In the fourth step, the centres of the pellets were determined and quantified for the whole tablet and for each selected half of the tablet. The centres of the pellets were counted instead of the numbers of pellets to prevent double counting of the pellets located at the border of the sectors. The results were compared with HPLC analysis of the Theo amount of the tablet halves. For a better comparison of both results, the number of the pellets detected on the surfaces was converted into the Theo amount, by multiplying the number of the pellets by the average Theo amount of one coated pellet. The average Theo amount in a coated pellet was determined by HPLC analysis of exactly 200 coated pellets (n = 3 for each coating). The average Theo amount of a pellet coated with the Eudragit$^®$ NE dispersion was 0.7 mg and 0.73 mg for a pellet coated with the ethyl cellulose dispersion.

2.2.6.   *High performance liquid chromatography (HPLC)*

The Theo content of each selected tablet half was determined by HPLC. For this purpose, each tablet half was dissolved in 100 ml of purified water and then boiled as described in the USP monograph "Theophylline Extended-Release Capsules" [176], in order to crack the coating and release the drug. Subsequently, the solution was continuously stirred for at least 18 h to guarantee complete drug release from the coated pellets. The volume of this solution was added up to 250 ml with purified water. In a next step, 10 ml of this solution were filtered through a 0.2 µm membrane cellulose acetate filter (VWR International, Hannover, Germany). The API content was determined by HPLC (Merck Hitachi D-7000, Tokyo, Japan) using a mixture (85 / 15%, v/v) of solution A (water / acetonitrile / trifluoroacetic acid (94.9% / 5.0% / 0.1%, v/v); pH 2) and solution B (acetonitrile / water (60% / 40%, v/v)); adjusted to pH 2 with phosphoric acid 85%, w/w) as mobile phase and a Prodigy™ RP-18 column (Phenomenex, Aschaffenburg, Germany; column size 250 x 4.6 mm, particle size 5 µm, pore size 100 Å). The flow rate was adjusted to 1.6 ml / min and the sample volume injected was 20 µl. UV detection of Theo was performed at 204 nm [177], because of the high absorption coefficient of Theo at that wavelength and the high radiant flux of the deuterium lamp both resulting in a high detection sensitivity. It was made sure that the excipients did not interfere with the UV spectrum of Theo (data not shown). The absorbance was linear in a concentration range between 1.7 and 50.0 mg / l ($R^2 = 0.999$). For calibration, Theo was dissolved in purified water. The run time of each sample was 5 min.

2.3. Methods of 'Multispectral UV imaging for determination of the tablet coating thickness'[7]

2.3.1. Tableting

The compositions of all investigated tablet formulations are listed in Table 3.

Table 3: Formulations of coated tablets.

Formulation	Composition of the tablets	Composition of the coating dispersions
Theo-NE	Theophylline pellets	22.7% (w/w) Eudragit® NE 30D
		6.8% (w/w) talc
		0.7% (w/w) polysorbate 80
		0.7% (w/w) HPMC
		69.1% (w/w) water
Theo-EC	Theophylline pellets	27.0% (w/w) Aquacoat® ECD
		24.0% (w/w) triethyl citrate
		10.0% (w/w) HPMC
		39.0% (w/w) water
Placebo-EC	95.5% (w/w) MCC	27.0% (w/w) Aquacoat® ECD
	2.0% (w/w) croscarmellose sodium	24.0% (w/w) triethyl citrate
	2.0% (w/w) lactose monohydrate	10.0% (w/w) Kollicoat® IR
	0.5% (w/w) magnesium stearate	39.0% (w/w) water
Theo-IR	Theophylline pellets	20.0% (w/w) Kollicoat® IR Sunset Yellow
		80.0% (w/w) water

---

[7]This chapter has been published as shown on page 167 in appendix B.

Placebo-EC tablets were compressed with a rotary tablet press (Fette 102i, Fette Compacting, Schwarzenbek, Germany) in fully automatic mode with 8 mm faceted flat-faced punches at 200 MPa. For compression of the placebo tablets a three-chamber Fill-O-Matic (Fette Compacting, Schwarzenbek, Germany) was used. The weight of the tablets was adjusted to approximately 160 mg to obtain tablets with a tablet thickness of 2.5 mm.

Tableting of plain Theo tablets was performed with the same rotary tablet press, again in fully automatic mode with 8 mm faceted flat-faced punches but at 320 MPa. In contrast to the placebo tablets, an automatically rotating filling wheel for multi-layer tablets (Fette 102i, Fette Compacting, Schwarzenbek, Germany) was used for compaction of the Theo tablets because of the high tackiness of Theo in the three-chamber Fill-O-Matic. Again, the weight of the tablets was adjusted to about 160 mg to obtain tablets with a tablet thickness of 2.5 mm.

The tablet weight and thickness were controlled at different time points using a tablet hardness tester (Erweka TBH425, Heusenstamm, Germany) for three randomly chosen tablets during compaction.

2.3.2. Preparation of coating dispersions

To prepare the ethyl cellulose coating dispersion the plasticiser triethyl citrate was slowly added to the Aquacoat® ECD while stirring with a propeller stirrer (Eurostar 100 digital, IKA, Staufen, Germany). As pore formers either HPMC (for Theo-EC) or Kollicoat® IR (for Placebo-EC) were homogenised in purified water with an Ultra Turrax® (IKA, Staufen, Germany). After a transparent solution was obtained it was slowly poured into the ethyl cellulose dispersion while stirring.

For the preparation of the Eudragit® NE coating dispersion HPMC (as a stabiliser) was homogenized in purified water with an Ultra Turrax® homogeniser. After a transparent solution was obtained polysorbate 80 (as plasticiser) and talc (as anti-tacking agent) were added and homogenised for at least 10 min. The resulting suspension was slowly poured into the Eudragit® NE 30D dispersion under continuous stirring for at least 5 min.

To prepare the Kollicoat® IR coating dispersion, Kollicoat® IR Sunset Yellow powder was homogenised in purified water. For this experiment Kollicoat® IR Sunset Yellow was chosen because the four absorption bands with maxima at wavelengths 237, 316, 400, and 483 nm of the pigment for sunset yellow [178] are in the UV range or close to the UV range of the imaging device. The compositions of the coating dispersions are shown in Table 3.

2.3.3. Film coating of the tablets

For each formulation 600 g of the different tablet cores were coated in a drum coater (Solidlab 1, Bosch, Schopfheim, Germany) with the respective coating dispersion. The coating process parameters for the investigated formulations are shown in Table 4. Throughout the coating process five samples were removed from the drum coater at predetermined time points to obtain tablets that cover the full range of coating thickness.

Table 4: Process parameters used for tablet coating in a drum coater.

Process parameters	Theo-NE	Theo-EC	Placebo-EC	Theo-IR
Inlet air temperature	15 °C	70 °C	70 °C	65 °C
Air flow rate	60 m^3 h^{-1}	60 m^3 h^{-1}	60 m^3 h^{-1}	60 m^3 h^{-1}
Atomizing air pressure	0.55 bar	0.50 bar	0.50 bar	0.50 bar
Microclimate	0.50 bar	0.50 bar	0.50 bar	0.50 bar
Drum rotation speed	26 rpm	24 rpm	24 rpm	24 rpm
Fluid spray rate	1.5 g min^{-1}	2.9 g min^{-1}	2.9 g min^{-1}	3.0 g min^{-1}
Nozzle diameter	0.8 mm	0.8 mm	0.8 mm	0.8 mm
Total number of sampling time points	50	34	38	36
Curing in an oven	48 h at 40 °C	24 h at 60 °C	24 h at 60 °C	24 h at 60 °C

2.3.4. Film coating analysis

2.3.4.1. Determination of tablet weight gain

Prior to the coating process several tablets were marked on one side of the tablet with a felt pen and weighed on an analytical scale (Mettler AT400, Greifensee, Switzerland). Once a coated tablet was removed from the pan and cured in the oven each sample was weighed again to determine the individual tablet weight gain.

2.3.4.2. Multispectral imaging

Multispectral images of the unmarked surface of each tablet were acquired using an UV imaging instrument equipped with a Mercury – Xenon lamp as the UV light source and a CCD camera to capture the diffusely reflected light (VideometerLabUV, Videometer, Hørsholm, Denmark). Twenty tablets were imaged simultaneously at six different wavelengths (254, 280, 300, 313, 334 and 365 nm). Each multispectral image had a size of 960 pixels ✕ 1280 pixels (7.4 cm x 9.9 cm field of view), with a pixel size of 77 µm. Image recording time was up to 30 s.

Multispectral images of the tablets (Theo-IR formulation) in the wavelength range between 385 nm and 1050 nm were acquired using a VideometerLab instrument (Videometer, Hørsholm, Denmark). The functional principal of this device is similar to the VideometerLabUV and has been described in detail by Rosas et al. [179]. The imager illuminates the samples by light emitting diodes at 20 wavelengths with the spatial resolution of 72.5 µm using this setup. Each image with a size of 1200 pixels ✕ 1200 pixels (covering a field of view of 8.7 cm ✕ 8.7 cm) was recorded in up to 10 s. For control of both instruments, the VideometerLab software (ver. 2.1, Videometer, Hørsholm, Denmark) was used.

Multivariate data analysis and related statistics were performed using an in-house written Matlab® (ver. R2013a, Mathworks, Natick, USA) script combined with the PLS_Toolbox (ver. 7.3, Eigenvector Research, Wenatchee, USA) and the Image Processing Toolbox (ver. 8.0, Mathworks, Natick, USA). To extract the reflectance from the acquired images, the reflectance was calculated from the reflected light intensity by an image calibration with two calibrated reflectance reference targets. The calibration targets are either bright with reflectance values of 99% or dark with reflectance values around 30%. To separate the tablets from the background, PCA was applied to the reflectance images followed by setting a hard threshold in the PC-1 scores [116]. Given the low contrast between the background and tablets with a coloured coating a circle-detecting algorithm based on the Circle Hough Transformation [174] was additionally applied to the binary image obtained by PCA for this type of tablets. All pixels within the circles were assigned to the tablets. Circular erosion based on a circular morphological structuring element with appropriate number of pixels in the radius was applied to all tablets to remove the edges of the tablets to avoid artefacts [180].

2.3.4.3. Terahertz pulsed imaging

The unmarked surfaces of the sample tablets were analysed using a TPI mapping system (TPI imaga 2000, TeraView Ltd., Cambridge, UK). Selected tablets from different sampling time points were measured in full scan mode: Theo-NE (n = 35), Theo-EC (n = 40) and Placebo-EC (n = 40). The unmarked side of each tablet was scanned with a spatial resolution of 200 µm and a time-domain range of a penetration depth of 1 mm in air. The data acquisition time was 15 min per tablet. Coating thickness analysis was performed with the TPIView software (ver. 3.0.3,

TeraView Ltd., Cambridge, UK). All subsequent imaging and statistical data analysis was performed with Matlab$^{®}$.

2.3.5. Data analysis

2.3.5.1. Analysis of the tablet weight gain with UV imaging

In order to predict the individual tablet weight gain based on the applied UV imaging method the mean reflectance spectra obtained from the UV images were correlated with the measured tablet weight gains of the respective tablets. Therefore, tablet weight gain and UV imaging data obtained from the tablets were randomly assigned to either a calibration or a test data set. PLS regression was applied to the test set using the standard SIMPLS algorithm of the PLS_Toolbox software [129]. The optimum number of LVs for the PLS models was chosen based on cross validation (random subsets, 2 splits, 6 iterations) that was applied to the respective calibration dataset. Therefore, the values of the RMSEC as well as the RMSECV were evaluated as a function of the number of LVs. The number of LVs, which showed the local minimum of the RMSECV, was chosen as optimum for the respective PLS model [102,175]. The PLS model was applied to predict the individual tablet weight gain of the tablets belonging to the test data set.

2.3.5.2. Analysis of the coating thickness and its distribution on the tablet surface

To predict the coating thickness as well as its distribution on the tablet surface the UV mean reflectance spectra were correlated with the coating thickness maps measured by TPI using a PLS approach. The optimum number of LVs for the PLS models was determined based on the results of cross validation (random subsets, 2 splits, 6 iterations) as described above (section 2.3.5.1), and the model was then applied to predict the coating thickness distribution on the tablet surface.

2.4. Methods of 'UV imaging of MUPS tablets: A stability study'[8]

2.4.1. Sample preparation

For the preparation of the ASA layered pellets, an ethanolic solution containing 10% (w/w) of ASA and 2.5% (w/w) of povidone was sprayed onto MCC pellets in a fluidized bed apparatus (Solidlab 1, Bosch Packaging Technology, Schopfheim, Germany). To prepare the SA layered pellets, again an ethanolic solution consisting of 10% (w/w) of SA and 2.5% (w/w) of povidone was applied onto the MCC pellets in the same apparatus. The drug layering process parameters for both ASA and SA layered pellets are shown in Table 5.

Table 5: Parameters of drug layering and coating processes.

Process / Process parameters	ASA layering of MCC pellets	SA layering of MCC pellets	Coating of ASA layered pellets	Coating of SA layered pellets
Inlet air temperature	30 °C	25 °C	35 °C	35 °C
Air flow rate	35 m^3 h^{-1}	35 m^3 h^{-1}	41 m^3 h^{-1}	41 m^3 h^{-1}
Atomizing air pressure	1.4 bar	1.4 bar	1.0 bar	1.0 bar
Microclimate	0.40 bar	0.35 bar	0.35 bar	0.32 bar
Fluid spray rate	3 - 4 g min^{-1}	3 - 4 g min^{-1}	5.0 g min^{-1}	2.5 g min^{-1}
Nozzle diameter	0.8 mm	0.8 mm	0.8 mm	0.8 mm
Post-drying in oven	24 h at 40 °C	24 h at 40 °C	24 h at 40 °C	24 h at 40 °C

---

[8]This chapter has been published as shown on page 167 in appendix B.

The obtained API layered pellets were each coated in the same apparatus with an organic Eudragit® RL PO solution. This solution was prepared by dissolving Eudragit® RL PO in a part of a solvent mixture of acetone and isopropanol (1:1) under continuous stirring. Talc and triethyl citrate were homogenised in the remaining part of the solvent mixture with an Ultra Turrax® (IKA, Staufen, Germany). The resulting suspension was slowly poured into the Eudragit® RL solution and continuously stirred for at least 10 min. The resulting coating dispersion contained 8.0% (w/w) Eudragit® RL PO, 4.0% (w/w) talc, and 0.8% (w/w) triethyl citrate. The coating parameters for both types of API layered pellets are shown in Table 5.

Tablets were compressed using an instrumented rotary tablet press (Fette 102i, Fette Compacting, Schwarzenbek, Germany) equipped with 10 mm flat-faced punches and operated in single-punch mode. To obtain plain ASA and SA tablets, 250 mg of the respective drug powder were manually filled into the die and compressed at 255 MPa. To compare the spectral information of the coated drug layered pellets, tablets consisting of only the coated ASA or SA layered pellets without tableting excipients were prepared. Therefore, 250 mg of the respective coated pellets were manually filled into the die and compressed at 382 MPa.

A stability study of ASA was performed with MUPS tablets containing the coated ASA layered pellets. The composition of these MUPS tablets is shown in

Fig. 10. For compression of these tablets again 250 mg of the formulation were manually filled into the die and compressed at 255 MPa. The initial API content of a MUPS tablet measured by HPLC was approximately 10 mg.
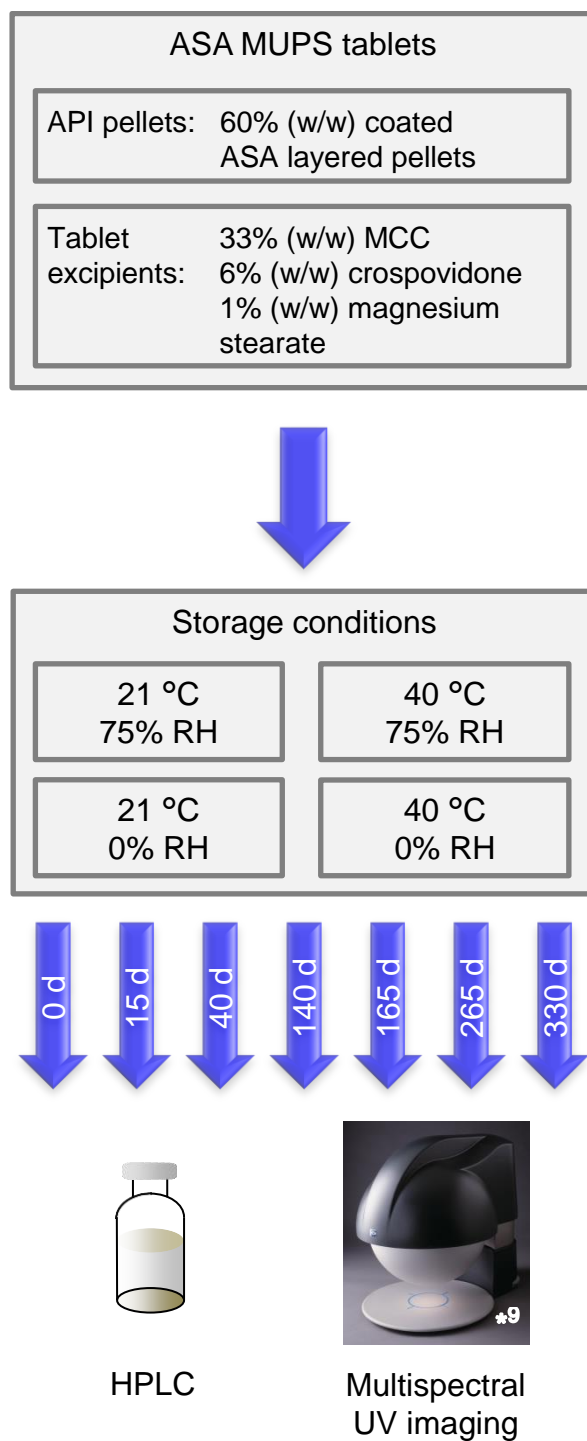
Fig. 10: ASA MUPS tablet formulation, storage conditions and analysis.

---

[9]Printed with permission of Videometer A/S

2.4.2. *UV imaging*

Multispectral images of the bottom and top side of the tablets were obtained with an UV imager (VideometerLabUV, Videometer, Hørsholm, Denmark) equipped with a Mercury-Xenon lamp as UV light source and a CCD camera capturing diffused reflected light at six wavelengths (254, 280, 300, 313, 334 and 365 nm). The instrument provides a pixel size of 77.9 µm and covers a field of view of 7.4 cm x 9.9 cm (960 pixels x 1280 pixels). Therefore, up to twenty tablets were imaged simultaneously in up to 30 s. The instrument was operated with the VideometerLab software (ver. 2.1, Videometer, Hørsholm, Denmark). The functional principle of the UV imager has been described in detail by Wu et al. [100]. Briefly, the UV light source transmits UV light into the integrating sphere where it is diffused by several internal reflections, illuminates the sample homogeneously and a CCD camera captures the reflected diffused light at six different wavelengths.

Analysis of the images was performed with an in-house written Matlab[®] (ver. 8.1, Mathworks, USA) script. The software was combined with the PLS_Toolbox (ver. 7.3, Eigenvector Research, Wenatchee, USA) for multivariate data analysis and the Image Processing Toolbox (ver. 8.0, Mathworks, Natick, USA) for image processing.

2.4.3. *High performance liquid chromatography (HPLC)*

For each MUPS tablet the amounts of ASA and SA were determined by HPLC. Each tablet was dissolved in 20 ml of acetonitrile. The obtained suspension was filtered through a 0.45 µm regenerated cellulose membrane filter (SPARTAN® RC 30, GE Healthcare UK, Buckinghamshire, UK) into a 50 ml volumetric flask and added up with acetonitrile. The obtained solution was analysed by HPLC (Merck Hitachi D-7000, Tokyo, Japan). A mixture of 59.9% (v/v) water, 39.9% (v/v) acetonitrile, and 0.2% (v/v) of 85% (w/w) phosphoric acid was used as mobile phase. The HPLC apparatus was equipped with a Prodigy® RP 18 column (Phenomenex, Aschaffenburg, Germany; column size 250 x 4.6 mm, particle size 5 µm, pore size 100 Å). The flow rate was adjusted to 1.0 ml / min and the injected sample volume was 10 µl. ASA was detected at 229 nm after 5.3 min and SA at 237 nm after 7.7 min. For calibration of the HPLC method the needed amounts of ASA and SA were dissolved in acetonitrile. The SA amount caused by degradation of ASA during tablet storage was calculated based on the initial amount of ASA. Linear absorbance of ASA was ensured for a concentration range between 3.6 and 109.6 mg / l ($R^2 = 0.999$) and the absorption of SA for a concentration range between 3.4 and 54.5 mg / l ($R^2 = 0.999$).

2.4.4. Stability investigation

All MUPS tablets prepared for the ASA stability study were imaged after tableting (sampling time point: 0 d) and the SA concentration in three sample tablets was determined by HPLC. To obtain tablets with different concentrations of the degradation product (SA), the tablets were stored under four different conditions (Fig. 10). At each sampling time point all tablets were imaged with an UV imager and the SA concentrations of three sample tablets for each storage condition were determined.

A total of 66 tablets was analysed in the stability study. The obtained UV imaging and HPLC data sets for the MUPS tablets were randomly assigned to either a calibration or a test set. The SA concentration of the tablets determined by HPLC was correlated with the estimated SA concentration based on UV reflectance spectra using a PLS. The standard SIMPLS algorithm of the PLS_Toolbox software was applied for the calculation of the PLS model [129].

2.5. Methods of 'A fast and non-destructive method for quality control of pellet distribution within a MUPS tablet by terahertz pulsed imaging'[10]

2.5.1. Sample preparation

To obtain coated Theo pellets for manufacturing of MUPS tablets, a Eudragit® NE coating dispersion was prepared by homogenising HPMC as a gelling agent in purified water at 40 °C using an Ultra Turrax® (IKA, Staufen, Germany). After a solution was formed, polysorbate 80 as a plasticiser and talc as anti-tacking agent were added and dispersed for at least 10 min and subsequently slowly poured into the Eudragit® NE 30 D dispersion under continuous stirring with a propeller stirrer (Eurostar 100 digital, IKA, Staufen, Germany) for at least 5 min. The resulting coating dispersion contained 22.7% Eudragit® NE 30 D, 6.8% talc, 0.7% polysorbate 80, and 0.7% HPMC (w/w). After preparation of the coating dispersion, Theo pellets (mesh 900 - 1000 µm) were coated in a bottom spray fluidized bed apparatus (Solidlab 1, Bosch Packaging Technology, Schopfheim, Germany). For this coating process, the coating parameters were adjusted as follows: Inlet air temperature 16 °C; inlet air flow rate 35 $m^3\ h^{-1}$; atomizing air pressure 1.5 bar; microclimate 0.4 bar; spraying rate 1.5 - 3.0 $g\ min^{-1}$. The nozzle diameter was 0.8 mm. The obtained coated pellets were subsequently dried in an oven at 40 °C for 48 h. A polymer coating level of 5% was applied onto the Theo pellets, defined as weight gain referring to the coating polymer mass.

The coated Theo pellets were mixed with MCC powder to obtain five batches of tablets with varying amounts of pellets (30%, 40%, 50%, 60%, and 70% (w/w)). 250 mg of each formulation were manually filled into the die and compacted at 255 MPa using the single punch mode of an instrumented rotary press (Fette 102i, Fette Compacting, Schwarzenbek, Germany), equipped with 10 mm flat-faced punches.

---

[10]This chapter has been published as shown on page 167 in appendix B.

2.5.2. Terahertz pulsed imaging

Five MUPS tablets, one from each batch, were imaged with a commercial TPI system (TPI™ imaga 2000, TeraView, Cambridge, UK) which represents an automated tablet scanner. As shown in Fig. 11 the TPI system scans across the x- and y-direction of the top and bottom side of the sample tablets and thereby records single depth profiles at 200 µm steps. The scanning procedure is based on a 3D model of the surface, which is generated prior to the THz measurements. This 3D model is further required for analysis of the THz data to allocate each waveform and thus to enable the 3D reconstruction of the sample. Each terahertz waveform within a tablet corresponds to a depth of 3.45 mm and the data acquisition time per tablet side was 25 min. The analysis of the images was performed with Matlab (ver. 8.1, Mathworks, Natick, USA). A wavelet denoising was applied on each THz waveform using 4-layer Daubechies wavelets and performing the wavelet decomposition at level 8. This procedure highlighted structures and supressed noise in the THz waveforms.
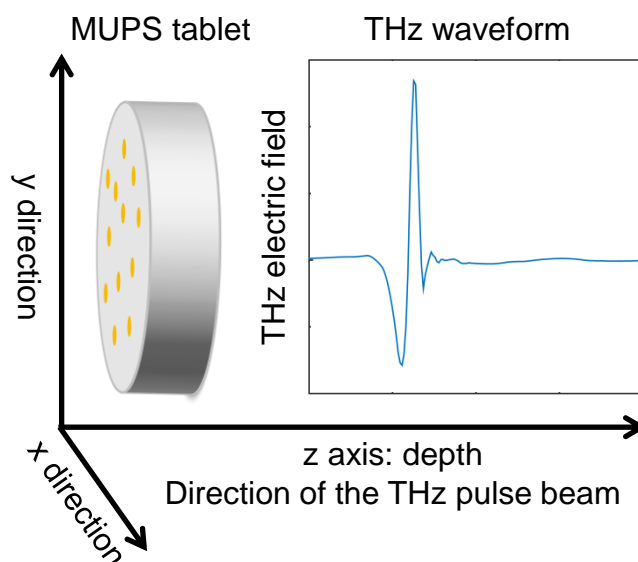
Fig. 11: Schematic visualisation of a MUPS tablet and the resulting THz waveform.

2.5.3. X-ray computed microtomography

The same MUPS tablets as analysed by TPI were scanned with microCT (Skyscan 1172, Bruker microCT, Kontich, Belgium) applying a source voltage of 59 kV. The tablets were rotated during the measurement, and 803 transmission images were recorded in steps of 0.25°. The exposure time for each transmission image was 780 ms. Scan duration for one whole tablet varied between 43 and 53 min. The reconstruction of the microCT images was performed with NRecon (ver. 1.6.8, Bruker microCT, Kontich, Belgium) and further analysis of the images was conducted by the dataviewer (ver. 1.5.2, Bruker microCT, Kontich, Belgium). The voxel size of the reconstructed images varies between 3.04 x 3.04 x 3.04 µm and 3.98 x 3.98 x 3.98 µm.

3. Results and Discussion

3.1. Results and discussion of 'Multispectral UV imaging for surface analysis of MUPS tablets with special focus on the pellet distribution '[11]

3.1.1. Detection of theophylline pellets in the tablet matrix

Initially, the suitability of multispectral UV imaging in combination with multivariate analysis to distinguish between coated Theo pellets and tablet excipients within a MUPS tablet was investigated. For this purpose, the surfaces (top and bottom) of tablets containing 70% (w/w) of pellets coated with the ethyl cellulose dispersion (n=3) and the Eudragit® NE dispersion (n=3), respectively, were analysed. Mean reflectance UV spectra of the reference Theo, MCC, and crospovidone tablets and the mean spectrum of three randomly chosen spectra of the pixels belonging to the coated pellets within the MUPS tablets are shown in Fig. 12a. The spectra of the coated pellets in a MUPS tablet (data shown for a coating level of 5%) are quite similar to the spectra of the plain Theo tablets, indicating that Theo may be detected through the coating polymer. The spectral differences between the reflectance spectra are illustrated by a PCA scores plot (Fig. 12b). All the Theo pellets, independent of the coating dispersion applied, form a cluster, presumably as a consequence of the greater absorption by Theo above 300 nm. PC-1 explains more than 90.80% of the spectral variance and shows the differences in the chemical information between the sample tablets. The loadings plot of PC-1 (Fig. 12c) resembles the UV spectrum of plain Theo tablets because the used excipients are barely UV active and allow a differentiation between Theo and the excipients. Thus, Theo in the pellets can be detected through the coating polymer by application of only six UV wavelengths. In comparison to PC-1, PC-2 explains only 7.91% of the spectral variance. Together, PC-1 and PC-2 cover more than 98.71% of the spectral variance. It is difficult to explain PC-2 in detail, nevertheless it is obvious that the

---

[11]This chapter has been published as shown on page 167 in appendix B.

loadings plot of PC-2 differs strongly from the loadings plot of PC-1. A more detailed analysis is difficult because of the only six applied wavelengths (Fig. 12c).
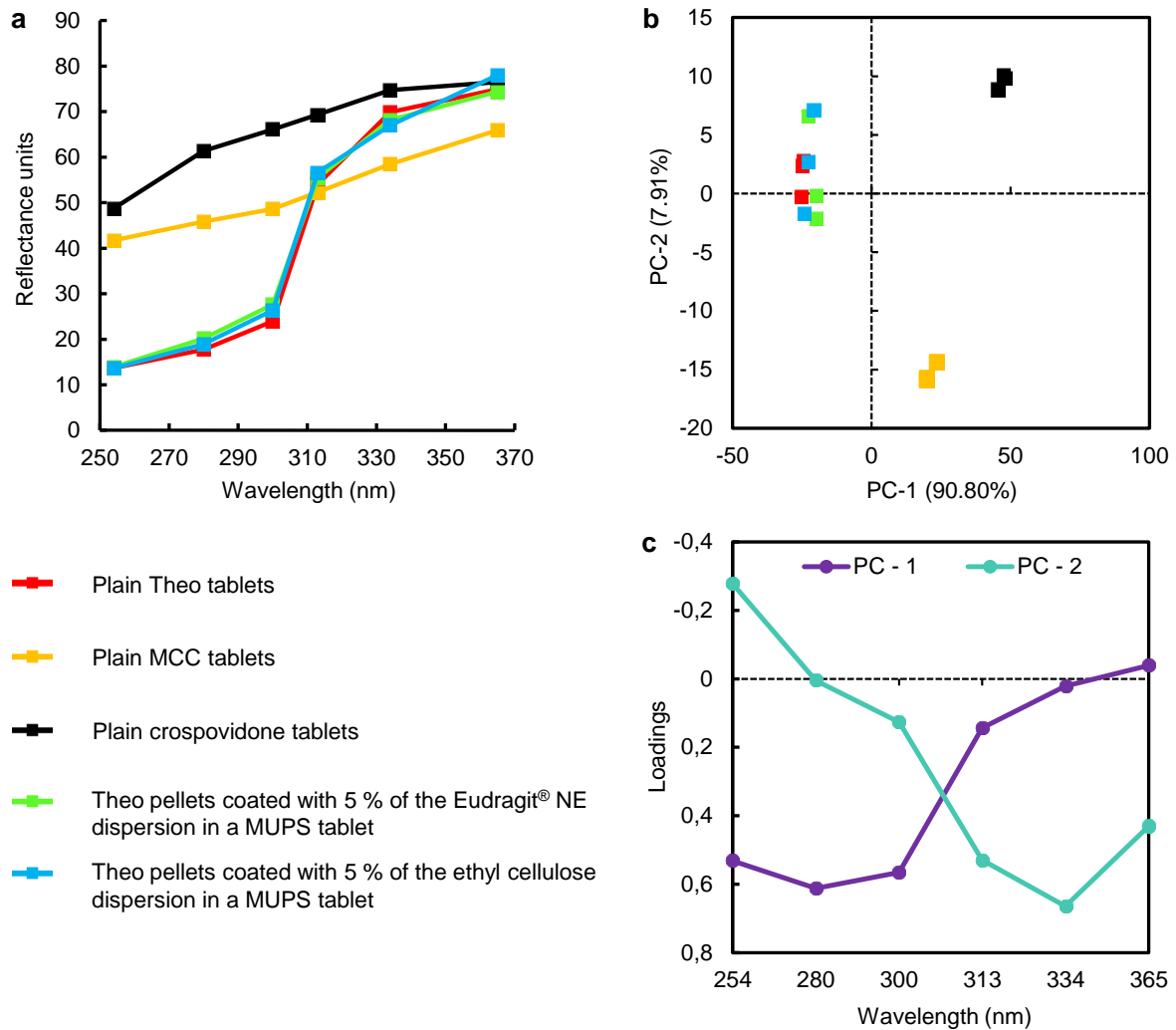
Fig. 12: Comparison of the spectral information of plain Theo, MCC, crospovidone tablets with the spectral information of coated Theo pellets in MUPS tablets: a) UV reflectance spectra, b) resulting PCA scores plot, c) resulting PCA loadings plots of PC-1 and PC-2.

Pellets coated with the Eudragit® NE coating were expected to be more difficult to analyse spectroscopically in a MUPS tablet compared to the pellets coated with the transparent ethyl cellulose coating because of the high talc content of the Eudragit® NE dispersion (1:1 ratio of polymer and talc). However, no clear difference between the spectrum of plain Theo tablets and the spectrum of Theo pellets coated with the Eudragit® NE dispersion was observed (Fig. 12a). Moreover, the PCA scores plot showed only one cluster for the spectra of plain Theo tablets and Theo pellets coated with the ethyl cellulose dispersion and the Eudragit® NE dispersion, respectively, within a MUPS tablet (Fig. 12b). To further confirm that the applied coating has no systematic effect on the Theo detection, a PCA only with Theo containing formulations was performed and no clustering was observed (data not shown).

As the PCA (Fig. 12b) does not reveal any differences between both pellet coatings, the Theo content of each tablet pixel of the UV image of a tablet was predicted by the PLS model (Section 2.2.5). Fig. 13 (left) shows the predicted values for the Theo content of both types of MUPS tablets. For pixels belonging to the Theo pellets coated with the ethyl cellulose dispersion a higher Theo content is predicted than for pixels belonging to pellets coated with the Eudragit® NE dispersion, visualised by a darker red colour of the pellets at the tablet surface. This observation can have different reasons: The preparation of pellets with exactly the same coating layer thickness of the two different polymer coatings is difficult, even though a coating level of 5% was applied to both types of pellets. Moreover, the Eudragit® NE dispersion contains a 1:1 ratio of polymer and talc, which can lead to a reduction in the Theo reflection intensity for a few pixels belonging to the API pellets because of the scattering properties of talc, whereas the ethyl cellulose dispersion does not contain talc and is therefore transparent. In addition, in the SEM images the surfaces of the

pellets coated with the ethyl cellulose dispersion in a tablet appear rather smooth, while the excipients are present as powder particles between the pellets (Fig. 13, right). In contrast, the SEM image of the MUPS tablet containing pellets coated with the Eudragit® NE dispersion shows a thin layer of excipients on the pellet surface, because of the stickiness of the polymer. This may also lead to a reduction in Theo reflectance intensity.
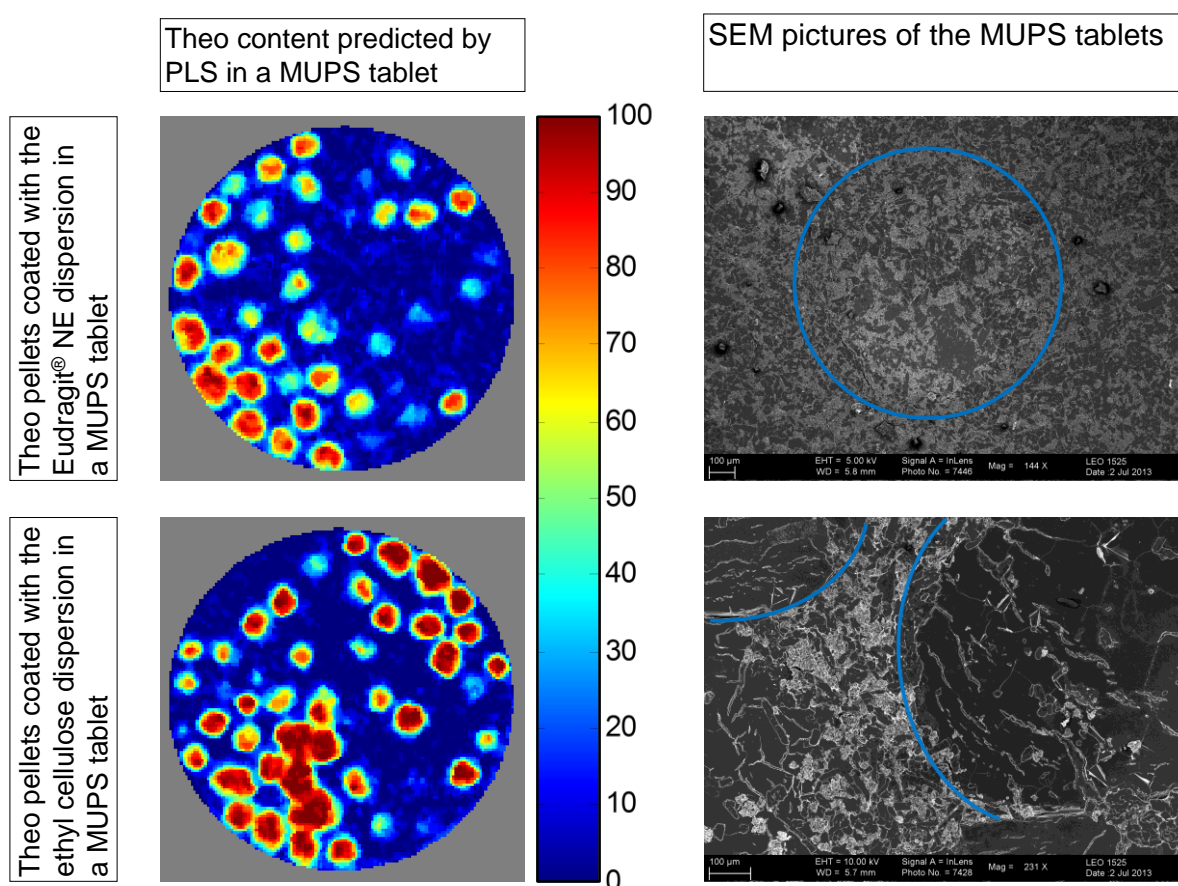
Fig. 13: left) Theo content in MUPS tablets predicted by PLS, right) SEM pictures of the MUPS tablets.

To visualise the influence of the coating layer thickness, Theo contents predicted by PLS for coated Theo pellets with three different coating levels compressed to a tablet are shown in Fig. 14. Only a slight decrease of the predicted Theo content can be observed with increasing coating layer thickness of pellets coated with the ethyl cellulose dispersion in the tablets, manifesting itself in a lighter red colour. In contrast, for the pellets coated with the Eudragit® NE dispersion the decrease of the predicted Theo content is more pronounced. As was shown in Fig. 12a and b, none of the coatings change the UV spectrum of plain Theo, as all samples cluster together with Theo in the PCA scores plot. Consequently, the large difference between the predicted Theo contents of pellets coated with the different coating levels of the Eudragit® NE dispersion can be explained by its high talc content. Thus, it is possible to differentiate the coated pellets from the excipients even at high coating levels. The highest coating level of 19% was chosen because it is close to the usually used upper limit for these two coating dispersions [181,182]. Thus, UV imaging allows the differentiation of coated Theo pellets from the excipients within a MUPS tablet for the whole range of coating layer thicknesses.
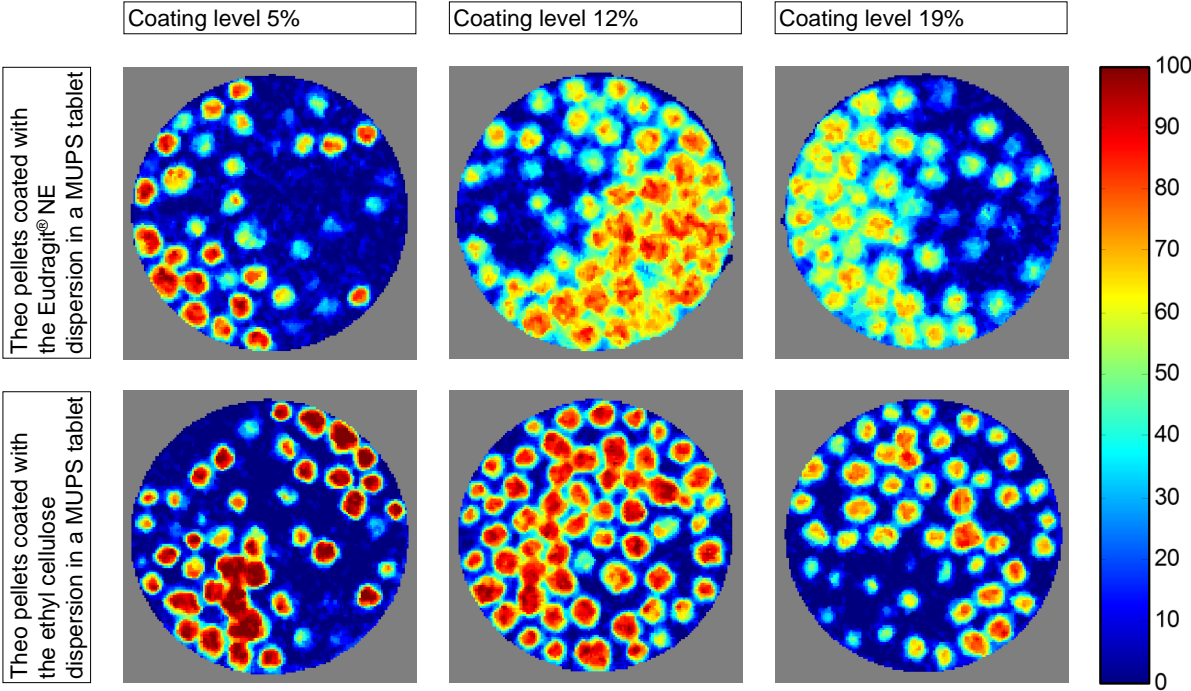
Fig. 14: Theo contents predicted by PLS for pellets with three different coating levels in MUPS tablets.

3.1.2. Pellet quantification in MUPS tablets

After having shown that it is possible to detect the pellets on the tablet surface, the pellet content and pellet distribution in the tablet was estimated by surface analysis. For this purpose, 10 tablets containing pellets coated with the ethyl cellulose dispersion (coating level 5%) at pellet contents of 30%, 50%, and 70% (w/w), respectively, were analysed. In addition, 10 tablets containing pellets coated with the Eudragit® NE dispersion (coating level 5%) at the same pellet contents were investigated. Thus, 30 tablets of each type of coated pellets with significantly varying Theo amount were obtained.

In Fig. 15a the correlation of the amount of Theo in the examined tablets determined by HPLC with the amount of Theo on the tablet surface calculated based on the determined number of pellets, is shown for both coating dispersions. A power trend line was expected to be the best fit because the amount of Theo in a whole tablet (volume) was correlated with the amount of Theo on the tablet surface (area) and is visualised in Fig. 15a and b by the green line. However, it was observed that a linear correlation was a better fit in most cases. Therefore, only a linear correlation is shown in other figures. The resulting linear correlation of MUPS tablets containing pellets coated with the ethyl cellulose dispersion shows an R^2 of 0.93 and a root mean square error (RMSE) of 10.85 mg, indicating that the pellet amount in each tablet can be estimated. As it has already been shown, the coating polymer has an effect on the predicted Theo content of each individual pixel of the tablet image and may therefore influence the detectability of the pellets in the tablet matrix. However, a linear correlation was also obtained with MUPS tablets containing pellets coated with the Eudragit® NE dispersion, resulting in an R^2 of 0.93 and an RMSE of 11.13 mg (Fig. 15b). Therefore, image analysis of the tablet surface with regard to the number of pellets provides information on the total Theo content in a MUPS tablet.

Furthermore, the same MUPS tablets were analysed using a PLS approach (Fig. 15c and d). For this purpose, a mean spectrum of all pixel reflectance spectra belonging to the top and bottom of a tablet was calculated. Subsequently, the spectra were SNV corrected to remove light scattering effects [102,116]. In accordance with the PLS approach, the resulting mean spectra of all tablets were correlated with the corresponding Theo amount detected by HPLC. Based on the results of preliminary cross validation (random subsets, 20 splits, 6 iterations) calibration models with 4 LVs each were calculated [102,175]. The PLS model for MUPS tablets containing pellets coated with the ethyl cellulose dispersion provides slightly better values compared to the pellet quantification procedure, resulting in an R^2 of 0.98 and RMSEC of 6.07 mg. The PLS model for MUPS tablets containing pellets coated with the Eudragit® NE dispersion also shows slightly better values than the pellet quantification procedure. However, for fully automatic predictions regarding future multiple-unit pellet systems in terms of the pellet amount in a tablet, the pellet quantification procedure is a more convenient approach compared to the setup of a valid PLS model.
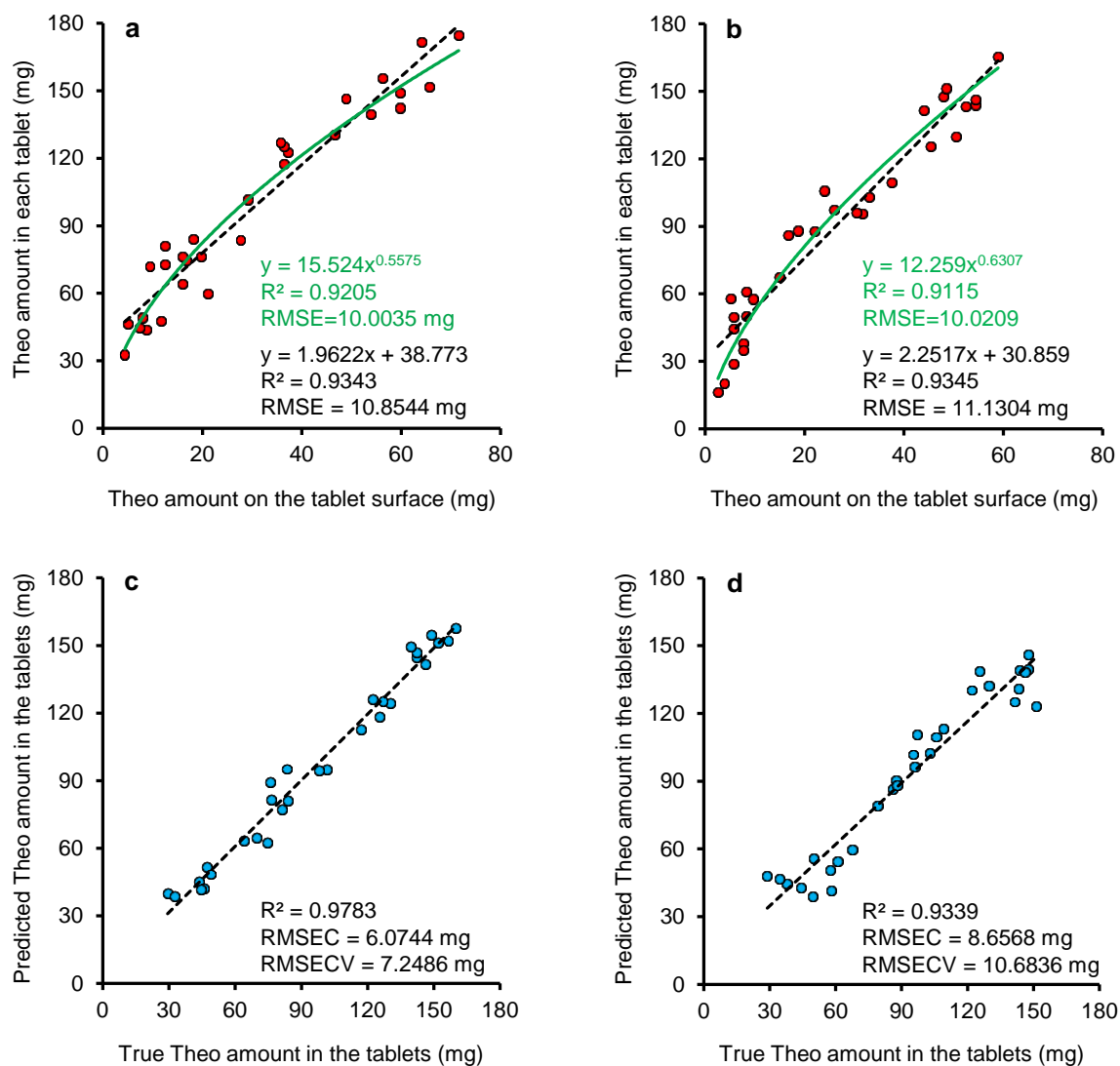
Fig. 15: Correlation data of MUPS tablets containing pellets coated with the ethyl cellulose dispersion (left, n = 30) and the Eudragit® NE dispersion (right, n = 30), respectively: a/b) correlation of the Theo amount detected by HPLC with the Theo amount on the tablet surface determined by UV imaging, c/d) correlation of the Theo amount predicted by a PLS approach with the true Theo amount detected by HPLC.

To examine whether the distribution of the pellets on the tablet surface may provide information on the distribution of the pellets within the tablet, the results of the surface analysis using UV imaging were correlated with the HPLC analysis of the two tablet halves. As described above, the UV images of the tablets were scanned to detect the most inhomogeneous pellet distribution after tablet division. To inspect if the distribution on the tablet surface correlates with the actual pellet distribution within the tablet, the tablets were divided into two halves and the Theo amount was measured by HPLC and correlated with the Theo amount determined on the surface of the tablet halves by UV imaging as illustrated in Fig. 16. The correlation for the tablet halves is not as good as the correlation for the whole tablets. As described in section 2.2.5 the most inhomogeneous division case for every tablet was determined and used for the models. This particular division case was analysed by HPLC. Unfortunately, it is physically impossible to divide the tablet exactly in the same way as suggested by the pellet counting procedure. Therefore, variances between the model and the exact division may arise. Nevertheless, a prediction of the Theo content in each half of MUPS tablets containing pellets coated with the ethyl cellulose dispersion based on surface analysis is possible, as illustrated by an R^2 of 0.91 and an RMSE of 7.04 mg. The results for tablets containing pellets coated with the Eudragit® NE dispersion show a slightly higher variation. However, the estimation of the true pellet amount in the tablet halves is still possible.
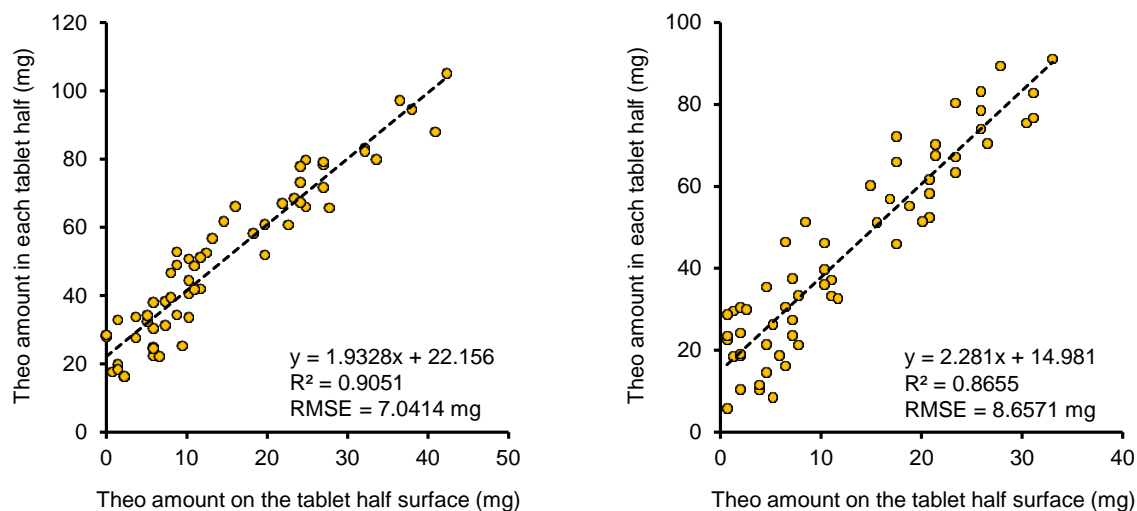
Fig. 16: Correlation of the Theo amount detected by HPLC in each tablet half with the Theo amount on the surface of each tablet half determined by UV imaging for MUPS tablets containing pellets coated with the ethyl cellulose dispersion (left, n = 60) and the Eudragit® NE dispersion (right, n = 60), respectively.

Consequently, the surface distribution of the pellets and thus the API provides information on the distribution of the pellets within the whole tablet. Surface analysis directly after tableting is therefore a valuable tool to determine whether the pellets are distributed homogeneously, or if an optimization of the manufacturing process and the formulation, respectively, is required. Compared to HPLC, which considers only one manual tablet division case, UV imaging has the advantage that all possible distribution cases can be investigated.

3.1.3. Influence of the tablet thickness on pellet quantification

To investigate the influence of the tablet thickness on the prediction model for pellet quantification, three batches of 10 tablets each with different average thicknesses (1.1 mm, 1.8 mm and 3.3 mm) containing pellets coated with the ethyl cellulose dispersion were examined. Calibration models were obtained for each of the batches and these models were compared on the basis of the parameters R^2 and RMSE, revealing that the tablet thickness of 1.8 mm provides the best correlation (Fig. 17b and c). For a tablet thickness of 1.1 mm, it is possible that one pellet may be detected on both top and bottom surfaces and might therefore be counted twice. Consequently, if the tablet thickness approximates the pellet diameter, predictive models for the analysis of one surface only as well as the combined analysis of both top and bottom surfaces should be compared with the results of HPLC to find the best correlation. In Fig. 17a PLS predicted images of the cross-sections of the tablets are shown with respect to their thicknesses. The percentage of pellets at the surface decreases with increasing tablet thickness due to a decreased surface to volume ratio. Thereby, the correlation decreases with increasing tablet thickness as indicated by the R^2 and RMSE values. Nevertheless, according to the R^2 of 0.7566 a statistically significant correlation was shown for the tablets with the thickness of 3.3 mm. A low R2 was expected, because as presented in Fig. 17a only 25% of the total pellet amount is detectable at the tablet surface. Therefore, the pellet amount at the tablet surface is less representative for the pellet amount in the whole tablet compared to tablets with other tablet thicknesses. As described above, during the exact tablet division, the pellets at the division line might be assigned to the respective other half than expected based on the surface analysis. However, because of the low R^2 of 0.3657, the model for the tablet halves cannot be used for the estimation for the pellet distribution.

Consequently, the pellet quantification procedure is applicable for the fast estimation of the pellet amount and the pellet distribution for tablet thicknesses up to 2.4 mm (see Fig. 15 and Fig. 16).
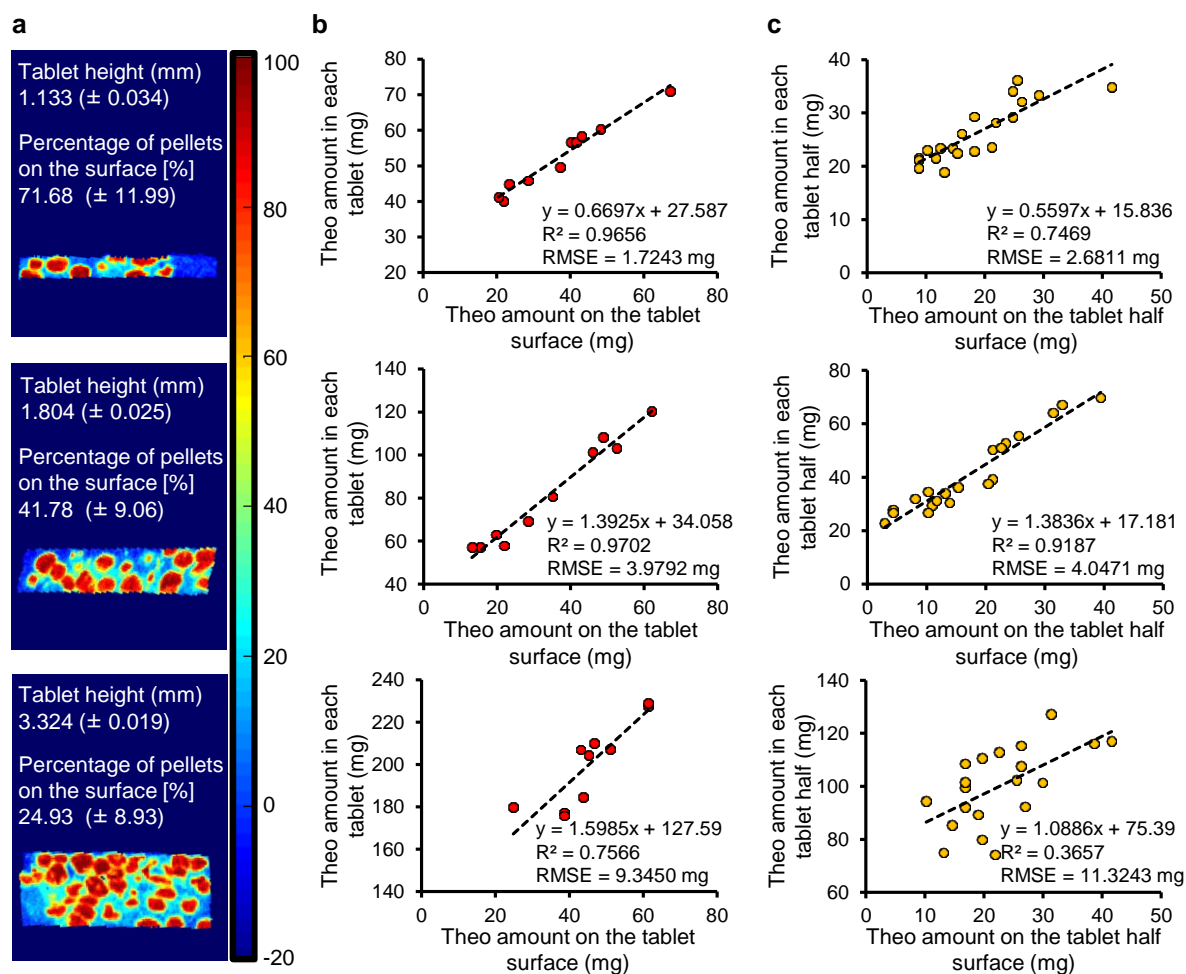
Fig. 17: Tablet thickness and correlation data of MUPS tablets containing pellets coated with the ethyl cellulose dispersion a) Visualisation of the predicted Theo content for every pixel of the tablet cross-section obtained by PLS, b) correlation of the Theo amount detected by HPLC with the Theo amount on the tablet surface determined by UV imaging (n = 10) and c) correlation of the Theo amount detected by HPLC with the Theo amount on the tablet half surface determined by UV imaging (n = 20).

3.1.4. Conclusion

Multispectral UV imaging in combination with multivariate image analysis has been shown to be a promising approach for fast analysis of the pellet distribution in MUPS tablets, suitable for inline measurements. It could be shown that pellets in MUPS tablets can be detected through coating layers even at high coating levels. The pellet quantification procedure proved to be a fast and simple analysis method for content uniformity and distribution of the pellets. This pellet quantification procedure provided similar results to the PLS model. It was found, that the coating material and the tablet height can influence the prediction model. For all tablet heights up to 2.4 mm good prediction models were obtained. In summary, UV imaging can be applied to predict the pellet distribution and content uniformity, but has to be pre-calibrated with regard to the formulation, tablet height and surface area. A fully automatic estimation of the pellet amount and distribution in MUPS tablets based on surface analysis immediately after tablet manufacturing using UV imaging thus appears possible.

3.2.   Results and discussion of 'Multispectral UV imaging for determination of the tablet coating thickness'[12]

3.2.1.   Prediction of the tablet weight gain based on UV spectra

In this study, the suitability of UV imaging to analyse the coating quality of single unit tablets during the coating process was investigated. For the first three investigated formulations (Table 3) the mean reflectance spectra were calculated for each sampling time point to visualise the intensity changes during the coating process. The reflectance spectra were plotted versus the tablet weight gain for each sampling time point, which corresponds to increasing coating thickness (Fig. 18). In coating formulations that do not contain UV absorbing ingredients the majority of UV radiation propagates through the polymer coating layer and is reflected by the tablet core. A small fraction of the radiation is typically scattered by the coating. With increasing coating thickness the intensity of the reflected light decreases, with the extent of this decrease depending on the coating formulation. The first formulation (Theo-NE) was designed to exhibit a particularily high talc particle content. It was expected that there would be a more pronounced decrease in the intensity of the reflected light with increasing coating thickness resulting from scattering of coatings that contain particles compared to the translucent coating of the second formulation (Theo-EC). At the beginning of the coating process the reflectance spectra of plain Theo were observed. During the coating process, the UV active core is continuously covered by the coating polymer and by talc, as the Eudragit® NE dispersion contains a one to one ratio of polymer and talc. Thus, a decrease of the intensity of the reflected light mainly at wavelengths above 313 nm was observed (Fig. 18a). The intensity changes of the reflected light for Theo-EC were slightly less pronounced (Fig. 18b), but the spectra still appeared similar to those of Theo-NE.

---

[12]Parts of this chapter have been published as shown on page 167 in appendix B.
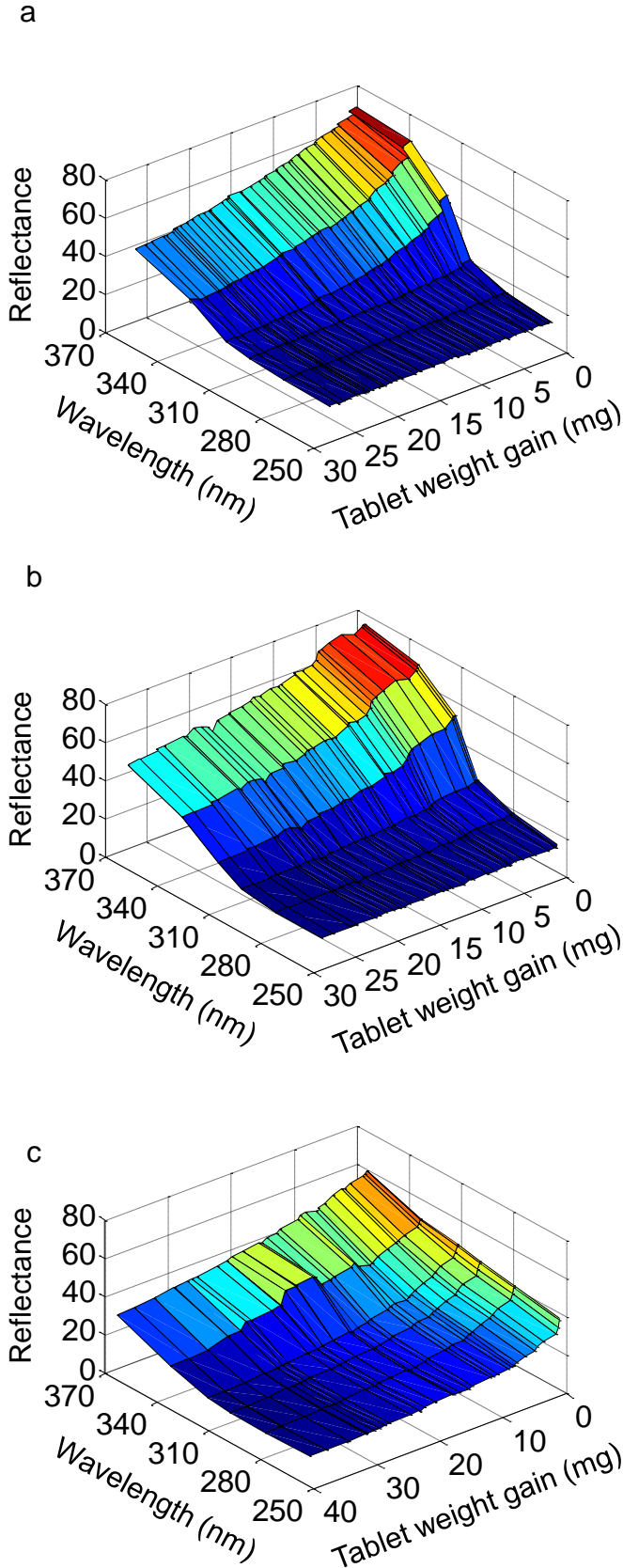
Fig. 18: Mean reflectance spectra versus mean tablet weight gain per sampling time

point for different formulations: a) Theo-NE b) Theo-EC c) Placebo-EC.

In contrast, the spectra of the Placebo-EC formulation showed a decrease in the intensity of the reflected light at all six wavelengths (Fig. 18c) during the coating process, indicating that these intensity changes were mainly caused by scattering losses. The extent of these intensity changes was significantly lower than for the formulations with the UV active core (Theo-NE, Theo-EC).

For the first three investigated formulations mean reflectance UV spectra of the calibration sets were correlated with the individual tablet weight gains using PLS. The resulting calibration models were used for prediction of the tablet weight gains for the tablets in the test sets (Fig. 19, Table 6). The applied PLS model for Theo-NE showed, that the intensity decrease of the reflected light correlates with the individual weight gain of each tablet. Based on the results of a preliminary random cross validation (2 splits, 6 iterations) with the calibration data set (n = 122 tablets), a PLS model with 2 LVs was established (RMSEC = 0.84 mg, RMSECV = 0.91 mg). This model was used for prediction of the individual tablet weight gain with an root mean squared error of prediction (RMSEP) of 0.83 mg and an R^2 of 0.990 for the test data set (n = 120 tablets, Fig. 19a).

As expected for the second formulation (Theo-EC), the intensity of the reflected light decreased only slightly with increasing thickness of the mainly translucent ethyl cellulose coating because of the absence of scattering talc particles (Fig. 18b). Nevertheless, it was possible to establish a correlation of the spectra with the tablet weight gain for the calibration data set (n = 84 tablets, Fig. 19b). An RMSEP of 0.87 mg was calculated using the test dataset (n = 85 tablets). This value is only slightly higher than the RMSEP of Theo-NE, but these values cannot be directly compared because the weight gain depends on the composition of the coating formulation and therefore corresponds to different coating thicknesses.

a

y = 0.9999x + 0.0138

b

y = 0.896x + 0.052

c

y = 0.9625x + 0.6751
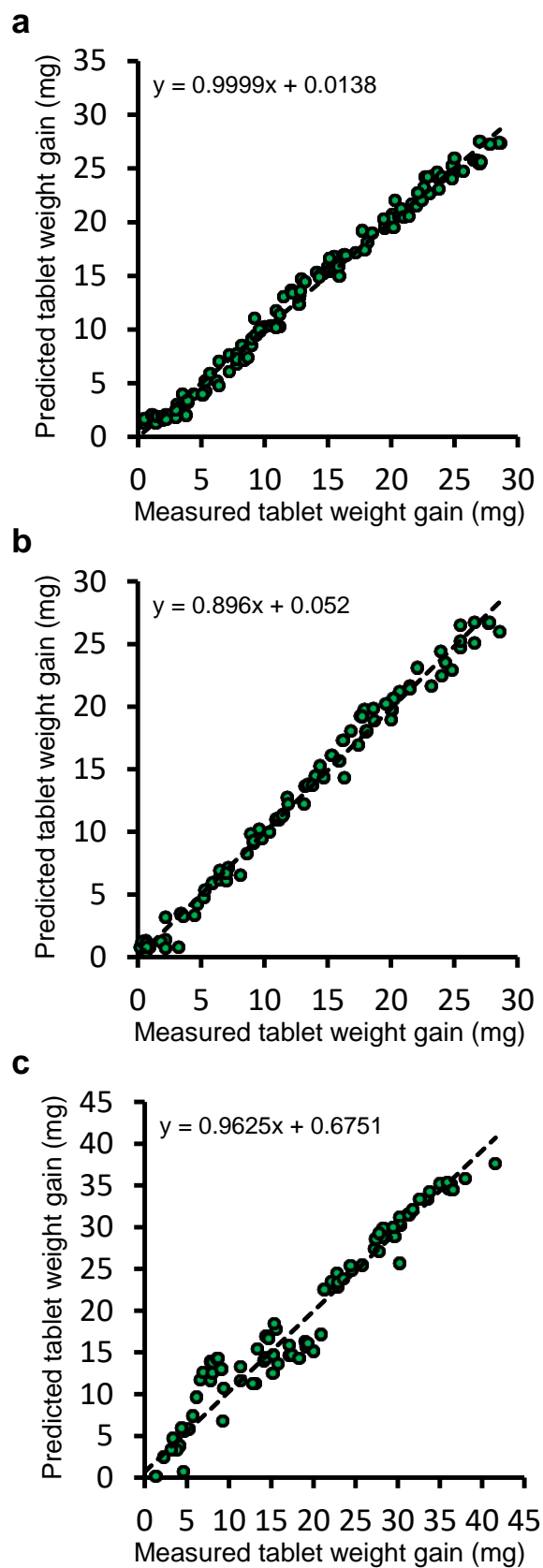
Fig. 19: PLS prediction models for the individual tablet weight gain applied to the test set tablets: a) Theo-NE b) Theo-EC c) Placebo-EC.

Table 6: Parameters of the PLS models for the weight gain prediction based on UV reflectance spectra and determined weight gain.

Model for the formulation	Pre-processing	LVs	$R^2 C^{1)}$	$R^2 CV^{2)}$	$R^2 P^{3)}$	RMSEC (mg)	RMSECV (mg)	RMSEP (mg)	$C^{1)}$ Bias	$CV^{2)}$ Bias	$P^{3)}$ Bias
Theo-NE	Mean centering	2	0.990	0.989	0.990	0.84	0.91	0.83	$3.0e^{-14}$	-0.01	0.01
Theo-EC	SNV, mean centering	2	0.988	0.985	0.989	0.92	1.18	0.87	$-2.1e^{-14}$	-0.04	-0.08
Placebo-EC	Mean centering	2	0.949	0.944	0.957	2.67	2.86	2.44	$-2.5e^{-14}$	-0.08	0.02

$C^{1)}$ = calibration, $CV^{2)}$ = cross validation, $P^{3)}$ = prediction.

The RMSEs for the prediction of the tablet weight gain of the Theo-NE formulation correspond to lower coating thicknesses than the RMSEs of the Theo-EC formulation, because the Eudragit® NE coating dispersion contains talc. Therefore, the PLS model for Theo-NE provides more precise predictions of the coating thickness than the PLS model for the Theo-EC.

The formulation Placebo-EC was expected to be even more problematic because of the UV inactive core and the translucency of the ethyl cellulose coating, resulting in only small changes of the intensity of the reflected light (Fig. 18c). Nevertheless, the UV spectra were correlated with the individual tablet weight gain (calibration data set: n = 94 tablets). Based on the preliminary cross validation, the calibration model was calculated with three LVs and applied to the test tablets (n = 95 tablets) resulting in an RMSEP of 2.44 mg (Fig. 19c). However, the PLS model can be used for prediction of the individual tablet weight gain with the Placebo-EC formulation.

For the first three investigated formulations it could be shown that UV spectra can be correlated with the tablet weight gain and that the obtained PLS models can be used for prediction of the individual tablet weight gain, which corresponds to different coating thicknesses. However, the extent of the intensity changes of the reflected light depends on the formulation resulting in a variation of the power of the PLS models.

3.2.2. Prediction of the coating thickness distribution

As shown before, UV imaging is suitable to determine the tablet weight gain. So far, in this study no information on the distribution of the coating thickness across the tablet surface was obtained. In contrast to the measurement of the tablet weight gain as an indirect method, the detection of the true coating thickness is possible with TPI. In addition to the mean coating thickness, TPI gives spatial information on the distribution of the coating thickness on the tablet surface (uniformity of the coating). In this study, the applicability of multispectral UV imaging for analysis of the spatial distribution of the coating thickness on the tablet surface was therefore investigated using TPI as a reference method.

For prediction of the coating distribution on the tablet surface the PLS calibration models were calculated based on the UV spectral information and the mean coating thickness determined by TPI. The resulting correlations between the measured mean coating thickness and the predicted coating thickness for the first three investigated formulations are shown in Fig. 20 and the details about the models are presented in Table 7.

As expected, the Theo-NE formulation leads to the best PLS calibration model (Fig. **20**a) because the Eudragit® NE coating dispersion mainly contains a one to one ratio of polymer and talc as mentioned above. Hence, the intensity of the reflected light decreases more noticeably with increasing coating thickness for Theo-NE than for Theo-EC. For this reason, the PLS model for Theo-EC is not quite as good as for Theo-NE, as the ethyl cellulose coating dispersion does not contain solid particles and is therefore mainly translucent (Fig. 20b). The Placebo-EC formulation was again expected to be more problematic because of its UV inactive core and mainly translucent coating. The resulting PLS prediction is based on the scattering

differences in the UV spectra between the sampling time points providing a slightly less suitable model than for the other two formulations (Fig. 20c). It could be shown that for the first three investigated formulations an acceptable calibration model may be obtained and used for prediction of the coating thickness. Accordingly, the UV imaging calibration models for coating thickness prediction are mainly based on the decrease in the intensity of the reflected light for the UV active cores and on the changes in the scattering for the UV inactive cores. In comparison to that, the PLS models for coating thickness prediction for the well-investigated NIR spectroscopy are based on other principles such as absorbance signals of the coating polymer for the pigment-free coatings and a baseline shift for pigment-containing coatings [65].

Table 7: Parameters for the PLS models for the coating thickness prediction based on UV reflectance spectra and coating thickness determined by TPI.

Model for the formulation	Pre-pro-cessing	LVs	$R^2 C^{1)}$	$R^2 CV^{2)}$	RMSEC (µm)	RMSECV (µm)	$C^{1)}$ Bias	$CV^{2)}$ Bias
Theo-NE	Mean centering	2	0.987	0.982	3.42	4.46	$5.7e^{-14}$	-0.19
Theo-EC	Autoscaling	2	0.982	0.978	6.10	6.74	0	-0.21
Placebo-EC	Mean centering	2	0.974	0.969	8.53	9.36	$2.8e^{-14}$	0.1

$C^{1)}$ = calibration, $CV^{2)}$ = cross validation.

a

b

c
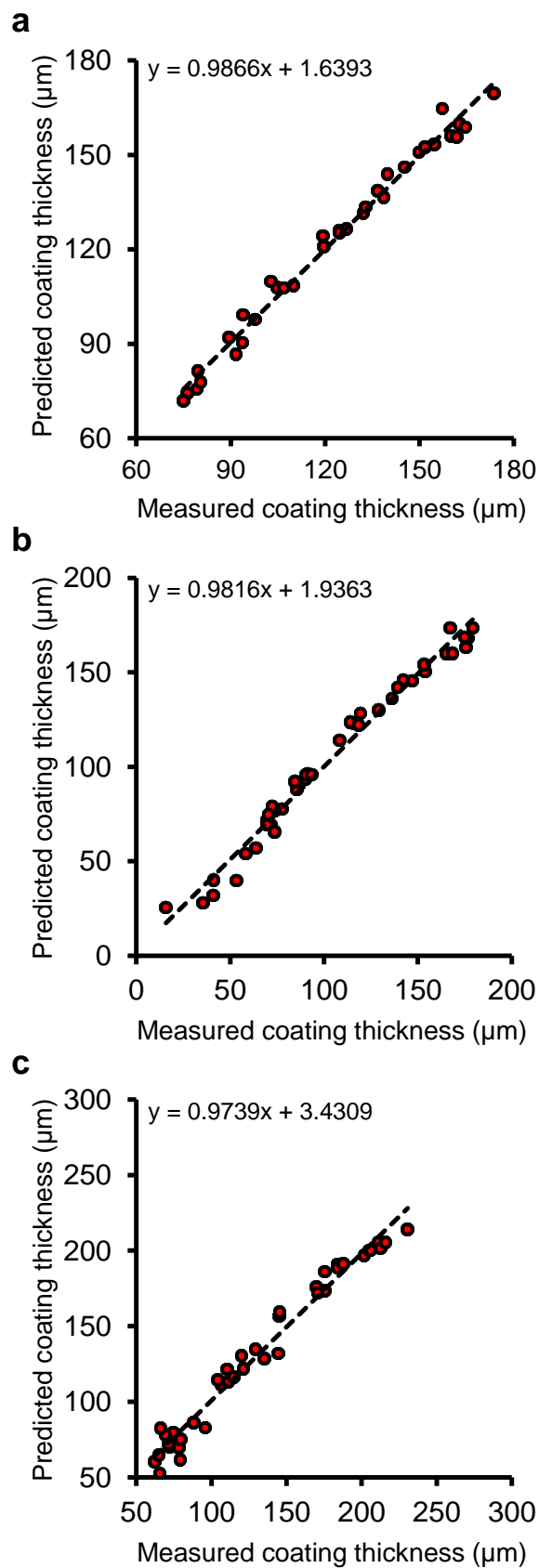
Fig. 20: PLS calibration models for the coating thickness based on UV imaging data correlated with TPI data: a) Theo-NE b) Theo-EC c) Placebo-EC.

The calculated PLS models were used for prediction of the coating thickness distribution on the tablet surface. In Fig. 21 the similarity between the predicted coating thickness based on the UV spectra (PLS) and the measured coating thickness (TPI) for the investigated formulations is visualised. Despite different spatial resolution, both methods showed comparable results with regard to the mean coating thickness and coating thickness distribution on the tablet surface.

However, the distribution of the coating thickness measured by TPI is narrower than that based on UV data because of the larger pixel size of TPI (200 μm) compared to the smaller UV imaging pixel size (77 μm). The larger pixel size of TPI compared to UV leads to data averaging of the coating thickness of the measurement area.

UV imaging is an indirect method, which detects changes in spectral information. Therefore, to determine the coating thickness a correlation between the spectral information and the reference data is needed. However, the main advantage of UV imaging is its fast acquisition speed: it takes up to only about 30 s to image a whole tablet surface with a spatial resolution of 77 μm. However, as a staring imaging technique UV imaging may show so-called 'edge effects'. The edge effect occurs if the light gets reflected in a different way at the edge of the tablet, resulting in a prediction of a slightly higher coating thickness at the edge compared to the true thickness. In this study, circular erosion of the tablet edge was applied to the UV images to account for these edge effects.
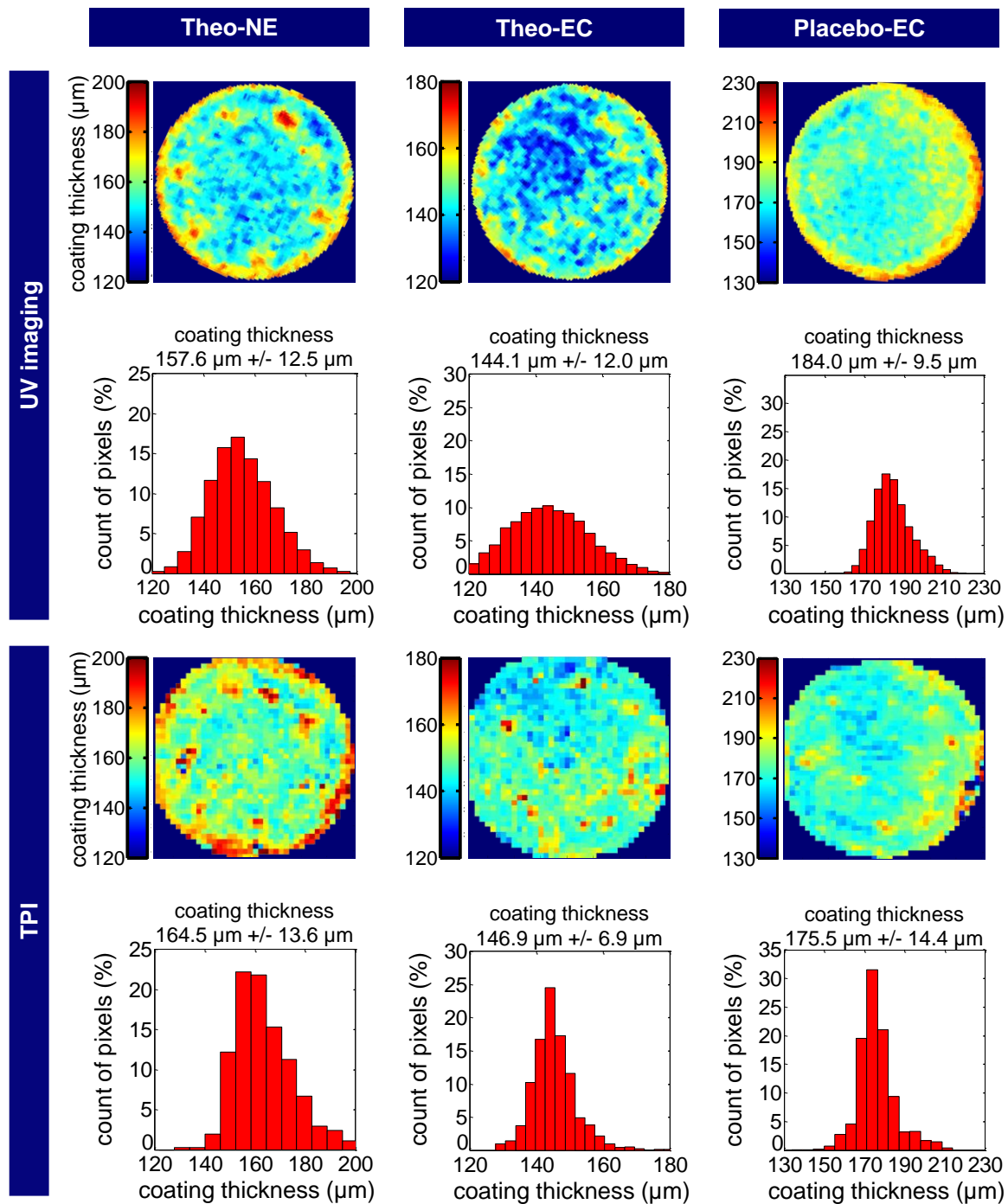
Fig. 21: Coating thickness distribution on the tablet surface predicted by PLS based on UV spectral information compared with that measured by TPI. UV: images and histograms of the predicted coating thickness based on UV spectral information, TPI: images of the coating thickness measured by TPI.

In contrast to UV imaging, TPI is a direct method because measurements are based on a delay of the terahertz pulse, which corresponds to a true coating thickness. As a mapping method TPI requires 15 min (50 ms for a single point [88]) with the lower spatial resolution of 200 µm for the surface analysis of one tablet. In TPI, the sample is measured point-by-point with the terahertz optics always at constant focus and normal to the surface. Hence, the edge effect resulting from the facet of the tablet can be mostly avoided (except for the extreme edge of the tablet where scattering of the terahertz pulse can occur). The main disadvantage of TPI is the thickness resolution limit. Hence, TPI is unsuitable to determine the coating thickness of thin coatings [96]. Therefore, recent publications suggest combining TPI with optical coherence tomography to improve the detectability of thin coatings [183]. In contrast, UV imaging in combination with multivariate data analysis was shown to be suitable to predict even low tablet weight gains corresponding to lower coating thicknesses based on UV spectra.

3.2.3. *UV imaging analysis of coloured coatings*

Kollicoat[®] IR Sunset Yellow is a coloured pigment coating resulting in a complete masking of the UV active core beyond a certain coating thickness. Thus, no differences in the spectral information beyond this thickness can be observed (Fig. 22a). The individual tablet weight gains at the initial sampling time points were too low to be significantly determined because for coloured coatings a lower amount of coating dispersion is usually applied compared to sustained release coatings. At low weight gains the accuracy of the weight gain methods to estimate the coating thickness is strongly affected by parameters such as abrasion of the tablets in a drum coater [160]. The thickness of these usually thin coloured films is also below the detection limit for TPI. Hence, a PLS regression was not possible. For better visualisation of spectral differences a PCA was performed with the mean UV spectra for each investigated tablet (Fig. 22b). PC-1 explains more than 96.5% of the spectral variance and shows the differences in the chemical information between the sample tablets resulting from the decrease of the Theo reflection intensity. The performed PCA analysis of the mean UV spectra reveals the differences between the tablets from the first 10 sampling time points corresponding to the first 50 tablets. Therefore, UV imaging may be suitable for determination of the thickness of thin coloured films and of the end point of the coating process when a homogeneous coating is achieved.
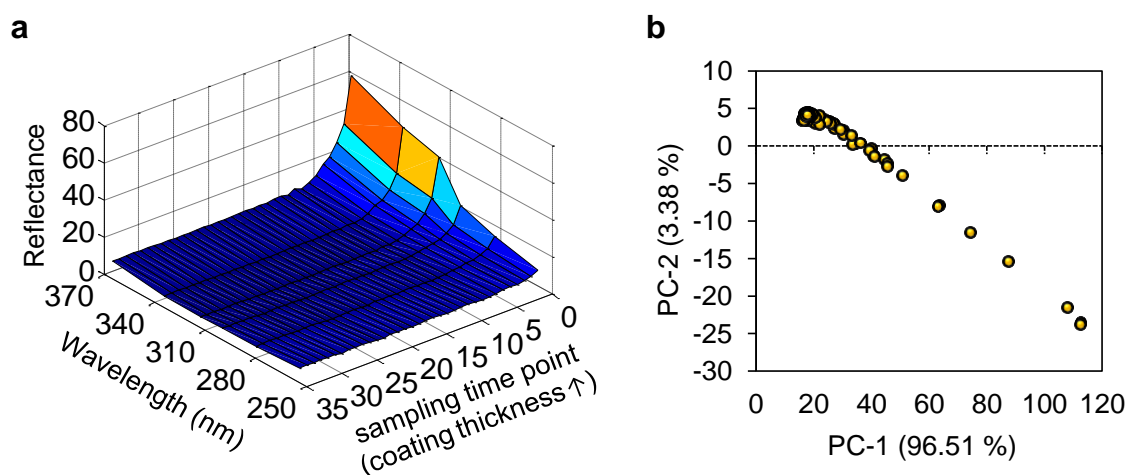
Fig. 22: a) Mean reflectance spectra for each sampling time point corresponding to the increasing coating thickness of the Theo-IR formulation, b) PC scores plot for 180 sample tablets of the Theo-IR formulation.

However, the mean coating thickness of coloured coatings may be determined using a similar imaging technique within a wavelength range between 385 nm and 1050 nm. Therefore, the Theo-IR formulation was also analysed using this wavelength range. Surprisingly, the reflectance spectra do not show pronounced differences after the 10th sampling time point (Fig. 23a). Nevertheless, using a PCA approach for the mean standard normal variate corrected reflectance spectra of the investigated tablet spectral differences were observed (Fig. 23b) [102,104]. PC-2 describes 38.89% of the spectral variance which corresponds to the increasing sampling time points. Therefore, based on the results of the preliminary cross validation a PLS calibration model for estimation of the sampling time points with 4 LVs for 178 tablets was calculated (Fig. 24). Hence, with the PLS approach it was possible to estimate the sampling time point corresponding to the mean coating thickness based on the mean reflectance spectra within the wavelength range between 385 nm and 1050 nm for each tablet in a data set.
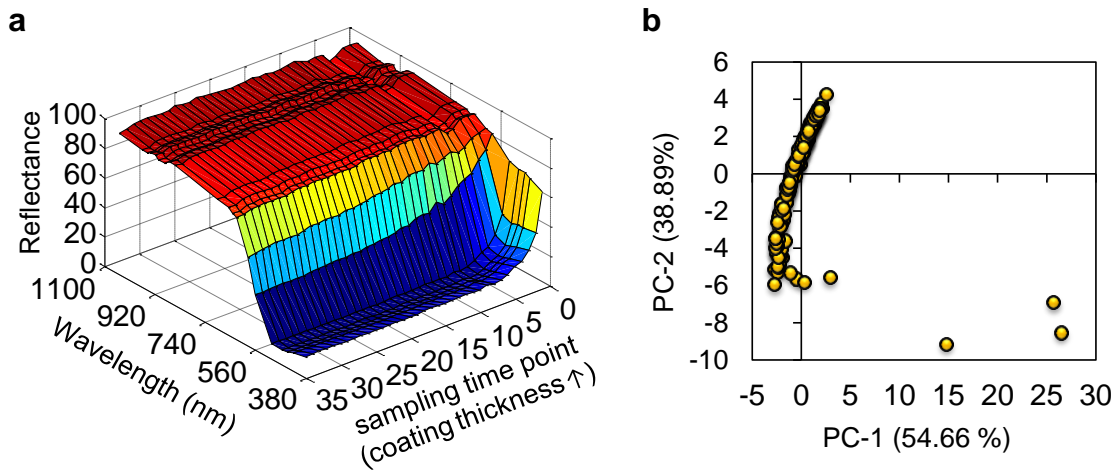
Fig. 23: a) Mean reflectance spectra (385 nm – 1050 nm) for each sampling time point corresponding to the increasing coating thickness of the Theo-IR formulation, b) PC scores plot of the mean reflectance spectra (385 nm – 1050 nm) for 180 sample tablets of the Theo-IR formulation.
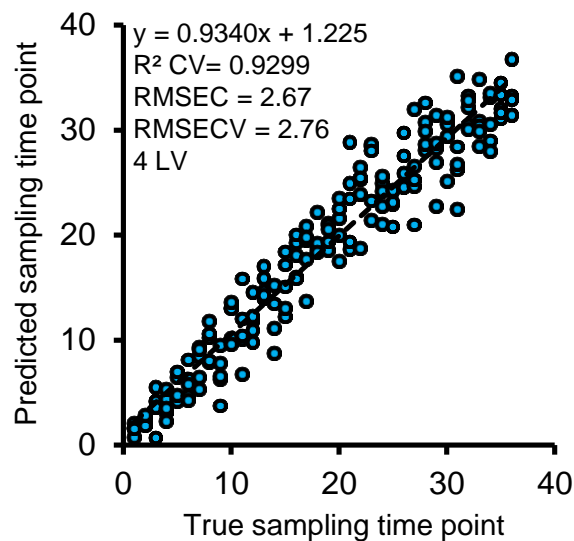
Fig. 24: PLS calibration model for the sampling time points based on the reflectance spectra (385 nm – 1050 nm) correlated with the true sampling time points of the Theo-IR formulation.

3.2.4. Conclusion

In the present study, it could be shown that the tablet weight gain during the coating process can be predicted based on UV imaging data for mainly translucent coatings as well as turbid, solid particles containing, coatings. As reference, the true coating thickness was measured by TPI and correlated with the UV spectra of the coated tablets using a PLS approach. The resulting PLS models were used for prediction of the coating thickness for every pixel of the UV image of the tablet surface and provided comparable surface coating thickness profiles to TPI.

For coloured pigment coatings UV imaging may be suitable on the one hand for thickness determination of particularly thin coatings and on the other hand for the endpoint determination of the coating process, because above a certain coating thickness the coatings become opaque and therefore no further spectral changes occur. Nevertheless, it could be shown that for the estimation of the sampling time points a similar imaging technique within the wavelength range between 385 nm and 1050 nm is applicable.

It could further be shown that UV imaging is a fast, non-destructive technique that allows recording of an image within 30 s. In addition, the use of only six wavelengths significantly reduces the amount of recorded data compared to other imaging methods. In comparison to TPI, UV imaging is not only a faster method, but also provides higher spatial resolution. However, it is an indirect measurement technique and, as an imaging technique, it can lead to false estimations of the coating thickness at the edge of the tablet.

Overall, further development of this technique to a PAT tool appears to be feasible.

3.3.   Results and discussion of 'UV imaging of MUPS tablets: A stability study'[13]

3.3.1.   *Differentiation between acetylsalicylic acid and salicylic acid by multispectral UV imaging*

In the present study the applicability of UV imaging to monitor the API stability with ASA as a model drug in coated drug pellets within a MUPS tablet was determined. First, it was investigated if ASA as API and SA as degradation product can be distinguished by UV imaging with 6 wavelengths even through the Eudragit® RL coating. For this purpose, the mean reflectance spectra of plain ASA and SA tablets (n = 4 tablets) were compared (Fig. 25a). The figure shows that the spectra of the plain substances without polymer coating can be clearly differentiated. In contrast, the mean reflectance spectra of tablets consisting of either coated ASA layered pellets or coated SA layered pellets without tableting excipients did not reveal a clear spectral difference (Fig. 25b). On the one hand, the degradation of ASA to SA starts already during the manufacturing process of coated pellets. For coated ASA layered pellets a SA concentration of approx. 2.5% was determined by HPLC. Thus, the reflectance spectra of coated ASA layered pellets are already mixed spectra of ASA and SA. On the other hand, the small fraction of the UV radiation is typically scattered by the ingredients of the coating leading to a decrease in the intensity of the reflected light. Hence, the UV spectra are altered by the coating and the spectral variances between ASA and SA are evened out.

---

[13]This chapter has been published as shown on page 167 in appendix B.
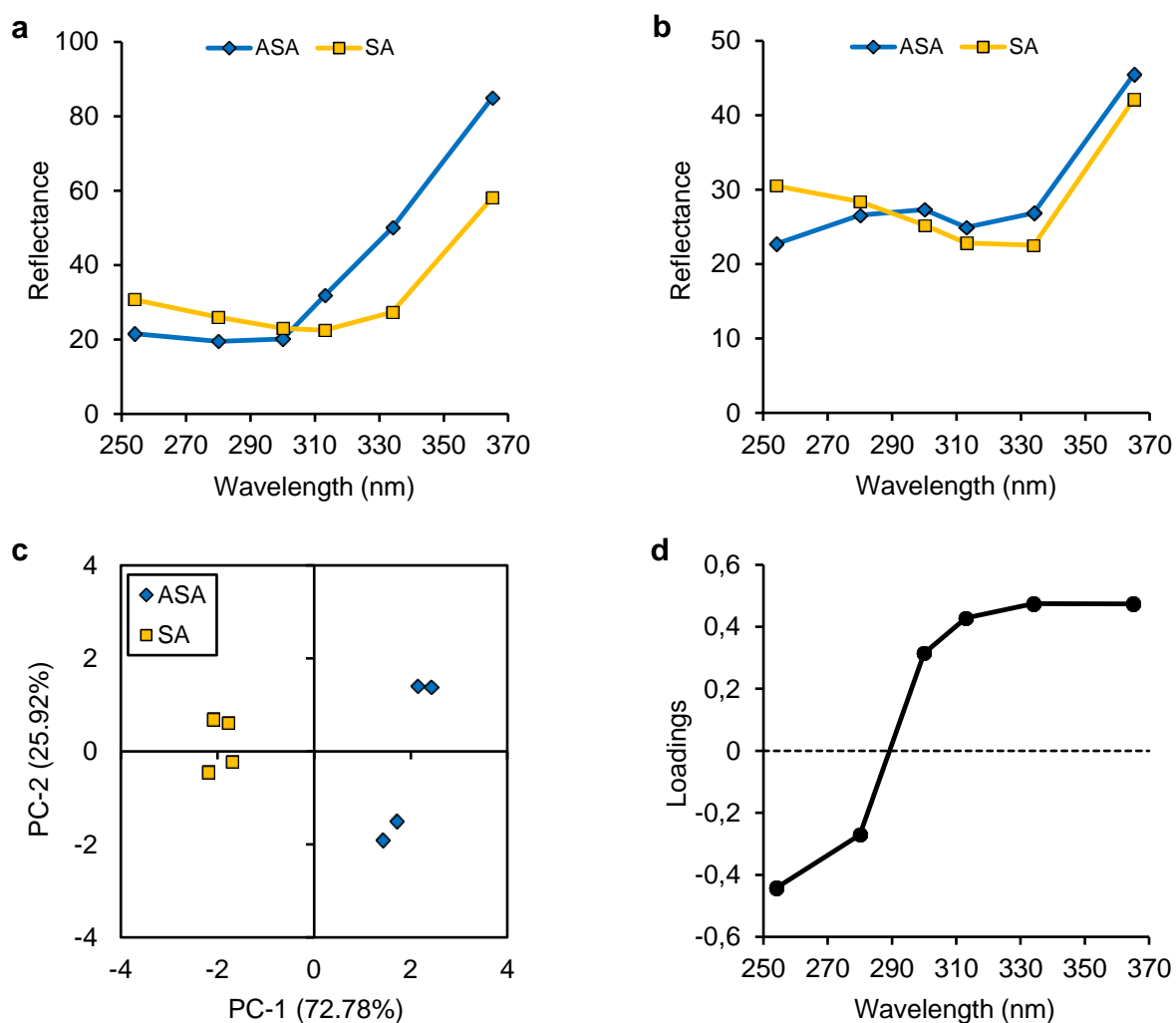
Fig. 25: a) UV mean reflectance spectra of plain API tablets (n = 4); b) UV mean reflectance spectra of API layered pellets coated with Eudragit® RL compressed to tablets without tableting excipients (n = 4); c) PCA scores plot of mean reflectance spectra for tablets consisting of coated ASA layered pellets (n = 4) and tablets consisting of coated SA layered pellets (n = 4); d) Loadings plot of PC-1.

The corresponding loadings plot of PC-1 reveals that the spectral variance can be observed for all six wavelengths (Fig. 25d). According to this information, the loadings plot shows that PC-1 differentiates the samples spectra based on chemical

information. Thus, by multivariate data analysis the spectral data of ASA and SA can

be clearly distinguished with six wavelengths even through the Eudragit® RL coating.

3.3.2. *Monitoring of acetylsalicylic acid degradation*

To investigate the suitability of UV imaging to monitor the ASA degradation to SA within a MUPS tablet, sample MUPS tablets were stored for different time periods under four different storage conditions. The Eudragit® RL coating was chosen because of its high water vapour permeability [181] and thus a significant degradation of ASA to SA was expected [67]. As a consequence, MUPS tablets with different SA concentrations were obtained. As described in section 2.4.3 three tablets from each sampling time point were analysed by HPLC. Based on the determined amount of ASA and SA in each tablet, the SA concentration was determined. The increase of the SA concentration in tablets during storage is shown in Fig. 26 for each storage condition. For 0 days of storage the SA concentration in three tablets was determined. Therefore, in all the graphs (a-d) the same three tablets are displayed for 0 days of storage. As expected, the fastest degradation was observed at a highest relative humidity (RH) of 75% and a temperature of 40 °C, followed by degradation at a RH of 75% and a temperature of 21 °C.
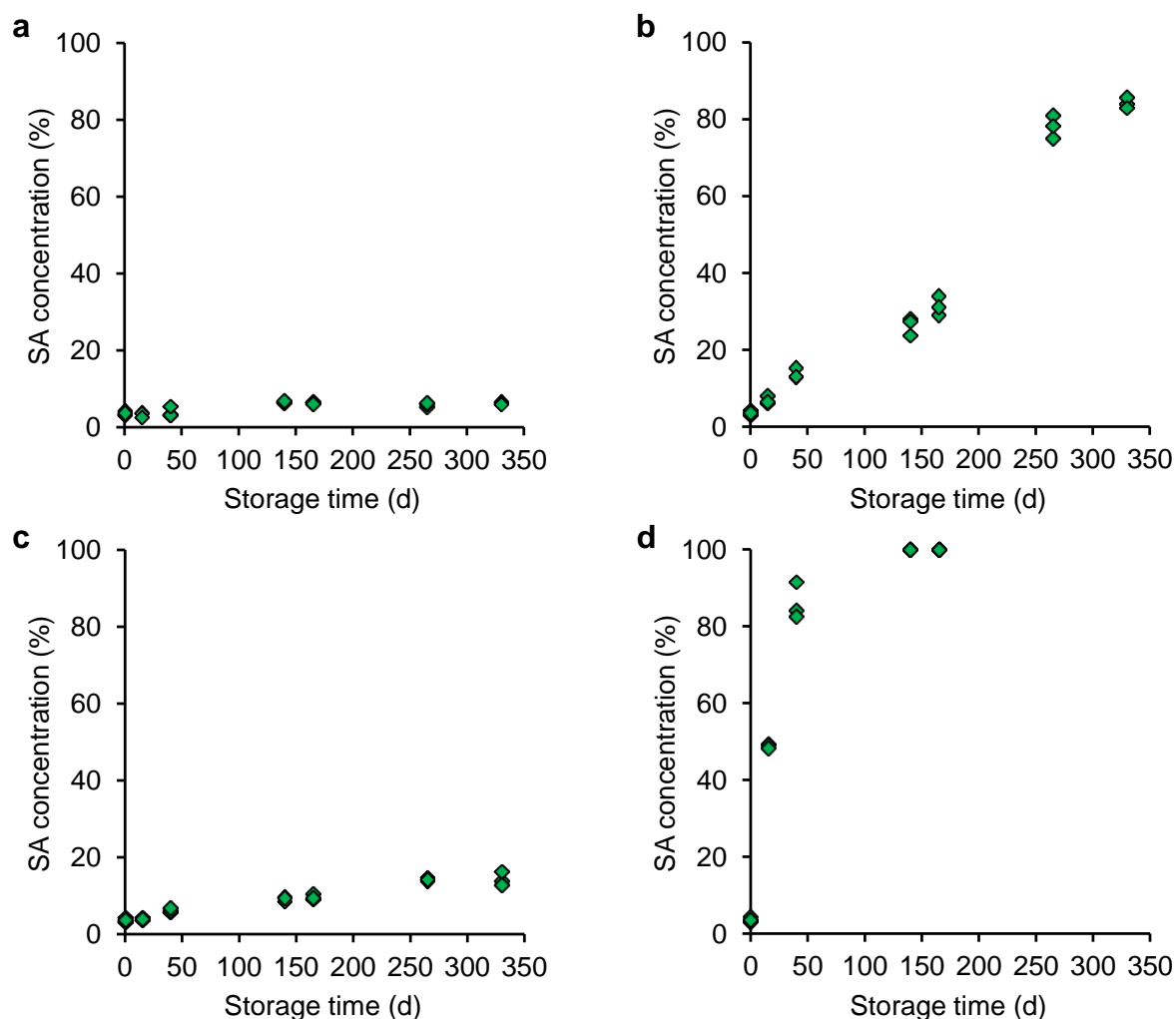
Fig. 26: SA concentration at the applied storage conditions versus storage time. a) 21 °C and 0% RH; b) 21 °C and 75% RH; c) 40 °C and 0% RH; d) 40 °C and 75% RH.

Multivariate data analysis was performed to correlate the SA concentration measured by HPLC with the UV imaging data. A PCA approach was applied to the top and bottom UV image of each MUPS tablet to separate the pixels belonging to the tablet surfaces from the pixels belonging to the background by setting a hard threshold in the PC-1 scores [116]. Subsequently, the pixels belonging to the API layered pellets were separated from the pixels belonging to the tablet excipients within a MUPS

tablet again by setting a hard threshold in the PC-1 scores. Subsequently, a mean reflectance spectrum of the UV spectra belonging to the API layered pellets on the top and bottom side of the tablet was calculated. The variation in the mean UV spectra of the coated API layered pellets within a single MUPS tablet as a function of storage time is shown in Fig. 27.
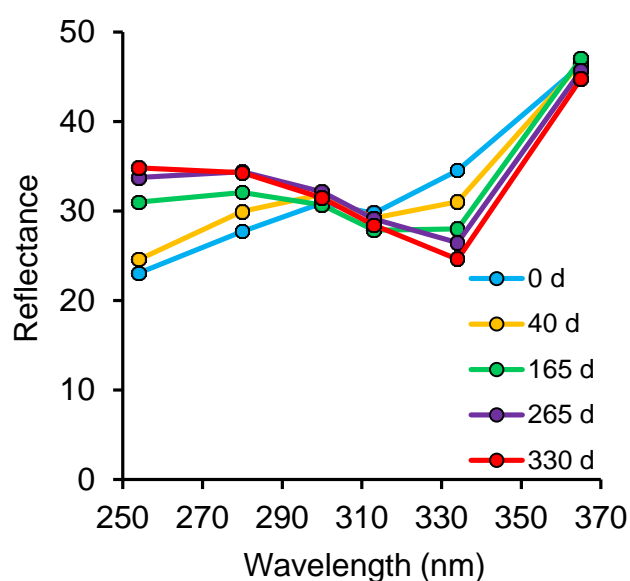
Fig. 27: Mean reflectance spectra for the coated API layered pellets in a MUPS tablet stored at 21 °C and 75% RH for the storage times of 0, 40, 165, 265 and 330 d.

The mean reflectance spectra for the tablets that were also analysed by HPLC, were used for the calculation of a PLS model. For these 66 tablets the mean UV reflectance spectra and SA concentrations were randomly assigned to either a calibration or a test set. To determine the optimal number of LVs for the PLS model, the obtained calibration set (n = 33 tablets) was used for a random cross validation. The SNV correction was used to remove the spectral variances caused by multiplicative interferences of light scattering and particle size [102,104]. This

algorithm led to the PLS model with the best RMSEC, RMSECV and R^2 values. Based on the RMSEC and RMSECV values as a function of the number of the LVs, a number of 3 LVs appeared to be the optimum for the calibration model [102,175]. The RMSECV values reach a plateau between the 4th and 5th LV, and there is only a small difference between the RMSECV values of the 3rd LV and the 4th LV (Fig. 28a). Therefore, to obtain a robust model and to avoid overfitting, a PLS model with 3 LVs was established based on the mean UV reflectance spectra and the SA concentration measured by HPLC. The resulting correlation between the PLS predicted SA concentration values and the SA concentration values measured by HPLC for the calibration set is shown in Fig. 28b. To assess the model performance, the PLS model was applied to the test set. In Fig. 28c the PLS predicted SA concentration is plotted versus the measured SA concentration for the test set. The SA concentration was well estimated for high and even for low SA concentration levels and for the tablets stored at all 4 storage conditions. Consequently, a PLS model with RMSEC of 3.55%, RMSECV of 4.37%, and RMSEP of 4.86% was obtained. This model was used for estimation of the SA concentration in whole tablets based on the surface UV spectra and thereby for monitoring of the ASA degradation in coated pellets within MUPS tablets.

a

b

c
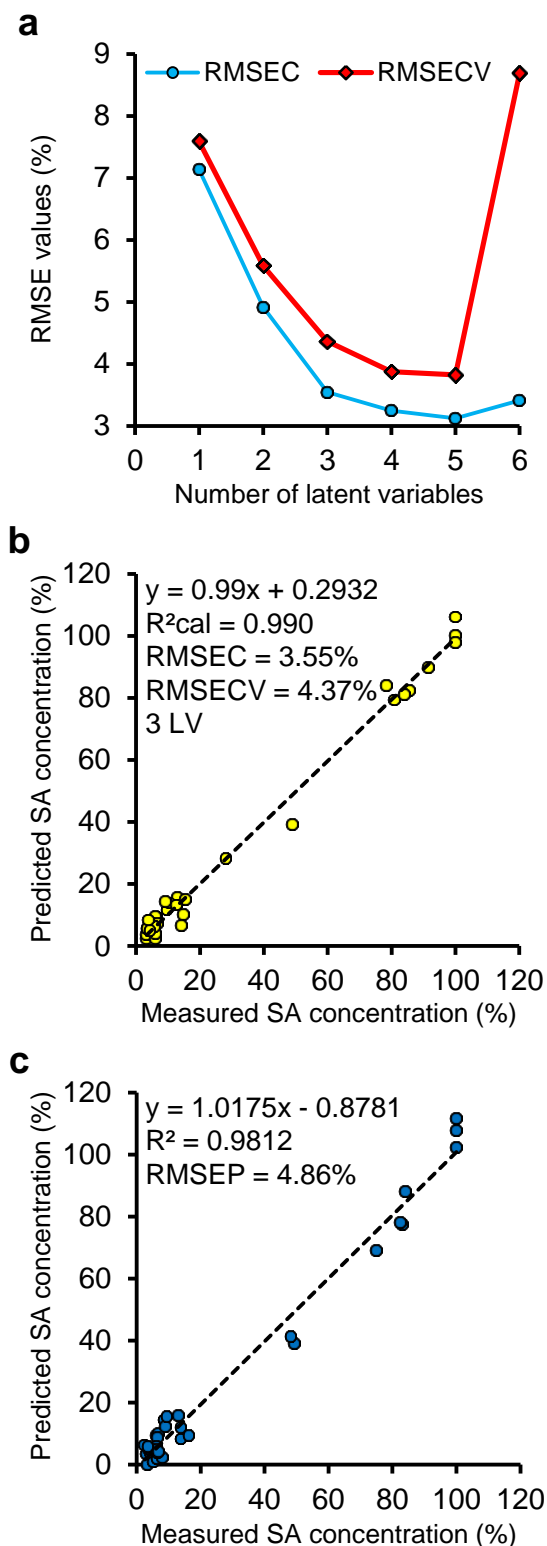
Fig. 28: a) RMSEC and RMSECV values versus the number of the latent variables; b) Predicted SA concentration versus measured SA concentration for the calibration set; c) Predicted SA concentration versus measured SA concentration for the test set.

3.3.3.   Visualisation of the acetylsalicylic acid degradation on the tablet surface

Compared to commonly used analytical methods for API content determination such as HPLC, imaging methods have the advantage of obtaining spatial information on the sample. To exploit this feature, the obtained PLS model was applied to the UV images for prediction of the SA concentration of each individual pixel of the pellets on the surface of a MUPS tablet. The distribution of the predicted SA concentration for the API layered pellets after separation from the background and from the tablet excipients matrix is shown in Fig. 29. The PLS model was applied to the UV images of a tablet, which was stored at 21 °C and 75% RH for 0, 40, 165, and 265 days. The left column of Fig. 29 shows the degradation of ASA during storage of one tablet. The SA concentration is illustrated by the colour code with blue and red pixels corresponding to low and high SA concentrations, respectively. The right column of Fig. 29 shows density distribution plots of the SA concentration corresponding to the tablet image in the left column. Overall, UV imaging was shown to be suitable for estimation of ASA degradation by quantification of the SA concentration in whole MUPS tablets based on surface analysis as well as for distribution analysis of the SA concentration on the surfaces of MUPS tablets.

As a rapid, non-destructive method UV imaging offers a better understanding of the API degradation process, because more frequent testing of the samples compared to destructive methods is possible. Furthermore, as shown by Klukkert et al., UV radiation passes through several types of sealing foil [153]. This would enable analysis of the mean concentration of the degradation product as well as its distribution on the tablet surface through the primary packaging during stability studies. UV imaging may also be used for monitoring of the API stability throughout the manufacturing process and transport. Thus, a decrease of API stability because of changing environmental conditions may immediately be measurable.
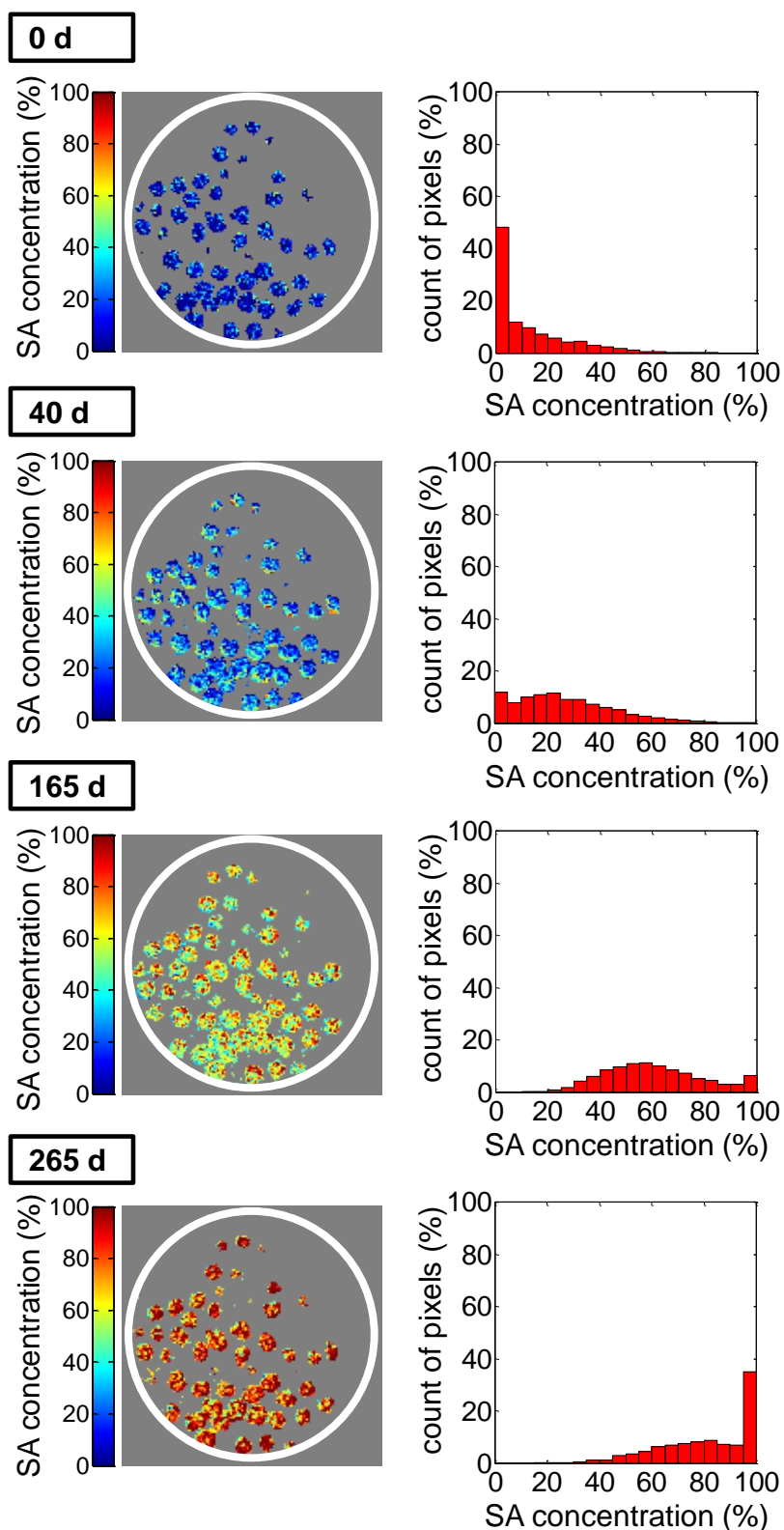
Fig. 29: Degradation of ASA to SA for a tablet stored at 21 °C and 75% RH visualised by the increase of the SA concentration predicted by PLS. Left column: increase of the SA concentration on the tablet surface during storage; Right column: density distribution plots of the SA concentration.

3.3.4. Conclusion

Multispectral UV imaging of the tablet surfaces in combination with chemometrics is a rapid and non-destructive method to investigate the stability of ASA layered pellets within a MUPS tablet through the coating polymer during storage. It could be shown that UV imaging is suitable to estimate the concentration of SA as degradation product of ASA in a whole MUPS tablet based on the mean reflectance spectra of the coated API layered pellets on the MUPS tablet surfaces. The calculated PLS model allowed the estimation of the SA concentration in the tablets at all investigated storage conditions, even at low SA concentration levels. In addition, the distribution of the SA concentration on the tablet surfaces was estimated and visualised by a PLS approach. Overall, this study demonstrates that UV imaging as a non-destructive technique has a high potential for monitoring of the API degradation during stability studies because of the high data acquisition speed, the high molar absorptivity of most APIs as well as the relatively low cost.

Moreover, it is worth to mention, that for practical implementation of UV imaging for stability testing, determination of the API degradation through the primary packaging material will have to be confirmed in future studies.

3.4.   Results and discussion of 'A fast and non-destructive method for quality control of pellet distribution within a MUPS tablet by terahertz pulsed imaging'[14]

3.4.1.   Quality control of pellet distribution within a MUPS tablet

In the present study, the suitability of TPI to analyse the inner structure of MUPS tablets was investigated. Firstly, the signals caused by propagation of the THz radiation through the MUPS tablets were correlated with the ingredients of the tablets. The THz radiation propagates through the tablet and is partly reflected by interfaces of materials with different refractive index [90]. The time delay between the reflections of two different interfaces can be measured and corresponds to a length (propagation depth). The sample THz waveform resulting from the reflection of the THz pulse beam at the interface of the materials in a MUPS tablet containing 30% (w/w) of coated Theo pellets is presented in Fig. 30a for a single example pixel. The THz electric field a.u. are plotted against propagation depth of a THz pulse beam in air which corresponds to the equivalent propagation depth of the THz pulse beam in the tablet. The first reflection peak (1) is caused by the THz pulse that is reflected by the tablet surface in the matrix area. Thereafter, the THz pulse propagates into the tablet matrix and is reflected at the interface between the tablet matrix (MCC) and a coated pellet resulting in a second peak (2). The contact region between the tablet matrix and the pellet includes both an interface between the tablet matrix and the coating and an interface between the coating and the pellet core. However, the coating (coating level 5%, approximately X µm) is thinner than the TPI depth resolution limit of about 35 µm [96]. Thus, the reflections at these interfaces result only in a single peak representing a "combined" interface caused by the small time delay between these signals. After the reflection at this "combined" interface, the THz

---

[14]This chapter has been published as shown on page 167 in appendix B.

pulse further propagates into the Theo pellet until it once again is reflected at the "combined" interface between the pellet and the tablet matrix resulting in a third peak (3).
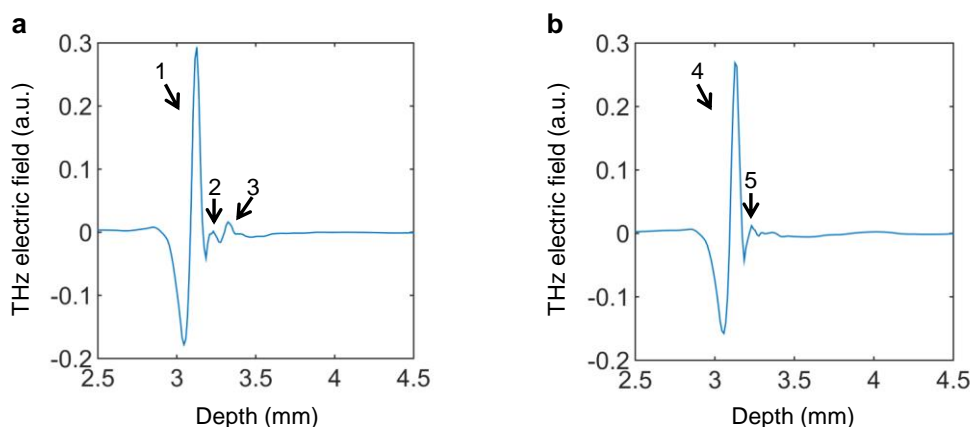
Fig. 30: Visualisation of two exemplary THz waveforms for a MUPS tablet containing 30% of coated pellets plotted as THz electric field (a.u.) against propagation depth equivalent (mm) in air: a) THz waveform for a pellet below the tablet surface, b) THz waveform for a pellet already visible on the tablet surface.

The waveform caused by the THz pulse beam that propagates into the MUPS at different spot is outlined in Fig. 30b. The first peak (4) is caused by THz pulse reflection at the surface of the tablet. The signal for the reflection of the THz pulse at the interface between the tablet matrix and pellet core is not detectable because this particular pellet is too close to the tablet surface and its signal is overlapped by the first peak, again because of the depth resolution limit [96]. The second peak (5) is the result of the reflection at the interface between the pellet core and the tablet matrix. Consequently, TPI enables the detection of pellets within a MUPS tablet.

These THz waveforms can be visualised up to certain depth of the tablet and allow analysis of the tablet structure below the surface. For better visualisation of the 3D structure of a MUPS tablet with a Theo pellet amount of 30% (w/w), images of six different depths (24 µm, 49 µm, 73 µm, 97 µm, 128 µm and 152 µm) below the tablet surface are presented in Fig. 31.

 The coated Theo pellets embedded in the MCC matrix can be identified in the THz data even below the tablet surface. A yellow colour of the pixels corresponds to a high THz electric field indicating the THz pulse reaches the surface of the pellet within the tablet and is reflected at this interface as described above. The first evaluable image was obtained for the depth of 24 µm below the tablet surface. As described above, the signals caused by the back-reflection of the THz pulse beam from the internal interfaces at the depths below than 24 µm are overlapped by the signal of the back-reflected THz pulse from the surface of the tablet. The pellets that can be detected based on the TPI data in the first image of Fig. 31 are marked with a red "1". These TPI results for the pellet distribution at a depth of 24 µm in the tablet were confirmed by the microCT data. The depth position of the pellets below the surface determined by TPI may slightly differ (several µm) from that determined by microCT. This difference is caused by the varying propagation velocity of THz radiation through different materials depending on their refractive indices [90]. Therefore, the matrix/pellet interface may be detected with TPI sooner than they are visible in the microCT images. However, in this study differences in propagation velocity were negligibly small and had no influence on the detected pellet positions.
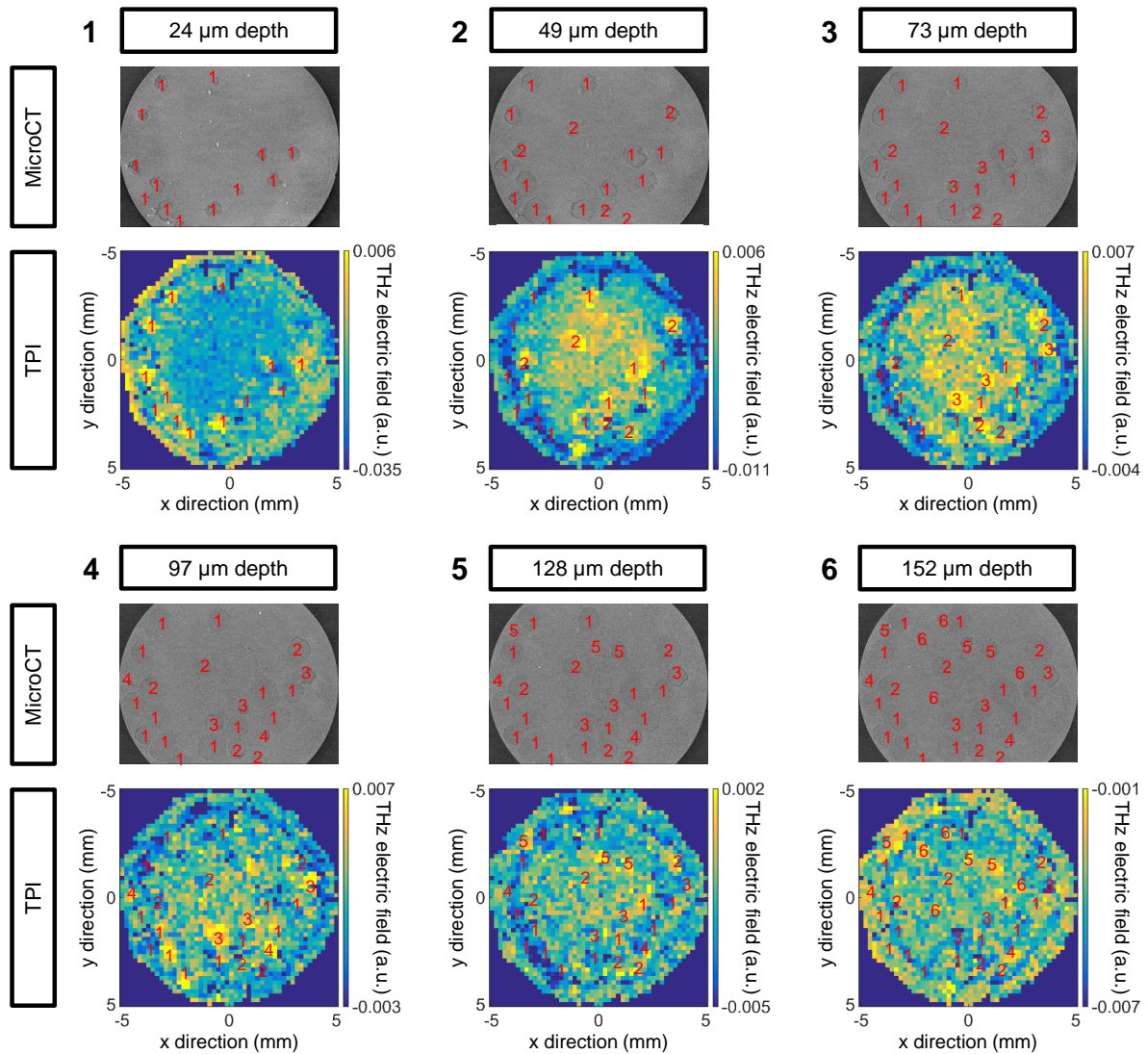
Fig. 31: MicroCT images and TPI images for six different depths below the tablet surface. The detected pellets are marked with the red number. The red numbers (1-6) in the images specify the number of the respective TPI image in which the pellets of the MUPS tablet were firstly detected. The detected pellets in the image of one depth were always transferred to the image of the respective following depth.

In the second image of Fig. 31 (depth of 49 µm) a change of the yellow colour for various pellets that are marked with "1" may be observed. This change results from the decrease of the THz electric field after the peak maximum, the peak being caused by the back-reflection of the THz pulse beam. However, the differentiation

between various pellets that are marked with "1" and the tablet matrix is impossible at this depth because there is no interface present. Therefore, to analyse the pellet distribution deep below the tablet surface of a MUPS tablet, the TPI images of the depths above should also be analysed. The pellets which were firstly detectable at the depth of 49 µm are marked with "2" (Fig. 31, image 2).

The shape of a pellet may vary at different depths below the surface of the MUPS tablet. Thus, several interface spots between the pellet and the matrix exist for one pellet at varying depths. The THz pulse beam is reflected at these interfaces resulting in a high THz electric field (yellow colour) for one pellet at varying depths. This can be observed for the pellets marked with "1" in the lower left corner of the TPI images. These pellets are characterised by a high THz electric field in the first image and then particularly again in the fourth image. As described above, the detectable interface spots of these pellets increase at the depth of 97 µm leading to new interfaces resulting in back-reflection of the THz pulse beams and therefore in high THz electric field values (yellow colour).

The optics of the TPI device are optimised to analyse the inner structure of samples with a thickness of up to 300 µm, as it was designed for the characterisation of pharmaceutical film-coated tablets. Therefore, it was possible to obtain evaluable images for at least 152 µm below the tablet surface, as visualised in the sixth image of Fig. 31. The analysis of depths > 152 µm below the tablet surface appears feasible with other optics, because Zeitler et al. demonstrated that internal interfaces up to 2 mm below the tablet surface of coated tablets can be detected [88]. Subsequently, a 3D structure visualisation and analysis of a whole MUPS tablet appears possible by THz imaging of the top and bottom side of the tablet.

The influence of the pellet amount on the detectability of the pellets embedded in the MCC matrix was investigated further. Therefore, MUPS tablets with different amounts of coated Theo pellets were imaged. As shown in Fig. 31 for the MUPS tablet with a pellet amount of 30% (w/w), all pellets which are present in the microCT images are also detected in the TPI images. In Fig. 32 images of four MUPS tablets with a pellet amount between 40 and 70% (w/w) are displayed. The images are presented only at one selected depth per tablet. To detect as many pellets as possible images at depths below the selected depths were analysed (data not shown). Pellets detected in the TPI images at depths below the selected depths are marked with "1". Furthermore, pellets detected in the TPI images of the selected depths are marked with "2". In the image of the tablet with the pellet amount of 40% (w/w) all pellets which are present in the microCT image, are also detected in the TPI image. In the microCT image of the MUPS tablet with the pellet amount of 50%, two pellets (marked with "0") are found, which are undetectable in the TPI images (Fig. 32b). Interestingly, these pellets are visible with microCT on the tablet surface. Thus, the peak caused by the back-reflection of the THz pulse at the interface between the pellet and the matrix may be overlapped by that at the interface between air and tablet surface (matrix). It is also possible that this surface peak is caused by the back-reflection of the THz pulse beam at the interface between air and pellet surface, because some of the pellets are located at the surface of the tablet. The two undetected pellets are located close to the edge of the tablet. Interestingly, in the TPI image of the MUPS tablet with the pellet amount of 60% (w/w) again two pellets (marked with "0"), which are also located close to the edge of the tablet, are not found in the TPI images. Apparently, edge effects are occurring in the THz waveforms acquired close to the tablet edge because of a diffraction-limited focal spot of about 200 μm.
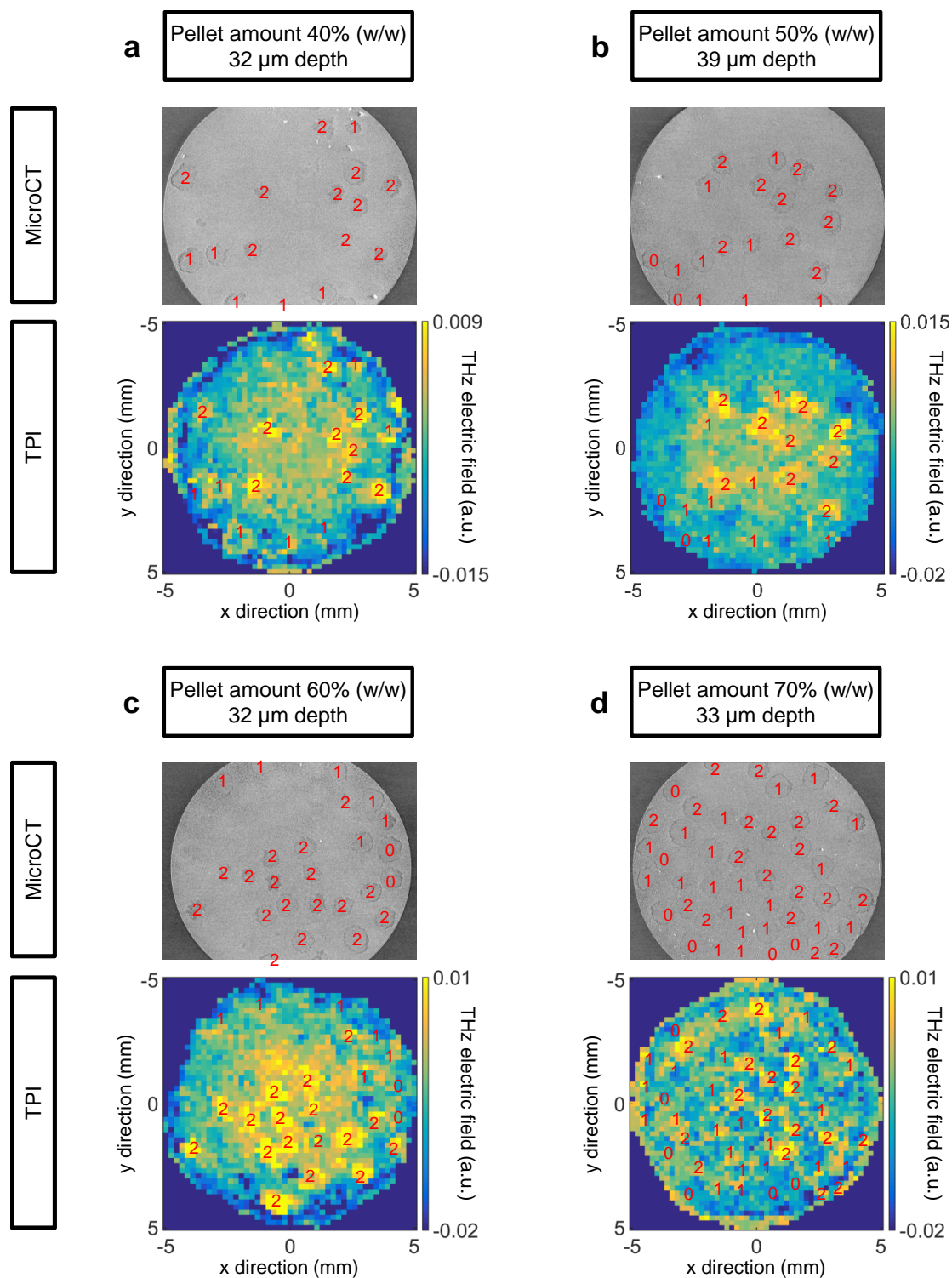
Fig. 32: MicroCT images and TPI images for MUPS tablets with varying pellet amount. 1 indicates pellets that were detected in the TPI images for the depths before the presented image (these images are not shown), 2 indicates pellets that were detected in the presented TPI images and 0 indicates pellets that were not detected in the TPI images.

As shown in Fig. 32d, for the MUPS tablet with a pellet amount of 70% (w/w) the number of undetected pellets increased to six (marked with "0"). Three of the undetected pellets are again located close to the tablet edge confirming the assumption that the applied optics decreases the pellet detectability at the edge of the tablet. The other three of the undetected pellets are not located close to the tablet edge, but are already visible on the tablet surface. This confirms the hypothesis that the back-reflection peak of the THz pulse beam at the interface between matrix and pellets which are visible on the tablet surface may be overlapped by the back-reflection peak of the THz pulse beam at the tablet surface. However, the detectability of the pellets based on the TPI images appears to decrease slightly with increasing pellet amount in the MUPS tablet. Nevertheless, it should be mentioned that these pellets may still be detected based on THz electric field values at other depths below the tablet surface.

In Table 8 the results regarding the number of pellets detected in the TPI and MicroCT images of MUPS tablets up to the selected depth are summarized. For better comparison of the results for the different pellet amounts within the MUPS tablets the percentage of the number of pellets detected in the TPI images with regard to the number of visible pellets in the microCT images was calculated. For tablets with a low pellet amount (30 and 40% (w/w)) all pellets that were visible in the microCT images, could also be detected in the TPI images. In the TPI images of tablets with pellet amounts of at least 50% (w/w) more than 87% of pellets that were visible with microCT, could be detected.

Table 8: Comparison of the numbers of pellet detected in MUPS tablets with varying pellet amounts by microCT and TPI.

Pellet amount in MUPS tablet:	30% (w/w)[1]	40% (w/w)[2]	50% (w/w)[2]	60% (w/w)[2]	70% (w/w)[2]
Number of pellets detected in microCT images	18	16	19	25	45
Number of pellets detected in TPI images	18	16	17	23	39
Percentage of pellets detected by TPI compared to microCT	100%	100%	89%	92%	87%

[1] Number of pellets detected up to the depth of 49 µm below the tablet surface.

[2] Number of pellets detected up to the selected depth below the tablet surface.

Generally, it was possible to detect most of the pellets in the TPI images up to the selected depth regardless of the pellet amount in the MUPS tablets and to confirm these results with the microCT images. Compared to micro-CT, TPI was shown to be a fast and safer method with a high depth resolution (approximately 5 µm) for the analysis of the inner structure of MUPS tablets.

The advantage of TPI compared to surface imaging methods is the possibility to obtain additional information on the pellet distribution below the tablet surface. As already mentioned, with the optics of the TPI device it was possible to analyse the pellet distribution up to at least 152 µm below the tablet surface. In the section 3.1 the suitability of UV imaging for analysis of the pellet distribution on the MUPS tablet surface was investigated. In this study it could be shown that the pellet amount in a MUPS tablet can be estimated based on the amount of pellets determined on the tablet surface. In addition, the pellet amount in a tablet half after tablet division could

be estimated based on the pellet amount determined on the surface of this tablet half. Based on the data of the present study, it seems possible that the determination of the pellet amount within a MUPS tablet by TPI analysis of the tablet might be more suitable, as the percentage of detected pellets in the tablet increases. Particularly for tablets with a low pellet amount and thus also a low number of detectable pellets at the tablet surface, the estimation of the pellet amount in the tablets based on TPI images may improve the quality of the determination. In the section 3.1.3 it has been also shown that for thicker tablets the quality of the estimation decreases. However, this problem might also be solved by application of TPI. Additionally, MUPS tablets are usually coated to achieve homogeneous, smooth surfaces. A coloured coating for example may decrease the detection by UV imaging significantly, as no UV signal from the tablet can be obtained above a certain coating thickness (section 3.2). THz radiation propagates through the coating and should allow analysis of the inner structure also of coated MUPS tablets. Therefore, TPI holds a great potential to analyse the quality of MUPS tablets.

3.4.2. Conclusion

In this study, the suitability of TPI for the detection of coated Theo pellets within a MUPS tablet was investigated. It was found, that a pellet in a tablet causes two peaks: one as soon as the THz pulse beam is back-reflected at the interface between the tablet matrix and the pellet surface and a second when the pulse beam leaves the pellet and is reflected at the interface between the pellet and the matrix. Thus, TPI allows the visualisation of the interfaces between the pellets and the tablet matrix. The first evaluable TPI images were achieved at approximately 25 µm below the tablet surface. With the applied optics it was possible to detect the pellets in the TPI images up to at least 152 µm below the tablet surface. Increasing the amount of pellets within the MUPS tablets appeared to slightly decrease the pellet detectability. However, the undetected pellets were located close to the tablet edge or at the tablet surface. In conclusion, TPI was shown to be a promising technique for fast and non-destructive analysis with a high depth resolution within the MUPS tablets. Therefore, the current study serves as a proof-of-concept for quality control of MUPS tablets by means of TPI. In future studies, the optimisation of the TPI optics for the analysis of the pellet distribution within entire MUPS tablets should be performed.

4. References

[1]   M. Jivraj, L.G. Martini, C.M. Thomson.

        An overview of the different excipients useful for the direct compression of

        tablets.

        Pharm. Sci. Technol. Today 3 (2000) 58–63.

[2]   K. Plumb.

        Continuous processing in the pharmaceutical industry.

        Chem. Eng. Res. Des. 83 (2005) 730–738.

[3]   S.V. Sastry, J.R. Nyshadham, J.A. Fix.

        Recent technological advances in oral drug delivery – A review.

        Pharm. Sci. Technol. Today 3 (2000) 138–145.

[4]   M. Celik.

        Pharmaceutical powder compaction technology.

        2nd ed., Informa Healthcare, London (2011).

[5]   F. Siepmann, A. Hoffmann, B. Leclercq, B. Carlin, J. Siepmann.

        How to adjust desired drug release patterns from ethylcellulose-coated

        dosage forms.

         J. Control. Release 119 (2007) 182–189.

[6]   H. Bechgaard, G.H. Nielsen.

        Controlled-release multiple-units and single-unit doses a literature review.

        Drug Dev. Ind. Pharm. 4 (1978) 53–67.

[7]   T.M. Feinblatt, E.A Ferguson.

        Timed-disintegration capsules: An in vivo roentgenographic study.

        N. Engl. J. Med. 254 (1956) 940–943.

[8]   S. Abdul, A.V. Chandewar, S.B. Jaiswal.

A flexible technology for modified-release drugs: Multiple-unit pellet system (MUPS).

J. Control. Release 147 (2010) 2–16.

[9]   C.D. Melia, S.S. Davis.

Review article: Mechanisms of drug release from tablets and capsules.

I: Disintegration.

Aliment. Pharmacol. Ther. (1989) 223–232.

[10]   J. Collet, C. Moreton.

Modified release peroral dosage forms.

In: M.E. Aulton (Ed.), Pharmaceutics: The science of dosage form design.

Churchill Livingstone, Edinburgh (2002) 289–305.

[11]   R. Bodmeier.

Tableting of coated pellets.

Eur. J. Pharm. Biopharm. 43 (1997) 1–8.

[12]   P. Bansal, S. Vasireddy, F. Plakogiannis, D. Parikh.

Effect of compression on the release properties of polymer-coated niacin granules.

J. Control. Release 27 (1993) 157–63.

[13]   S.R. Bechard, J.C. Leroux.

Coated pelletized dosage form: effect of compaction on drug release.

Drug Dev. Ind. Pharm. 18 (1992) 1927–44.

[14]   T.E. Beckert, K. Lehmann, P.C. Schmidt.

Verpressen von magensaftresistent überzogenen Pellets zu zerfallenden Arzneiformen: Einfluss von Auftragsmenge und Elastizität der Filmbildner.

Österreichische Apotheker Verlangsgesellschaft, Wien (1995).

[15]   R. Bodmeier, O. Paeratakul.

Mechanical properties of dry and wet cellulosic and acrylic films prepared

from aqueous colloidal polymer dispersions used in the coating of solid

dosage forms.

Pharm. Res. 11 (1994) 882–888.

[16]   K. Lehmann.

Chemistry and application properties of polymethacrylate coating systems.

Drugs Pharm. Sci. 36 (1989) 153–245.

[17]   K. Lehmann, H.-U. Petereit, D. Drehe.

Fast disintegrating controlled release tablets from coated particles.

Drugs Made Ger. 37 (1994) 53.

[18]   K. Lehmann, T. Süfke.

New methacrylic acid copolymers for improved coating technology.

Pharm. Res 12 (1995) S137.

[19]   F.J. López-rodríguez, J.J. Torrado, S. Torrado, C. Escamilla, R. Cadórniga,

L.L. Augsburger.

Compression behavior of acetylsalicylic acid pellets.

Drug Dev. Ind. Pharm. 19 (1993) 1369–1377.

[20]   L. Maganti, M. Çelik.

Compaction studies on pellets: II. Coated pellets.

Int. J. Pharm. 103 (1994) 55–67.

[21]   C. Rong-Kun, E.M. Rudnic.

The effect of various polymeric coating systems on the dissolution and

tableting properties of potassium chloride microcapsules.

Int. J. Pharm. 70 (1991) 261–270.

[22]   K. Lehmann, H.-U. Petereit, D. Dreher.

       Schnellzerfallende Tabletten mit gesteuerter Wirkstoffabgabe.

       Pharm. Ind. 55 (1993) 940–947.

[23]   L.A. Felton, J.W. McGinity.

       Influence of plasticizers on the adhesive properties of an acrylic resin

       copolymer to hydrophilic and hydrophobic tablet compacts.

       Int. J. Pharm. 154 (1997) 167–178.

[24]   J.C. Gutiérrez-Rocca, J.W. McGinity.

       Influence of water soluble and insoluble plasticizers on the physical and

       mechanical properties of acrylic resin copolymers.

       Int. J. Pharm. 103 (1994) 293–301.

[25]   A. Dashevsky, K. Kolter, R. Bodmeier.

       Compression of pellets coated with various aqueous polymer dispersions.

       Int. J. Pharm. 279 (2004) 19–26.

[26]   W. Sawicki, R. Łunio.

       Compressibility of floating pellets with verapamil hydrochloride coated with

       dispersion Kollicoat SR 30 D.

       Eur. J. Pharm. Biopharm. 60 (2005) 153–158.

[27]   M.E. Aulton, A.M. Dyer, K.A. Khan.

       The Strength and Compaction of Millispheres: The design of a controlled-

       release drug delivery system for ibuprofen in the form of a tablet comprising

       compacted polymer-coated millispheres.

       Drug Dev. Ind. Pharm. 20 (1994) 3069–3104.

[28]   La Felton, N.H. Shah, G. Zhang, M.H. Infeld, A.W. Malick, J.W. McGinity.

Compaction properties of individual nonpareil beads coated with an acrylic

resin copolymer.

STP pharma sciences. 7 (1997) 457–462.

[29]   J.B. Schwartz, N.H. Nguyen, R.L. Schnaare.

Compaction studies on beads: Compression and consolidation parameters,

Drug Dev. Ind. Pharm. 20 (1994) 3105–3129.

[30]   C. Wang, G. Zhang, N. H. Shah, M. H. Infeld, A. W. Malick, J. W. McGinity.

Compaction properties of spheronized binary granular mixtures.

Drug Dev. Ind. Pharm. 21 (1995) 753–779.

[31]   B. Johansson, M. Wikberg, R. Ek, G. Alderborn.

Compression behaviour and compactability of microcrystalline cellulose

pellets in relationship to their pore structure and mechanical properties.

Int. J. Pharm. 117 (1995) 57–73.

[32]   B. Johannson, F. Nicklasson, G. Alderborn.

Tabletting properties of pellets of varying porosity consisting of dicalcium

phosphate and microcrystalline cellulose.

Pharm. Res. 12 (1995) 164.

[33]   G. P. Millili, J. B. Schwartz.

The strength of microcrystalline cellulose pellets: The effect of granulating

with water/ethanol mixtures.

Drug Dev. Ind. Pharm. 16 (1990) 1411–1426.

[34]   T.E. Beckert, K. Lehmann, P.C. Schmidt.

Compression of enteric-coated pellets to disintegrating tablets.

Int. J. Pharm 143 (1996) 13–22.

[35]   U.H. Opitz.

        Multipartikuläre Tabletten.

        Apothekenmagazin 23 (2005) 136–141.

[36]   G. Ragnarsson, A. Sandberg, U. E. Jonsson, J. Sjögren.

        Development of a new controlled release metoprolol product.

        Drug Dev. Ind. Pharm. 13 (1987) 1495–1509.

[37]   J.L. Haslam, A.E. Forbes, G.S. Rork, T.L. Pipkin, D.A. Slade, D. Khossravi.

        Tableting of controlled release multiparticulates, the effect of millisphere size

        and protective overcoating.

        Int. J. Pharm. 173 (1998) 233–242.

[38]   P. Kühl.

        Tablettieren von Pellets: Komprimierbarkeit, Kompaktierbarkeit und Integrität

        in Kombination mit mikrokristalliner Cellulose und Polyethylenglykol,

        Von-Melle-Park 3, 20146 Hamburg (1999).

[39]   K.M. Picker.

        "Soft Tableting": A new concept to tablet pressure sensitive materials.

        Pharm. Dev. Technol. 9 (2004) 107–121.

[40]   S.A. Altaf, S.W. Hoag, J.W. Ayres.

        Bead compacts. I. Effect of compression on maintenance of polymer coat

        integrity in multilayered bead formulations.

        Drug Dev. Ind. Pharm. 24 (1998) 737–746.

[41]   J.J. Torrado, L.L. Augsburger.

        Effect of different excipients on the tableting of coated particles.

        Int. J. Pharm 106 (1994) 149–55.

[42]   M.E. Bhad, S. Abdul, S.B. Jaiswal, A.V. Chandewar, J.M. Jain, D.M.
        Sakarkar.

        MUPS tablets - A brief review.

        Int. J. Pharmtech Res. 2 (2010) 847–855.

[43]   K.G. Wagner, M. Krumme, P.C. Schmidt.

        Investigation of the pellet-distribution in single tablets via image analysis.

        Eur. J. Pharm. Biopharm. 47 (1999) 79–85.

[44]   K.G. Wagner, M. Krumme, T.E. Beckert, P.C. Schmidt.

        Development of disintegrating multiple-unit tablets on a high-speed rotary
        tablet press.

        Eur. J. Pharm. Biopharm. 50 (2000) 285–292.

[45]   J.M. Juran.

        Juran on quality by design: the new steps for planning quality into goods and
        services.

        The free press, New York (1992).

[46]   Food and Drug Administration.

        Guidance for industry: Quality systems approach to pharmaceutical CGMP
        regulations (2006).

        http://www.fda.gov/downloads/Drugs/.../Guidances/UCM070337.pdf

        Accessed 8 November 2016.

[47]   Food and Drug Administration.

        Pharmaceutical CGMPs for the 21st Century- A risk-based approach (2004).

        http://www.fda.gov/downloads/Drugs/DevelopmentApprovalProcess/M
        anufacturing/QuestionsandAnswersonCurrentGoodManufacturingPractic
        escGMPforDrugs/UCM176374.

        Accessed 8 November 2016.

[48]   Food and Drug Administration.

Guidance for industry PAT - A framework for innovative pharmaceutical

development, manufacturing, and quality assurance (2004).

http://www.fda.gov/downloads/Drugs/Guidances/ucm070305.

Accessed 8 November 2016.

[49]   L.X. Yu, G. Amidon, M.A. Khan, S.W. Hoag, J. Polli, Raju, G. K.,

J. Woodcock.

Understanding pharmaceutical quality by design.

AAPS J. 16 (2014) 771–783.

[50]   International Conference on Harmonisation of Technical Requirements for

Registration of Pharmaceuticals for Human Use.

Guideline on pharmaceutical development Q8 (2R) (2009).

http://www.ich.org/fileadmin/Public_Web_Site/ICH_Products/Guidelines/Quali

ty/Q8_R1/Step4/Q8_R2_Guideline.pdf

Accessed 8 November 2016.

[51]   European Medicines Agency.

Directive 2003/94/EC for medicines and investigational medicines for human

use (2003).

http://eur-lex.europa.eu/legal-content/EN/TXT/?uri=celex:32003L0094.

Accessed 8 November 2016.

[52]   Food and Drug Administration.

Code of federal regulations title 21. Part 211. Current good manufacturing

practice for finished pharmaceuticals (2014).

http://www.accessdata.fda.gov/scripts/cdrh/cfdocs/cfcfr/CFRSearch.cfm?CF

RPart=211.

Accessed 8 November 2016.

[53]   Food and Drug Administration.

        Code of federal regulations title 21. Part 210. Current Good Manufacturing

        Practice in manufacturing, processing, packing, or holding of drugs (2014).

        http://www.accessdata.fda.gov/scripts/cdrh/cfdocs/cfcfr/CFRSearch.cfm?CF

        RPart=210.

        Accessed 8 November 2016.

[54]   G. Clark.

        FDA's PAT initiative.

        Pharm. Technol. Eur. 10 (2004).

[55]   T. De Beer, A. Burggraeve, M. Fonteyne, L. Saerens, J.P. Remon, C.

        Vervaet.

        Near infrared and Raman spectroscopy for the in-process monitoring of

        pharmaceutical production processes.

        Int. J. Pharm. 417 (2011) 32–47.

[56]   H.W. Siesler, Y. Ozaki, S. Kawata, H.M. Heise.

        Near-infrared spectroscopy: principles, instruments, applications.

        2st ed., Wiley-VCH, Weinheim (2008).

[57]   M. Klukkert.

        New aspects of quality control of pharmaceutical tablets with special focus on

        enzyme tablets.

        Von-Melle-Park 3, 20146 Hamburg (2015).

[58]   X.Y. Lawrence, R. Lionberger, M.C. Olson, G. Johnston, G. Buehler, H.

        Winkle.

        Quality by design for generic drugs.

        Pharm. Technol. 33 (2009) 122–127.

[59]   Food and Drug Administration.

         Guidance for industry. Process validation: General principles and practices

         (2011).

         http://www.fda.gov/downloads/Drugs/.../Guidances/UCM070336.pdf

         Accessed 8 November 2016.

[60]   J. Popp, V.V. Tuchin, A. Chiou, S.H. Heinemann.

         Handbook of biophotonics: Photonics in pharmaceutics, bioanalysis and

         environmental research.

         1st ed., Wiley-VCH, Weinheim (2012).

[61]   R. Guenard, G. Thurau.

         Implementation of process analytical technologies.

         In: Process analytical technology, John Wiley & Sons, Chichester (2010)

         17-36.

[62]   M. Blanco, M. Alcalá, J.M. González, E. Torras.

         A process analytical technology approach based on near infrared

         spectroscopy: tablet hardness, content uniformity, and dissolution test

         measurements of intact tablets.

         J. Pharm. Sci. 95 (2006) 2137–2144.

[63]   K.C. Gordon, C.M. McGoverin.

         Raman mapping of pharmaceuticals.

         Int. J. Pharm. 417 (2011) 151–162.

[64]   A.A. Gowen, C.P. O'Donnell, P.J. Cullen, S.E.J. Bell.

         Recent applications of chemical imaging to pharmaceutical process

         monitoring and quality control.

         Eur. J. Pharm. Biopharm. 69 (2008) 10–22.

[65]   G. Reich.

         Near-infrared spectroscopy and imaging: Basic principles and

         pharmaceutical applications.

         Adv. Drug Deliv. Rev. 57 (2005) 1109–1143.

[66]   H.P. Patel, J.K. Patel, M.P. Patel, R.R. Patel.

         Multiple unit particles system of ramipril: An approach to enhance stability.

         J. Young Pharm. 3 (2011) 90–96.

[67]   H.-U. Petereit, W. Weisbrod.

         Formulation and process considerations affecting the stability of solid dosage

         forms formulated with methacrylate copolymers.

         Eur. J. Pharm. Biopharm. 47 (1999) 15–25.

[68]   J. Rantanen.

         Process analytical applications of Raman spectroscopy.

         J. Pharm. Pharmacol. 59 (2007) 171–177.

[69]   C.J. Strachan, T. Rades, K.C. Gordon, J. Rantanen.

         Raman spectroscopy for quantitative analysis of pharmaceutical solids.

         J. Pharm. Pharmacol. 59 (2007) 179–192.

[70]   S. Folestad, M. Josefson, A. Sparén, J. Johansson.

         Method and apparatus for spectrometric analysis of turbid, pharmaceutical

         samples (2004).

         https://www.google.com/patents/US6794670.

         Accessed 8 November 2016

[71]   J. Workman Jr, L. Weyer.

         Practical guide and spectral atlas for interpretive near-infrared spectroscopy,

         2nd ed., CRC Press, Boca Raton (2012).

[72]   C. Gendrin, Y. Roggo, C. Collet.

Pharmaceutical applications of vibrational chemical imaging and

chemometrics: A review.

J. Pharm. Biomed. Anal. 48 (2008) 533–553.

[73]   B.C. Smith.

Fundamentals of Fourier transform infrared spectroscopy.

2nd ed., CRC Press, Boca Raton (2011).

[74]   J.M. Amigo, J. Cruz, M. Bautista, S. Maspoch, J. Coello, M. Blanco.

Study of pharmaceutical samples by NIR chemical-image and multivariate

analysis.

Trends. Analyt. Chem. 27 (2008) 696–713.

[75]   P.R. Griffiths.

Infrared and Raman instrumentation for mapping and imaging.

In: R. Salzer, H.W. Siesler (Eds.), Infrared and Raman spectroscopic

imaging, 1st ed., Wiley-VCH, Weinheim (2009) 3–64.

[76]   M. Rios.

New dimensions in tablet imaging.

Pharm. Technol. 3 (2008).

[77]   B. Boldrini, W. Kessler, K. Rebner, R. Kessler.

Hyperspectral imaging: A review of best practice, performance and pitfalls for

inline and online applications.

J. Near Infrared Spectrosc. 20 (2012) 438.

[78]   P.L. Geladi, H.F. Grahn, J.E. Burger.

Multivariate images, hyperspectral imaging: background and equipment.

In: Techniques and applications of hyperspectral image analysis, John Wiley

& Sons, Chichester (2007) 1–15.

[79]   R.W. Kessler.

Perspectives in process analysis.

J. Chemom. 27 (2013) 369–378.

[80]   M. Jamrogiewicz.

Application of the near-infrared spectroscopy in the pharmaceutical

technology.

J. Pharm. Biomed. Anal. 66 (2012) 1–10.

[81]   M.J. Pelletier, C.C. Pelletier.

Spectroscopic theory for chemical imaging.

In: S. Šašić, Y. Ozaki (Eds.), Raman, infrared, and near-infrared chemical

imaging, Wiley, Hoboken (2010) 1–20.

[82]   P. Larkin.

Infrared and Raman spectroscopy; principles and spectral interpretation.

1st ed., Elsevier, Waltham (2011).

[83]   T. Vankeirsbilck, A. Vercauteren, W. Baeyens, G. Van der Weken, F.

Verpoort, G. Vergote, J.P. Remon,.

Applications of Raman spectroscopy in pharmaceutical analysis.

Trends Analyt. Chem. 21 (2002) 869–877.

[84]   R.K. May, K. Su, L. Han, S. Zhong, J.A. Elliott, L.F. Gladden, M. Evans, Y.

Shen, J.A. Zeitler.

Hardness and density distributions of pharmaceutical tablets measured by

terahertz pulsed imaging.

J. Pharm. Sci. 102 (2013) 2179–2186.

[85]   J.A. Zeitler, P.F. Taday, D.A. Newnham, M. Pepper, K.C. Gordon, T. Rades.

        Terahertz pulsed spectroscopy and imaging in the pharmaceutical setting - A

        review.

        J. Pharm. Pharmacol. 59 (2007) 209–223.

[86]   A.J. Fitzgerald, B.E. Cole, P.F. Taday.

        Nondestructive analysis of tablet coating thicknesses using terahertz pulsed

        imaging.

        J. Pharm. Sci. 94 (2005) 177–183.

[87]   Y.-C. Shen.

        Terahertz pulsed spectroscopy and imaging for pharmaceutical applications:

        A review.

        Int. J. Pharm 417 (2011) 48–60.

[88]   J.A. Zeitler, Y. Shen, C. Baker, P.F. Taday, M. Pepper, T. Rades.

        Analysis of coating structures and interfaces in solid oral dosage forms by

        three dimensional terahertz pulsed imaging.

        J. Pharm. Sci. 96 (2007) 330–340.

[89]   Y.-C. Shen, P.F. Taday.

        Development and application of terahertz pulsed imaging for nondestructive

        inspection of pharmaceutical tablet.

        IEEE J. Sel. Top. Quantum Electron. 14 (2008) 407–415.

[90]   J.A. Zeitler, Y.-C. Shen.

        Industrial applications of terahertz imaging.

        In: K.-E. Peiponen, A. Zeitler, M. Kuwata-Gonokami (Eds.), Terahertz

        spectroscopy and imaging, Springer, Berlin (2013) 451–489.

[91]   M. Walther, B.M. Fischer, P.U. Jepsen.

         Noncovalent intermolecular forces in polycrystalline and amorphous

         saccharides in the far infrared.

         Chem. Phys. 288 (2003) 261–268.

[92]   Y.C. Shen, P.F. Taday, D.A. Newnham, M. Pepper.

         Chemical mapping using reflection terahertz pulsed imaging.

         Semicond. Sci. Technol. 20 (2005) S254.

[93]   C.J. Strachan, T. Rades, D.A. Newnham, K.C. Gordon, M. Pepper,

         P.F. Taday.

         Using terahertz pulsed spectroscopy to study crystallinity of pharmaceutical

         materials.

         Chem. Phys. Lett. 390 (2004) 20–24.

[94]   K. Ajito, J.-Y. Kim, Y. Ueno, H.-J. Song, K. Ueda, W. Limwikrant,

         K. Yamamoto, K. Moribe.

         Nondestructive multicomponent terahertz chemical imaging of medicine in

         tablets.

         J. Electrochem. Soc. 161 (2014) B171–B175.

[95]   K. Yamamoto, M. Yamaguchi, M. Tani, M. Hangyo, S. Teramura, T. Isu,

         N. Tomita.

         Degradation diagnosis of ultrahigh-molecular weight polyethylene with

         terahertz-time-domain spectroscopy.

         Appl. Phys. Lett. 85 (2004), 5194-5197

[96]   M. Haaser, K.C. Gordon, C.J. Strachan, T. Rades.

         Terahertz pulsed imaging as an advanced characterisation tool for film

         coatings—A review.

         Int. J. Pharm. 457 (2013) 510–520.

[97]   R.K. May, M.J. Evans, S. Zhong, I. Warr, L.F. Gladden, Y. Shen, J.A. Zeitler.

        Terahertz in-line sensor for direct coating thickness measurement of

        individual tablets during film coating in real-time.

        J. Pharm. Sci. 100 (2011) 1535–1544.

[98]   B.L. Diffey.

        Sources and measurement of ultraviolet radiation.

        Methods 28 (2002) 4–13.

[99]   R.W. Kessler, W. Kessler.

        Spectral imaging in quality and process control.

        In: G. Gauglitz, D.S. Moore (Eds.), Handbook of spectroscopy, Wiley-VCH,

        Weinheim (2014) 1409–1418.

[100]   J.X. Wu, S. Rehder, F. van den Berg, J.M. Amigo, J.M. Carstensen,

        T. Rades, C.S. Leopold, J. Rantanen.

        Chemical imaging and solid state analysis at compact surfaces using UV

        imaging.

        Int. J. Pharm. 477 (2014) 527–535.

[101]   M. Klukkert, J.X. Wu, J. Rantanen, J.M. Carstensen, T. Rades, C.S. Leopold.

        Multispectral UV imaging for fast and non-destructive quality control of

        chemical and physical tablet attributes.

        Eur. J. Pharm. Sci. 90 (2016) 85–95.

[102]   Å. Rinnan, F. van den Berg, S.B. Engelsen.

        Review of the most common pre-processing techniques for near-infrared

        spectra.

        Trends Analyt. Chem. 28 (2009) 1201–1222.

[103] J.X. Wu, van den Berg, F., J. Rantanen, T. Rades, M. Yang.

Current advances and future trends in characterizing poorly water-soluble

drugs using spectroscopic, imaging and data analytical techniques.

Curr. Pharm. Des. 20 (2014) 436–453.

[104] A. Candolfi, R. de Maesschalck, D. Jouan-Rimbaud, P.A. Hailey,

D.L. Massart.

The influence of data pre-processing in the pattern recognition of excipients

near-infrared spectra.

J. Pharm. Biomed. Anal. 21 (1999) 115–132.

[105] Å. Rinnan.

Pre-processing in vibrational spectroscopy – When, why and how.

Anal. Methods 6 (2014) 7124.

[106] S. Haswell.

Practical guide to chemometrics.

Marcel Dekker Inc., New York (1992).

[107] K.R. Beebe, R.J. Pell, M.B. Seasholtz.

Chemometrics: A practical guide.

John Wiley & Sons, Hoboken (1998).

[108] R. Bro, A.K. Smilde.

Centering and scaling in component analysis.

J. Chemom. 17 (2003) 16–33.

[109] L. Zhang, M.J. Henson, S.S. Sekulic.

Multivariate data analysis for Raman imaging of a model pharmaceutical

tablet.

Anal. Chim. Acta 545 (2005) 262–278.

[110] C.A. Drumm, M.D. Morris.

Microscopic Raman line-Imaging with principal component analysis.

Appl. spectrosc. 49 (1995) 1331–1337.

[111] A.S. El-Hagrasy, M. Delgado-Lopez, J.K. Drennen.

A process analytical technology approach to near-infrared process control of

pharmaceutical powder blending: Part II: Qualitative near-infrared models for

prediction of blend homogeneity.

J. Pharm. Sci. 95 (2006) 407–421.

[112] P.-Y. Sacré, C. de Bleye, P.-F. Chavez, L. Netchacovitch, P. Hubert,

E. Ziemons.

Data processing of vibrational chemical imaging for pharmaceutical

applications.

J. Pharm. Biomed. Anal. 101 (2014) 123–140.

[113] S. Šašić, D. Blackwood, A. Liu, H.W. Ward, H. Clarke.

Detailed analysis of the online near-infrared spectra of pharmaceutical blend

in a rotary tablet press feed frame.

J. Pharm. Biomed. Anal. 103 (2015) 73–79.

[114] I. Tho, A. Bauer-Brandl.

Chemometrics (PCA) in pharmaceutics: Tablet development, manufacturing

and quality assurance.

In: P. Sanguansat (Ed.), Principal component analysis - Multidisciplinary

applications, InTech, Rijeka, 2012, 43–58.

[115] K. Pearson.

On lines and planes of closest fit to systems of points in space.

Philos. Mag. 2 (1901) 559–572.

[116]   M. Vidal, J.M. Amigo.

        Pre-processing of hyperspectral images. Essential steps before image

        analysis.

        Chemometr. Intell. Lab. Syst. 117 (2012) 138–148.

[117]   S. Wold, K. Esbensen, P. Geladi.

        Principal component analysis.

        Chemom. Intell. Lab. Syst. 2 (1987) 37–52.

[118]   B.K. Lavine.

        Clustering and classification of analytical data.

        In: R.A. Meyers (Ed.), Encyclopedia of analytical chemistry, John Wiley &

        Sons, Chichester (2006).

[119]   T. Rajalahti, O.M. Kvalheim.

        Multivariate data analysis in pharmaceutics: A tutorial review.

        Int. J. Pharm. 417 (2011) 280–290.

[120]   H. Abdi, L.J. Williams.

        Principal component analysis.

        WIREs Comp Stat 2 (2010) 433–459.

[121]   H. Wold.

        Causal flows with latent variables.

        Eur. Econ. Rev. 5 (1974) 67–86.

[122]   S. Wold, H. Martens, H. Wold.

        The multivariate calibration problem in chemistry solved by the PLS method.

        In: B. Kågström, A. Ruhe (Eds.), Matrix Pencils, Springer, Berlin (1983)

        286-293.

123]   S. Wold, A. Ruhe, H. Wold, W. J. Dunn III.

        The collinearity problem in linear regression. The partial least squares (PLS)

        approach to generalized onverses.

        SIAM J. Sci. Comput. 5 (1984) 735–743.

[124]   M. Otsuka, I. Yamane.

        Prediction of tablet properties based on near infrared spectra of raw mixed

        powders by chemometrics: Scale-up factor of blending and tableting

        processes.

        J. Pharm. Sci. 98 (2009) 4296–4305.

[125]   H. Abdi.

        Partial least squares regression (PLS-regression).

        In: M. Lewis-Beck., A. Bryman, T. Futing (Eds.), Encyclopedia of social

        sciences research methods, Sage, New York (2003).

[126]   L.A. Berrueta, R.M. Alonso-Salces, K. Héberger.

        Supervised pattern recognition in food analysis.

        J. Chromatogr. A 1158 (2007) 196–214.

[127]   W.J. Dunn, D.R. Scott, W.G. Glen.

        Principal components analysis and partial least squares regression.

        Tetrahedron Comput. Methodol. 2 (1989) 349–376.

[128]   L. Eriksson.

        Multi-and megavariate data analysis.

        2nd ed., Umetrics AB, Umea (2006).

[129]   S. de Jong.

        SIMPLS: An alternative approach to partial least squares regression.

        Chemom. Intell. Lab. Syst. 18 (1993) 251–263.

[130]   R. Rosipal, N. Krämer.

Overview and Recent Advances in Partial Least Squares.

In: Proceedings of the 2005 international conference on subspace, latent

structure and feature selection, SLSFS (2005) 34–51.

DOI: 10.1007/11752790_2

[131]   W. Kessler.

Multivariate Datenanalyse: für die Pharma-, Bio-und Prozessanalytik.

Wiley-VCH, Weinheim (2007).

[132]   Y. Roggo, P. Chalus, L. Maurer, C. Lema-Martinez, A. Edmond, N. Jent.

A review of near infrared spectroscopy and chemometrics in pharmaceutical

technologies.

J. Pharm. Biomed. Anal. 44 (2007) 683–700.

[133]   C. Gendre, M. Genty, M. Boiret, M. Julien, L. Meunier, O. Lecoq, M. Baron,

P. Chaminade, J.M. Pean.

Development of a process analytical technology (PAT) for in-line monitoring

of film thickness and mass of coating materials during a pan coating

operation.

Eur. J. Pharm. Sci. 43 (2011) 244–250.

[134]   T.R.M. De Beer, C. Bodson, B. Dejaegher, B. Walczak, P. Vercruysse,

A. Burggraeve, A. Lemos, L. Delattre, Y. Van der Heyden, J.P. Remon,

C. Vervaet, W.R.G Baeyens.

Raman spectroscopy as a process analytical technology (PAT) tool for the in-

line monitoring and understanding of a powder blending process.

J. Pharm. Biomed. Anal. 48 (2008) 772–779.

[135] J.J. Moes, M.M. Ruijken, E. Gout, H.W. Frijlink, M.I. Ugwoke.

Application of process analytical technology in tablet process development

using NIR spectroscopy: Blend uniformity, content uniformity and coating

thickness measurements.

Int. J. Pharm 357 (2008) 108–118.

[136] R.B. Shah, M.A. Tawakkul, M.A. Khan.

Process analytical technology: chemometric analysis of Raman and near

infra-red spectroscopic data for predicting physical properties of extended

release matrix tablets.

J. Pharm. Sci. 96 (2007) 1356–1365.

[137] P.R. Wahl, G. Fruhmann, S. Sacher, G. Straka, S. Sowinski, J.G. Khinast.

PAT for tableting: Inline monitoring of API and excipients via NIR

spectroscopy.

Eur. J. Pharm. Biopharm. 87 (2014) 271–278.

[138] H. Wikström, S. Romero-Torres, S. Wongweragiat, J.A. Williams ,

E.R. Grant, L.S. Taylor.

On-line content uniformity determination of tablets using low-resolution

Raman spectroscopy.

Appl. spectrosc. 60 (2006) 672–681.

[139] J.M. Amigo, C. Ravn.

Direct quantification and distribution assessment of major and minor

components in pharmaceutical tablets by NIR-chemical imaging.

Eur. J. Pharm. Sci. 37 (2009) 76–82.

[140] J. Cruz, M. Blanco.

Content uniformity studies in tablets by NIR-CI.

J. Pharm. Biomed. Anal. 56 (2011) 408–412.

[141]   F. Franch-Lage, J.M. Amigo, E. Skibsted, S. Maspoch, J. Coello.

         Fast assessment of the surface distribution of API and excipients in tablets

         using NIR-hyperspectral imaging.

         Int. J. Pharm. 411 (2011) 27–35.

[142]   E. Lee, W.X. Huang, P. Chen, E.N. Lewis, R.V. Vivilecchia.

         High-throughput analysis of pharmaceutical tablet content uniformity by near-

         infrared chemical imaging.

         Spectrosc. 21 (2006) 24–32.

[143]   A. Palou, J. Cruz, M. Blanco, J. Tomas, J. de los Rios, M. Alcala.

          Determination of drug, excipients and coating distribution in pharmaceutical

         tablets using NIR-CI.

         J. Pharm. Anal. 2 (2012) 90–97.

[144]   N. Zhao, A. Zidan, M. Tawakkul, V.A. Sayeed, M. Khan.

         Tablet splitting: Product quality assessment of metoprolol succinate extended

         release tablets.

         Int. J. Pharm. 401 (2010) 25–31.

[145]   M. Boiret, A.d. Juan, N. Gorretta, Y.-M. Ginot, J.-M. Roger.

         Distribution of a low dose compound within pharmaceutical tablet by using

         multivariate curve resolution on Raman hyperspectral images.

         J. Pharm. Biomed. Anal. 103C (2014) 35–43.

[146]   T. Firkala, A. Farkas, B. Vajna, I. Farkas, G. Marosi.

         Investigation of drug distribution in tablets using surface enhanced Raman

         chemical imaging.

         J. Pharm. Biomed. Anal. 76 (2013) 145–151.

[147] S. Sasić.

Raman mapping of low-content API pharmaceutical formulations. I. Mapping

of alprazolam in alprazolam/xanax tablets.

Pharm. Res. 24 (2007) 58–65.

[148] S. Sasić,

An in-depth analysis of Raman and near-infrared chemical images of

common pharmaceutical tablets.

Appl. spectrosc. 61 (2007) 239–250.

[149] M.N. Slipchenko, H. Chen, D.R. Ely, Y. Jung, M.T. Carvajal, J.-X. Cheng.

Vibrational imaging of tablets by epi-detected stimulated Raman scattering

microscopy.

Analyst 135 (2010) 2613–2619.

[150] B. Vajna, G. Patyi, Z. Nagy, A. Bódis, A. Farkas, G. Marosi.

Comparison of chemometric methods in the analysis of pharmaceuticals with

hyperspectral Raman imaging.

J. Raman Spectrosc. 42 (2011) 1977–1986.

[151] R.P. Cogdill, S.M. Short, R. Forcht, Z. Shi, Y. Shen, P.F. Taday,

C.A. Anderson, J.K. Drennen.

An efficient method-development strategy for quantitative chemical imaging

using terahertz pulse spectroscopy.

J. Pharm. Innov. 1 (2006) 63–75.

[152] Y.-C. Shen, R.J. Hwu, K.J. Linden, P.F. Taday, D.A. Newnham, M.C. Kemp,

M. Pepper.

3D chemical mapping using terahertz pulsed imaging.

In: Integrated Optoelectronic Devices 2005, SPIE, 2005, 24.

[153]   M. Klukkert, J.X. Wu, J. Rantanen, S. Rehder, J.M. Carstensen, T. Rades,

        C.S. Leopold.

        Non-destructive quality control of tablets and blister packs by UV imaging.

        Pharm. Ind. 78 (2016) 108–120.

[154]   M. Klukkert, J.X. Wu, J. Rantanen, S. Rehder, J.M. Carstensen, T. Rades,

        C.S. Leopold.

        Rapid assessment of tablet film coating quality by multispectral UV imaging.

        AAPS PharmSciTech 17 (2016) 958–67.

[155]   L. Maurer, H. Leuenberger.

        Terahertz pulsed imaging and near infrared imaging to monitor the coating

        process of pharmaceutical tablets.

        Int. J. Pharm. 370 (2009) 8–16.

[156]   D. Brock, J.A. Zeitler, A. Funke, K. Knop, P. Kleinebudde.

        A comparison of quality control methods for active coating processes.

        Int. J. Pharm. 439 (2012) 289–295.

[157]   G. Heinicke, J.B. Schwartz.

        Ammonio polymethacrylate-coated diltiazem: Drug release from single

        pellets, media dependence, and swelling behaviour.

        Pharm. Dev. Technol. 12 (2007) 285–296.

[158]   M. Andersson, M. Josefson, F.W. Langkilde, K.-G. Wahlund.

        Monitoring of a film coating process for tablets using near infrared reflectance

        spectrometry.

        J. Pharm. Biomed. Anal. 20 (1999) 27–37.

[159]   M.-J. Lee, D.-Y. Seo, H.-E. Lee, I.-C. Wang, W.-S. Kim, M.-Y. Jeong, G.J.

        Choi, In line NIR quantification of film thickness on pharmaceutical pellets

        during a fluid bed coating process, Int. J. Pharm. 403 (2011) 66–72.

[160] C.-V. Möltgen, T. Puchert, J.C. Menezes, D. Lochmann, G. Reich.

A novel in-line NIR spectroscopy application for the monitoring of tablet film

coating in an industrial scale process.

Talanta 92 (2012) 26–37.

[161] J.D. Pérez-Ramos, W.P. Findlay, G. Peck, K.R. Morris.

Quantitative analysis of film coating in a pan coater based on in-line sensor

measurements.

AAPS PharmSciTech 6 (2005) E127.

[162] J. Müller, K. Knop, J. Thies, C. Uerpmann, P. Kleinebudde.

Feasibility of Raman spectroscopy as PAT tool in active coating.

Drug Dev. Ind. Pharm. 36 (2010) 234–243.

[163] M. Wirges, A. Funke, P. Serno, K. Knop, P. Kleinebudde.

Development and in-line validation of a process analytical technology to

facilitate the scale up of coating processes.

J. Pharm. Biomed. Anal. 78–79 (2013) 57–64.

[164] C. Cairós, J.M. Amigo, R. Watt, J. Coello, S. Maspoch.

Implementation of enhanced correlation maps in near infrared chemical

images: Application in pharmaceutical research.

Talanta 79 (2009) 657–664.

[165] N. Futscher, P. Schumacher.

Climatic zones of the earth.

Pharm. Ind. 34 (1972) 479–483.

[166]   WHO Expert Committee on Specifications for Pharmaceutical Preparations.

Guidelines for stability testing of pharmaceutical products containing well

established drug substances in conventional dosage forms.

WHO technical report series No. 863, 34th Report (1996) 65–79.

http://apps.who.int/medicinedocs/en/d/Js5516e/.

Accessed 8 November 2016.

[167]   WHO Expert Committee on Specifications for Pharmaceutical Preparations.

WHO technical report series No. 937, 40th Report (2006) 12.

http://apps.who.int/iris/bitstream/10665/43443/1/WHO_TRS_937_eng.pdf

Accessed 8 November 2016.

[168]   International Conference on Harmonisation of Technical Requirements for

Registration of Pharmaceuticals for Human Use.

Stability testing of new drug substances and products Q1A(R2) (2003).

http://www.ich.org/fileadmin/Public_Web_Site/ICH_Products/Guidelines/Quali

ty/Q1A_R2/Step4/Q1A_R2__Guideline.pdf

Accessed 8 November 2016.

[169]   M. Bakshi, S. Singh.

Development of validated stability-indicating assay methods - Critical review.

J. Pharm. Biomed. Anal. 28 (2002) 1011–1040.

[170]   A.H. Beckett, J.B. Stenlake.

Practical Pharmaceutical Chemistry: Part II

4th ed., Bloomsbury, London (2001).

[171]   J.K. Drennen, R.A. Lodder.

Nondestructive near-infrared analysis of intact tablets for determination of

degradation products.

J. Pharm. Sci. 79 (1990) 622–627.

[172] I. Malik, M. Poonacha, J. Moses, R.A. Lodder.

Multispectral imaging of tablets in blister packaging.

AAPS PharmSciTech 2 (2001) 1–7.

[173] C. Wang, T.J. Vickers, C.K. Mann.

Direct assay and shelf-life monitoring of aspirin tablets using Raman

spectroscopy.

J. Pharm. Biomed. Anal. 16 (1997) 87–94.

[174] T.J. Atherton, D.J. Kerbyson.

Size invariant circle detection.

Image Vision Comput. 17 (1999) 795–803.

[175] S. Wiklund, D. Nilsson, L. Eriksson, M. Sjöström, S. Wold, K. Faber.

A randomization test for PLS component selection.

J. Chemom. 21 (2007) 427–439.

[176] The United States Pharmacopeial Convention Inc.

United States Pharmacopeia and National Formulary, Vol 2, USP 30-NF 25

(2007) 3321–3322.

[178] A.J. Quattrone, R.S. Putnam.

A single liquid-chromatographic procedure for therapeutic monitoring of

theophylline, acetaminophen, or ethosuximide.

Clin. Chem. 27 (1981) 129–32.

[179] B. Fanget, H. Najb, D. Dumas, M. Mietton.

Optimization of streamflow measurements by the dilution of the food colorant

E110.

Hydrol. Sci. J. 54 (2009) 474–483.

[179]   J.G. Rosas, M. Blanco.

         A criterion for assessing homogeneity distribution in hyperspectral images.

         Part 1: Homogeneity index bases and blending processes.

         J. Pharm. Biomed. Anal. 70 (2012) 680–690.

[180]   R.C. Gonzalez, R.E. Woods, S.L. Eddins.

         Digital image processing using MATLAB.

         1st ed., Prentice Hall, Upper Saddle River (2004).

[181]   B. Skalsky, H.-U. Petereit.

         Chemistry and application properties of polymethacrylate systems.

         In: J.W. McGinity, L.A. Felton (Eds.), Aqueous polymeric coatings for

         pharmaceutical dosage forms, Informa Healthcare, New York (2008)

         237-277.

[182]   D.A. Miller, J.W. McGinity.

         Aqueous polymeric film coating.

         In: L.L. Augsburger, S.W. Hoag (Eds.), Pharmaceutical dosage forms:

         Tablets, Informa Healthcare, New York (2008) 399-437.

[183]   S. Zhong, Y.-C. Shen, L. Ho, R.K. May, J.A. Zeitler, M. Evans, P.F. Taday,

         M. Pepper, T. Rades, K.C. Gordon, R. Müller, P. Kleinebudde.

         Non-destructive quantification of pharmaceutical tablet coatings using

         terahertz pulsed imaging and optical coherence tomography.

         Opt. Lasers Eng. 49 (2011) 361–365.

5. Appendix

A Curriculum vitae

The CV is not published for reasons of data protection.

B Conference contributions and publications

In context with this work, the following contributions have been presented at conferences and journal articles have been published.

Conference contributions - oral presentations

Modern methods of spectroscopic analysis in pharmaceutical technology. I.M.Sechenov First Moscow State Medical University 2013, Moscow, Russia

---

UV imaging for determination of the coating layer thickness of coated tablets. 9th Pharmaceutical Solid-State Research Cluster Symposium 2015, Ghent, Belgium

---

UV imaging versus terahertz pulsed imaging for analysis of tablet coating. 10th World Meeting on Pharmaceutics, Biopharmaceutics and Pharmaceutical Technology 2016, Glasgow, UK

UV imaging for quality control of MUPS tablets. 10th Pharmaceutical Solid-State Research Cluster Symposium 2016, Copenhagen, Denmark

---

Conference contributions - poster presentations

Design of experiments approach for the development of coated pellets for MUPS tablets. 40th Annual Meeting & Exposition of the Controlled Release Society 2013, Honolulu, USA

UV imaging of MUPS tablets: Surface analysis of the pellet distribution. 9th World Meeting on Pharmaceutics, Biopharmaceutics and Pharmaceutical Technology 2014, Lisbon, Portugal

UV imaging of MUPS tablets: A stability study, 28th Meeting of the American Association of Pharmaceutical Scientists 2014, San Diego, USA

UV imaging of MUPS tablets: pellet content and distribution analysis. 7th pan-European QbD & PAT Science Conference 2015, Graz, Austria

Pellet Distribution Analysis by UV Imaging and HPLC: A comparative Study. 42nd Annual Meeting & Exposition of the Controlled Release Society 2015, Edinburgh, UK

Determination of the coating layer thickness of coated tablets by UV imaging. 29th Meeting of the American Association of Pharmaceutical Scientists 2015, Orlando, USA

Terahertz pulsed imaging of multiple unit pellet system tablets. 30th Meeting of the American Association of Pharmaceutical Scientists 2015, Denver, USA

Journal articles with authors contributions and reference chapters.

Title	Journal	Authors	Contribution to the work	Percentage	Reference chapters
Multispectral UV imaging for surface analysis of MUPS tablets with special focus on the pellet distribution	International Journal of Pharmaceutics (accepted)	Novikova, A. Carstensen, J.M. Rades. T. Leopold. C.S.	Project plan, experiments, data analysis, publication Supervisor Supervisor Supervisor	100%	1.5.2; 2.2; 3.1
UV imaging of MUPS tablets: A stability study	European Journal of Pharmaceutics and Biopharmaceutics (submitted)	Novikova, A. Carstensen, J.M. Zeitler, J.A. Rades, T. Leopold, C.S.	Project plan, experiments, data analysis, publication Supervisor Supervisor Supervisor Supervisor	100%	1.5.4; 2.4; 3.3
Multispectral UV imaging for determination of the tablet coating thickness	Journal of Pharmaceutical Sciences (submitted)	Novikova, A. Castensen, J.M. Rades, T. Leopold, C.S.	Project plan, experiments, data analysis, publication Supervisor Supervisor Supervisor	100%	1.5.3; 2.3; 3.2
A fast and non-destructive method for quality control of pellet distribution within a MUPS tablet by terahertz pulsed imaging	European Journal of Pharmaceutical Sciences (submitted)	Novikova, A. Markl, D. Zeitler, J.A. Rades, T. Leopold, C.S.	Project plan, experiments, data analysis, publication Data analysis Supervisor Supervisor Supervisor	95% 5%	1.5.2; 2.5; 3.4;

C Hazardous materials

Substance	Supplier	Danger symbol	Hazard statements	Precautionary statements
Aceton	Biesterfeld, Spezialchemie, Germany		H225, H319, H336	P210, P233, P305+P338+P351
Acetonitrile	VWR, Germany		H225, H302, H312, H332, H319	P210,P280, P305+P338+P351
Acetylsalicylicacid	Fagron, Germany		H302, H315, H319, H335	P261, P305+P338+P351
Hydrochloric acid	Roth, Germany		H290, H314, H335	P234, P390
Isopropanol	Biesterfeld Spezialchemie, Germany		H225, H319, H336	P210, P233, P305+P338+P351
Phosphoric acid	Roth, Germany		H290, H314,	P280, P301+P330+P331, P303+P361+P353, P305+P338+P353, P310
Salicylic acid	Caelo, Germany		H302, H318	P280, P305, P351, P313

Theophylline	Caelo, Germany		H301	P301 + P310
Trifluoroacetic acid	Roth, Germany		H290, H314, H332, H412	P260, P280, P303+P351+P338, P305+P338+P353, P310

<u>Declaration on oath (affirmation in lieu of oath)</u> / Eidesstattliche Versicherung

Hiermit versichere ich an Eides statt, die vorliegende Dissertation selbst verfasst und keine anderen als die angegebenen Hilfsmittel benutzt zu haben. Die eingereichte schriftliche Fassung entspricht der auf dem elektronischen Speichermedium. Ich versichere, dass diese Dissertation nicht in einem früheren Promotionsverfahren eingereicht wurde.

Datum, Unterschrift